

DEPARTMENT OF PHYSICS AND ASTRONOMY "A. RIGHI"

SECOND CYCLE DEGREE

PHYSICS

Diagrammatic Monte Carlo for the Froehlich polaron in materials with anisotropic non-degenerate band extrema

Supervisor

Prof. Cesare Franchini

Co-supervisor

Dr. Thomas Hahn

Defended by Samuele De Amicis

Abstract

The polaron is a quasiparticle made of an electron and a cloud of phonons coupled to it through the electron-phonon interaction. This quasiparticle state is common at the bottom of the conduction band or at the top of the valence band (hole polaron) in ionic semiconductors and insulators such as III-V compounds (GaAs, GaP, AlAs) and oxides (BaO, CaO). In this thesis we will be focusing on the large polaron model, also known as the Froehlich polaron, which assumes that the material can be modelled as a dielectric continuum. The main features of the Froehlich model will be discussed, including also a generalization for our more complex case, and then the Many Body formalism will be explained together with the main aspects of the Monte Carlo method (introducing also Markov chains), in order to provide the theoretical basis for the Diagrammatic Monte Carlo method applied to the large polaron.

The simulations performed using Diagrammatic Monte Carlo were used to compute the ground state energy and polaron effective masses in the specific case of the conduction band of a range of cubic materials (AlAs, AlP, GaN, GaP, SiC, ZnSe) with parameters found using ab-initio methods.

The materials simulated had both isotropic and anisotropic conduction bands, a significant difference with respect to previously performed Diagrammatic Monte Carlo simulations, which were all based on an isotropic model for the electron band.

The results obtained are in agreement with previously computed values found in literature using different numerical methods and the obtained model can be used as a starting point for more complex simulations.

CONTENTS

Contents

Abstract					
Lis	List of Figures List of Tables Introduction				
Lis					
Int					
1	1.1 1.2 1.3 1.4 1.5	Ehlich Polaron Electrons in crystals	3 6 12 13 16 22		
2	2.1 2.2 2.3 2.4 2.5 2.6	Creen's function formalism	24 24 26 28 31 33		
3	The 3.1 3.2 3.3 3.4 3.5	Diagrammatic Monte Carlo method The Monte Carlo sampling method	41 42 44 47 51		
4	Diag 4.1 4.2	MC for the Froehlich Polaron Updates	54 56 64		
5	Met 5.1 5.2	hods and results Input data	68 68 69		

References			
Appendix			
Acknowledgement 5.4 Acknowledgment			
Conclusions			
5.3 Results	69		
CONTENTS	iii		

LIST OF FIGURES iv

List of Figures

1.1	DFT calculated low-temperature GaAs Wurtzite structure with relative DOS [1].	6
1.2	Computed polaron energy using perturbation theory, strong coupling theory	
	and all coupling Feynman technique [2]	15
1.3	GaAs crystal structure, the cubic structure of the zincblende unit cell is here	
	clearly displayed	16
1.4	DFT calculated AlAs band structure [3], the conduction band minimum is on the high symmetry line Δ between Γ and X	17
1.5	Polaron effective mass breakdown limit in the uniaxial case [4]	21
2.1	Feynman diagram of the free electron propagator together with its Green's function	34
2.2	Feynman diagram of the free phonon propagator together with its Green's	
	function	34
2.3	Feynman diagrams of the electron-phonon interaction	35
2.4	Order 4 diagram.	35
2.5	Disconnected order 4 diagram	36
2.6	Order 2 diagram	36
2.7	Order 4 diagram	36
2.8	Order 4 diagram	37
2.9	Order 2 diagram with one external phonon	38
3.1	Graphical representation of π estimation using the simple direct Monte Carlo	
	integration method	45
3.2	Schematic representation of the Metropolis algorithm procedure [5]	50
3.3	Diagrammatic Monte Carlo algorithm procedure [6]	53
4.1	Diagram length update	57
4.2	Diagram add/remove internal phonon update	59
4.3	Diagram add/remove external phonon update	60
4.4	Diagram swap update	62

LIST OF TABLES v

List of Tables

1	Input values used for the simulations from [7] and [4], the coupling strengths	
	are given as averages over the solid angle 4π	68
2	Obtained polaron ground state energy with DMC (0 is the reference for the	
	conduction band minimum), the values for Froehlich and Feynman were re-	
	trieved from [4]	69
3	Obtained polaron effective masses using DMC, the values for Froehlich and	
	Feynman were retrieved from [4]	70

Introduction

In Condensed Matter Physics, polarons are coherent states that are formed when an electron (or a hole) couples to a phonon bath in an ionic material (tipically the optical phonons): this usually happens at the bottom of the conduction band for the electron polaron and at the top of the valence band for hole polarons and leads to a renormalization of the electron ground state energy and effective mass.

This coupling is not easily described using standard ab-initio methods such as DFT (Density Functional Theory), which decouples the ionic degrees of freedom from the electronic ones, and some approximations are necessary in order to provide a description of the polaron. Nevertheless, the formalism provided by Quantum Many Body theory is necessary in order to analytically describe the physics of polarons.

Two different models for the polaron exist: the Froehlich polaron [8], which assumes that the characteristic size d of the electron with its phonon cloud, which together form the polaron, is much greater than the lattice spacing a of the material, and the Holstein polaron [9][10] which is suitable to describe polarons where the actual crystalline arrangement of the material cannot be neglected (and thus d is of the order of the lattice parameter).

In this thesis we will be focusing on the first case, and we will provide a way to compute relevant quantities about Froehlich polarons in a range of real materials using the Diagrammatic Monte Carlo method. For this scope, a model which includes anisotropies in the electron band and multiple phonon modes will be provided.

Here the organization of the thesis is briefly explained:

- In Chapter 1 the standard Froehlich model is presented and it is explained how its Hamiltonian is derived together with the main techniques to solve it. It is then explained how this relatively simple model can be generalized to have multiple anisotropic electronic bands and multiple optical phonon modes without altering the basic features of the model from which it was derived.
- In Chapter 2 the main Many-Body techniques employed to make the Froehlich model treatable using the Diagrammatic Monte Carlo method are explained: this includes using Green's functions as solutions for the Froehlich Hamiltonian together with the Matsubara imaginary time formalism and Wick's theorem to perturbatively expand the interacting Green's function in an integral series of non-interacting terms. In this way it becomes possible to use Feynman diagrams to solve the model, with the added bonus of obtaining a Green's function that is real and non-negative (thanks to the imaginary time formalism).
- In Chapter 3 the Monte Carlo method is explained, from Monte Carlo integration to Markov chain Monte Carlo, a technique which can be used to obtain random samples distributed as a target distribution, even if it unnormalized, using the Metropolis-

Hastings algorithm. Markov chain Monte Carlo is at the basis of the Diagrammatic Monte Carlo method, which also needs to implement ways to add or remove internal variables (since we are describing a system which can be described as an expansion of terms each with a different weight).

- In Chapter 4 the implementation of the algorithm is discussed: the basic features of the DMC simulation, the way free electron propagators and free phonon propagators were modelled in the computer, the updates that were implemented in order to obtain an ergodic simulation, and the main estimators that were used in order to obtain the results, among these the most important are the exact ground state energy estimator and the exact effective mass estimator.
- In Chapter 5 the results obtained together with the input parameters employed are compared to the same quantities computed with different methods (namely the perturbative method for the generalized cubic Froehlich model and the Feynman variational approach).

1 FROEHLICH POLARON 3

1 Froehlich Polaron

1.1 Electrons in crystals

The study of electrons inside a solid crystal is an important field due to their role in the determination of transport and optical properties of such materials [11].

Multiple experiments involving X-ray or electron scattering from suitable solid samples have demonstrated that a crystalline solid, whether a metal, an insulator or a semiconductor, is described by a periodic arrangement of atoms consisting of a unit cell (usually the primitive one, defined as the smallest unit cell possible in a determined material) with a suitable atomic basis: some examples are Iron (Fe), described by a BCC (Body-Centered Cubic) unit cell with a single Fe atom basis, rock salt (NaCl), described by by a FCC (Face-Centered Cubic) unit cell with a basis composed of one Na atom and one Cl atom, and crystalline silicon (Si), which is characterized by the diamond structure, an FCC structure with a basis composed of 2 silicon atoms (geometrically different from that seen in rock salt).

Given the periodic nature of crystal structures, it is natural to consider the electrostatic potential generated by the crystal to be periodic too. Such is the basic assumption which underlies the treatment of electrons in crystals, which was first described by Felix Bloch in his famous 1928 paper *Uber die Quantenmechanik der Elektronen in Kristallgittern* [12].

The model proposed by Bloch assumed independent electrons (no electron-electron interactions terms): each electron behaves as if only an average contribution to the potential from the other electrons (with the same periodicity of the lattice) exists, thus retrieving an **effective one-electron potential**.

The resulting Hamiltonian for the single independent electron is:

$$H\psi(\mathbf{r}) = \left(-\frac{\hbar^2}{2m}\nabla^2 + U(\mathbf{r})\right)\psi(\mathbf{r}) = E\psi(\mathbf{r}),\tag{1.1}$$

where $U(\mathbf{r})$ is a periodic potential with the lattice periodicity, given a lattice translation vector

$$T = n_1 \mathbf{a}_1 + n_2 \mathbf{a}_2 + n_3 \mathbf{a}_3, \qquad n_1, n_2, n_3 \text{ integers,}$$
 (1.2)

with a_1 , a_2 and a_3 primitive translation vectors. Therefore, we have

$$U(\mathbf{r} + \mathbf{T}) = U(\mathbf{r}),\tag{1.3}$$

this means that the potential can be expanded in Fourier series

$$U(\mathbf{K}) = \sum_{\mathbf{K}} U_{\mathbf{K}} e^{i\mathbf{K} \cdot \mathbf{r}}, \tag{1.4}$$

and is consequently useful to expand the wavefunction in the same way. For this reason the Born-von Karman boundary conditions are applied [13]

$$\psi(\mathbf{r} + N_i \mathbf{a}_i) = \psi(\mathbf{r}), \qquad i = 1, 2, 3.$$
(1.5)

where $N_i \mathbf{a}_i$ is a chosen vector such that $U(\mathbf{r} + N_i \mathbf{a}_i) = U(\mathbf{r})$ (it is a translation vector for the lattice). This is a normalizing condition for the wavefunction which corresponds to taking N_i unit cells in each direction and periodically repeating them. In this way it is possible to write the wavefunction in the following way:

$$\psi(\mathbf{r}) = \sum_{\mathbf{q}} c_{\mathbf{q}} e^{i\mathbf{q} \cdot \mathbf{r}}.$$
 (1.6)

Going back to the periodic potential $U(\mathbf{r})$ we observe that the Fourier terms $U_{\mathbf{K}}$ are related to $U(\mathbf{r})$ by

$$U_{\mathbf{K}} = \frac{1}{V} \int_{cell} dr e^{-i\mathbf{K} \cdot \mathbf{r}} U(\mathbf{r})$$
(1.7)

with V unit cell volume and ${\bf K}$ reciprocal lattice vector (vector in k-space such that $e^{i{\bf K}\cdot{\bf a}_i}=1$). If it is assumed that the potential $U({\bf r})$ is real and $U(-{\bf r})=U({\bf r})$ (valid for every Bravais lattice) it follows that the coefficients $U_{\bf K}$ are real.

Substituting in 1.1 we obtain:

$$(\mathbf{H} - E)\psi(\mathbf{r}) = \sum_{\mathbf{q}} \left(\frac{\hbar^2}{2m} q^2 - E \right) c_{\mathbf{q}} e^{i\mathbf{q} \cdot \mathbf{r}} + \sum_{\mathbf{K}\mathbf{q}'} U_{\mathbf{K}} c_{\mathbf{q}' - \mathbf{K}} e^{i\mathbf{q}' \cdot \mathbf{r}} = 0,$$
(1.8)

which yields the following result:

$$\left(\frac{\hbar^2}{2m}(\mathbf{k} - \mathbf{K})^2 - E\right)c_{\mathbf{k} - \mathbf{K}} + \sum_{\mathbf{K}'} c_{\mathbf{K}' - \mathbf{K}}c_{\mathbf{k} - \mathbf{K}'} = 0.$$
(1.9)

From this equation it becomes clear that for a fixed k only the coefficients $c_{\mathbf{k}}, c_{\mathbf{k}-\mathbf{K}}, \dots$ whose wavevector differs from \mathbf{k} by a reciprocal lattice vector are coupled. In this way the original problem has been divided in N independent equations for each allowed value of \mathbf{k} (in the first Brillouin zone, the primitive unit cell in the reciprocal space).

Going back to the expansion 1.6 the wavefunction now becomes:

$$\psi_k(\mathbf{r}) = \sum_{\mathbf{K}} c_{\mathbf{k} - \mathbf{K}} e^{i(\mathbf{k} - \mathbf{K}) \cdot r}, \tag{1.10}$$

which can be recast as

$$\psi_k(r) = e^{i\mathbf{k}\cdot\mathbf{r}} \sum_{\mathbf{k}} c_{\mathbf{k}-\mathbf{K}} e^{-i\mathbf{K}\cdot\mathbf{R}}; \tag{1.11}$$

in this form it is easy to recognize that

$$u_{\mathbf{k}}(\mathbf{r}) = \sum_{\mathbf{K}} c_{\mathbf{k} - \mathbf{K}} e^{-i\mathbf{K} \cdot \mathbf{R}}$$
 (1.12)

has the periodicity of the (reciprocal) Bravais lattice.

The shape of the Bloch wavefunction as stated in the Bloch theorem is thus retrieved

$$\psi_{\mathbf{k}}(\mathbf{r}) = e^{i\mathbf{k}\cdot\mathbf{r}} u_{\mathbf{k}}(\mathbf{r}) \tag{1.13}$$

and its square modulus (from which important properties such as charge distribution follow) $|\psi_{\mathbf{k}}(\mathbf{r})|^2$ has the periodicity of the lattice.

The new Hamiltonian eigenvalues equation using Bloch wavefunction reads

$$\mathbf{H}_{\mathbf{k}} u_{n\mathbf{k}} = \left(\frac{\hbar^2}{2m} \left(\frac{1}{i} \nabla + \mathbf{k}\right)^2 + U(\mathbf{r})\right) u_{n\mathbf{k}}(\mathbf{r}) = E_{n\mathbf{k}} u_{n\mathbf{k}}(\mathbf{r}), \tag{1.14}$$

which yields a different energy eigenvalue for each ${\bf k}$ in the first Brillouin zone. The index n arises from the fact that for each ${\bf k}$ value infinite discrete solutions to the eigenvalue equation exist, in the same way as in the particle in a box problem. Going to the thermodynamic limit $(N_i \to \infty \text{ for each component } i)$ the entire first Brillouin zone is sampled and the typical band structure of the solids is recovered.

All the methods employed in solid state calculations rely on this "simple" equation to determine band structures, granted an analytical form for the periodic potential $U(\mathbf{r})$ can be retrieved.

The most used and effective computation method is **Density Functional Theory** [14] or **DFT** for short, which does not directly compute the eigenvalue equation for each single k and n value, which would be impossible since the potential $U(\mathbf{r})$ is a many-body object that includes electron-electon interactions, but rather computes all the physical quantities of interest starting from the ground state charge density $\rho_0(\mathbf{r})$. This is made possible by the two Hohenberg-Kohn theorems [15], which respectively state that the external potential (the periodic $U(\mathbf{r})$ from the electron point of view) is uniquely determined up to a constant by the ground state charge density $\rho_0(\mathbf{r})$ and that this density can be computed variationally by minimizing a suitable functional $F[\rho]$.

Nevertheless, the functional $F[\rho]$ exact form is unknown: for this reason the **Kohn-Sham scheme** [16] is used. The idea at the basis of this practical setup is to substitute the real interacting system (many-body) with an auxiliary non-interacting one (single particle) which has the same ground state as the original. In this system the total potential $U(\mathbf{r}) = U_{ion}(\mathbf{r}) + U_{ee}(\mathbf{r})$ is replaced with an effective potential $U_{eff}(\mathbf{r})$ defined as

$$U_{eff}(\mathbf{r}) = U_{ion}(\mathbf{r}) + U_H(\mathbf{r}) + U_{xc}(\mathbf{r}), \tag{1.15}$$

where U_{ion} is the ionic potential, often modelled using pseudopotentials [17], $U_H(\mathbf{r})$ is the Hartree term, the electrostatic potential due to the mean field distribution of all the other electrons, and $U_{xc}(\mathbf{r})$ the exchange-correlation term, an approximate potential which includes Pauli exclusion principle (exchange), higher order electron-electron interactions (correlation) and many body corrections to kinetic energy. The exchange-correlation term is usually computed using **LDA** (Local Density Approximation) or **GGA** (Generalized Gradient Approximation),

both based on the the Uniform Electron Gas (UEG) [18]. Despite the inevitable approximations, DFT calculations are able to provide extremely accurate band structure calculations with few drawbacks, such as inaccurate gap estimations in insulators and semiconductors.

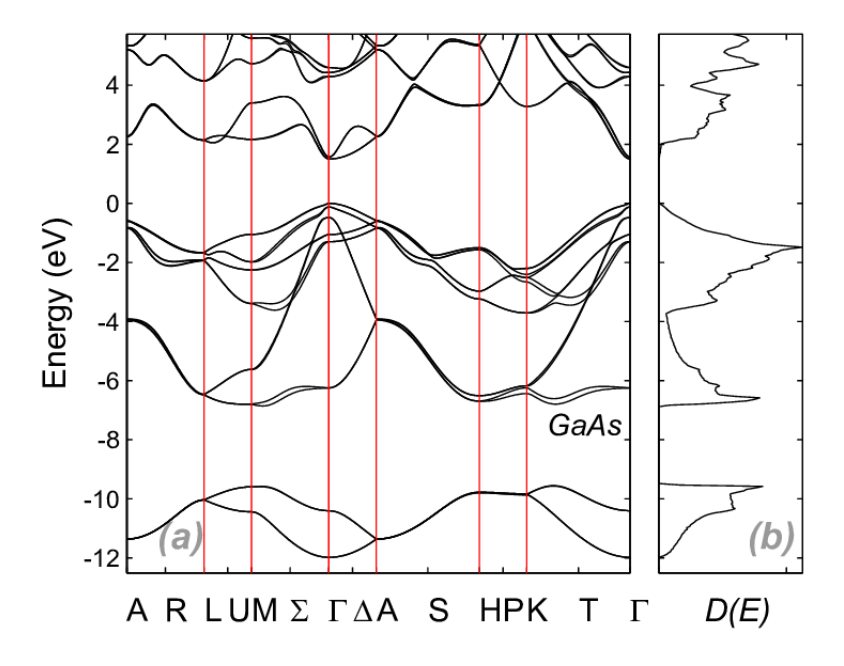


Figure 1.1: DFT calculated low-temperature GaAs Wurtzite structure with relative DOS [1].

As it can be seen in Figure 1.1 for GaAs, at the band extrema (at the edge between the allowed band states and the forbidden gap) the bands have a quadratic dispersion akin to that of a free electron: an electron in these regions feels only a very weak external potential $U(\mathbf{r})$ and can be considered free provided that the free electron mass m is substituted with an effective mass m^* which takes into account the potential acting on it.

In a general case the effective mass is a tensorial quantity (bands are anisotropic in general with respect to the wavevector) and their value can be computed with

$$m_{ij}^{*-1} = \frac{1}{\hbar^2} \frac{\partial^2 E}{\partial k_i \partial k_j},\tag{1.16}$$

provided that the quadratic approximation is valid. This approximation is really useful when calculating quantities near band extrema, providing an effective description of an otherwise complex interaction.

1.2 The polaron problem: the Froehlich model

The treatment described up until now for electrons in solids relies on a basic assumption: electron dynamics is much faster than ion dynamics. This is the so-called **Born-Oppenheimer**

approximation, which assumes that the motion of the much heavier ions is slow compared to the fast dynamics of the electrons (the characteristic time are of the order of ps for ions and fs for electrons). As a result, electrons are considered to respond instantaneously to changes in the positions of the ions, allowing the separation of electronic and ionic degrees of freedom in the analysis. Given M ions and n electrons the wavefunction $\Psi(\mathbf{R}_1,...,\mathbf{R}_M,\mathbf{r}_1,...,\mathbf{r}_n)$ with \mathbf{R}_α ionic positions and \mathbf{r}_i electron positions can be decomposed in the following way:

$$\Psi(\mathbf{R}_1, ..., \mathbf{R}_M, \mathbf{r}_1, ..., \mathbf{r}_n) = \chi(\mathbf{R}_1, ..., \mathbf{R}_M) \psi(\mathbf{r}_1, ..., \mathbf{r}_n), \tag{1.17}$$

and only the electronic wavefunction $\psi(\mathbf{r}_1,...,\mathbf{r}_n)$ is taken into consideration, decoupling ionic degrees of freedom and treating ionic potential as a constant energy surface $U_{ion}(\mathbf{r})$.

This approximation, although extremely effective in computing electronic bands, fails by design to describe systems where there is a strong coupling between electrons and ions (for example electron-phonon interaction).

Such is the case of charge doped polar crystals: in these materials single electrons at the bottom of the conduction band (or holes at the top of the valence band) couple to the strongly polarized ions and distort the unit cell: an electron-phonon interaction is thus present in the lattice and the electron properties (such as energy and effective mass) are renormalized due to this coupling [8].

The basic assumption of the Froehlich model is that the polaron is "large", namely the characteristic size of the polaron (electron together with its phonon cloud) is much larger than the lattice constant a. In this way it is possible to ignore the atomic details of the actual material and treat it as a uniform dielectric medium.

It is assumed that the electron which takes part in the formation of the polaron lies at the bottom of the valence band, in this way it is expected to have a quadratic energy dispersion characterized (as already seen in 1.16) by an effective mass

$$\epsilon(k) = \frac{\hbar^2 k^2}{2m^*},\tag{1.18}$$

where the effective mass m^* encapsulates all the interactions due to crystal structure (for a hole polaron the dispersion is similar considering a negative effective mass).

Given the fact that we are dealing with the large polaron model, it is possible to treat the material as an homogeneous continuum which is polarized by the excess charge (the conduction electron). We also assume that the material is isotropic. Let $\mathbf{P}(\mathbf{r})$ be the electric polarization at the point \mathbf{r} , the total electric field is then:

$$\mathbf{D}(\mathbf{r}) = \mathbf{E}(\mathbf{r}) + 4\pi \mathbf{P}(\mathbf{r}),$$

$$\mathbf{D}(\mathbf{r}) = \epsilon_0 \mathbf{E}(\mathbf{r}),$$
(1.19)

considering the electric permittivity in vacuum equal to 1.

The only free charge present in the material is the conduction electron in excess, this means

8

that $\mathbf{D}(\mathbf{r})$ is completely determined by it:

$$D(\mathbf{r}, \mathbf{r}_{el}) = -\nabla \frac{e}{|\mathbf{r} - \mathbf{r}_{el}|},$$

$$\nabla \cdot \mathbf{D}(\mathbf{r}, \mathbf{r}_{el}) = 4\pi \delta(\mathbf{r} - \mathbf{r}_{el}),$$
(1.20)

with \mathbf{r}_{el} the coordinate of the conduction electron. Developing the equations the following relation is obtained:

$$4\pi \mathbf{P}(\mathbf{r}) = \left(1 - \frac{1}{\epsilon_0}\right) \mathbf{D}(\mathbf{r}). \tag{1.21}$$

 $\mathbf{P}(\mathbf{r})$ is the total polarization, which has contributions both from electrons and ionic displacements, since only the second contribution is relevant in our treatment, a method to tell apart this two contributions is needed.

To obtain this we imagine a system where a field is slowly applied and then rapidly switched off [19]: only electrons are able to keep up with the variation of the field. A formula connecting polarization and $\mathbf D$ (dropping the $\mathbf r$ dependence for simplicity since an isotropic and homogeneous medium is assumed) is then retrieved as

$$4\pi\delta\mathbf{P} = -\left(1 - \frac{1}{\epsilon_{\infty}}\right)\mathbf{D},\tag{1.22}$$

it is then obtained the lattice contribution to the polarization:

$$4\pi \mathbf{P}_{lat} = 4\pi (\mathbf{P} - \delta \mathbf{P}) = \left(\frac{1}{\epsilon_{\infty}} - \frac{1}{\epsilon_{0}}\right) \mathbf{D}.$$
 (1.23)

We now consider a model for the polar crystal lattice: we assume it to be constituted of individual oscillating discrete dipoles located at fixed sites of the crystal with characteristic frequency ω . The energy of each one of these oscillators is

$$\frac{M}{2}(\dot{q}^2 + \omega^2 q^2).$$
 (1.24)

The next step is to move from a discrete set of fixed oscillators to a continuum of dipoles: it is assumed that the dipoles are not coupled. Defining the effective charge as e^* , the following substitution is made:

$$e^*\mathbf{q}_n \to \mathbf{P}_{lat}(\mathbf{r}),$$
 (1.25)

which relates the dipole moment to the polarization field. We also write the following relation:

$$\frac{M}{e^{*2}} = \gamma d^3 r,\tag{1.26}$$

where $M = nd^3r$ is the mass density of the medium.

It is now possible to define the kinetic and potential energy of the freely oscillating polarization

field:

$$T = \int \frac{\gamma}{2} \dot{\mathbf{P}}_{lat}^{2}(\mathbf{r}) d^{3}r,$$

$$V = \int \frac{\gamma \omega^{2}}{2} \mathbf{P}_{lat}^{2}(\mathbf{r}) d^{3}r.$$
(1.27)

We identify ω with the optical phonon frequency ω_{LO} , but the constant γ has not yet been given a physical definition. For this reason we consider the interaction between electrons and dipole moment, given by

$$e\frac{\mathbf{r} - \mathbf{r}'}{|\mathbf{r} - \mathbf{r}'|^3}\mathbf{P}_{lat},\tag{1.28}$$

which, using a continuous charge distribution and the polarization field, becomes

$$\rho(\mathbf{r})d^3r \frac{\mathbf{r} - \mathbf{r}'}{|\mathbf{r} - \mathbf{r}'|^3} \mathbf{P}_{lat}(\mathbf{r}')d^3r'. \tag{1.29}$$

The interaction energy E_I is thus

$$E_I = \iint \rho(\mathbf{r}) \frac{\mathbf{r} - \mathbf{r}'}{|\mathbf{r} - \mathbf{r}'|^3} \mathbf{P}_{lat}(\mathbf{r}') d^3 r d^3 r'. \tag{1.30}$$

The Lagrangian is then built as follows:

$$L = T - U - E_I \tag{1.31}$$

and the equation of motion are found solving the Lagrange equations

$$\frac{d}{dt}\frac{\delta L}{\delta \dot{P}_{lat_i}} - \frac{\delta L}{\delta P_{lat_i}} = 0 \tag{1.32}$$

for i = 1, 2, 3. The explicit formula of the equation of motion is:

$$\gamma(\ddot{\mathbf{P}}_{lat}(\mathbf{r}') + \omega^2 \mathbf{P}_{lat}(\mathbf{r}')) = -\int \frac{\mathbf{r} - \mathbf{r}'}{|\mathbf{r} - \mathbf{r}'|^3} \rho(\mathbf{r}) d^3r$$
(1.33)

keeping fixed $\rho(\mathbf{r})$. The term on the right side is simply the dielectric displacement $\mathbf{D}(\mathbf{r}')$ and, in the static limit, the equation simplifies to

$$\gamma \omega^2 \mathbf{P}_{lat}(\mathbf{r}') = \mathbf{D}(\mathbf{r}'). \tag{1.34}$$

Comparing this equation with 1.23, the value of γ is obtained:

$$\gamma = \frac{4\pi}{\omega^2} \left(\frac{1}{\epsilon_{\infty}} - \frac{1}{\epsilon_0} \right)^{-1}. \tag{1.35}$$

It is now time to define the complete polaron Hamiltonian. We start by defining the free electron term (the interaction lies inside the effective mass m^*), considering that the electron charge density operator is defined as:

$$\rho(\mathbf{r}) = -e\psi^{\dagger}(\mathbf{r})\psi(\mathbf{r}) \tag{1.36}$$

using the second quantization formalism with field operators, then the electron kinetic term is

$$H_{el} = \int \psi^{\dagger}(\mathbf{r}) \left(-\frac{\hbar^2}{2m^*} \nabla^2 \right) \psi(\mathbf{r}) d^3 r. \tag{1.37}$$

If we use a suitable basis for the field operator

$$\psi(\mathbf{r}) = \frac{1}{\sqrt{V}} \sum_{\mathbf{k}} c_{\mathbf{k}} e^{i\mathbf{k} \cdot \mathbf{r}}$$
(1.38)

with V (unit cell) volume, then 1.37 becomes

$$H_{el} = \sum_{\mathbf{k}} \frac{k^2}{2m^*} c_{\mathbf{k}}^{\dagger} c_{\mathbf{k}}, \tag{1.39}$$

with $c_{\bf k}^{\dagger}$ and $c_{\bf k}$ creation and annihilation operators for the free electron.

We now turn our attention to the polarization field, taking into account that it can be modelled as a harmonic oscillator with a form similar to 1.37 can be recovered (P_{lat} is substituted by P in the following equations):

$$H_{ph} = \int \left(\frac{1}{2\gamma} \mathbf{\Pi}^2(\mathbf{r}) + \frac{\gamma}{2} \omega^2 \mathbf{P}^2(\mathbf{r})\right) d^3r, \tag{1.40}$$

where $\Pi(\mathbf{r})$ is the conjugate momentum to $\mathbf{P}(\mathbf{r})$.

Using the canonical substitution for the operator P(r)

$$\mathbf{P}(\mathbf{r}) = \frac{1}{\sqrt{V}} \sum_{\mathbf{q}} \sqrt{\frac{\hbar}{2\gamma\omega}} \frac{\mathbf{q}}{q} e^{i\mathbf{q}\cdot\mathbf{r}} (a_{\mathbf{q}} - a_{-\mathbf{q}}^{\dagger})$$
(1.41)

and the corresponding one for $\Pi(\mathbf{r})$ we obtain the equation for a quantum harmonic oscillator:

$$H_{ph} = \hbar\omega \sum_{\mathbf{q}} a_{\mathbf{q}}^{\dagger} a_{\mathbf{q}}, \tag{1.42}$$

with $a_{\mathbf{q}}^{\dagger}$ and $a_{\mathbf{q}}$ bosonic phononic creation and annihilation operators.

With the same formalism, the interaction term is instead written in the following way:

$$H_{EPC} = \iint \psi^{\dagger}(\mathbf{r})\psi(\mathbf{r}) \frac{e}{|\mathbf{r} - \mathbf{r}'|} (-\nabla_{\mathbf{r}'} \cdot \mathbf{P})(\mathbf{r}') d^3r d^3r', \qquad (1.43)$$

using the same substitution in 1.41 for P(r) the following form is obtained:

$$H_{EPC} = \int \psi^{\dagger}(\mathbf{r})\psi(\mathbf{r}) \left[4\pi i \left(\frac{e^2 \hbar}{2\gamma \omega V} \right)^{1/2} \sum_{\mathbf{q}} \frac{1}{q} (a_{\mathbf{q}}^{\dagger} e^{-i\mathbf{q}\cdot\mathbf{r}} - a_{\mathbf{q}} e^{i\mathbf{q}\cdot\mathbf{r}}) d^3 r \right]. \tag{1.44}$$

The term is simplified even more if we substitute the electron field operator using 1.41, then the final form of the coupling term is reached

$$H_{EPC} = \sum_{\mathbf{k},\mathbf{q}} (V_{\mathbf{q}} c_{\mathbf{k}+\mathbf{q}}^{\dagger} c_{\mathbf{k}} a_{\mathbf{q}} + V_{\mathbf{q}}^{*} c_{\mathbf{k}-\mathbf{q}}^{\dagger} c_{\mathbf{k}} a_{-\mathbf{q}}^{\dagger}), \tag{1.45}$$

where the coupling parameter is given as

$$V_{\mathbf{q}} = 4\pi i \left(\frac{e^2}{2\hbar\gamma\omega V}\right)^{1/2} \frac{1}{q}.$$
(1.46)

It is possible to rewrite the coupling parameter in terms of the dimensionless coupling strength α :

$$\alpha = \frac{2\pi e^2}{\hbar \gamma \omega} \sqrt{\frac{2m^* \omega}{\hbar}} = \frac{1}{2} \left(\frac{1}{\epsilon_{\infty}} - \frac{1}{\epsilon_0} \right) \frac{e^2}{\hbar \omega} \sqrt{\frac{2m^* \omega}{\hbar}},\tag{1.47}$$

with ϵ_0 static dielectric constant and ϵ_∞ the optical dielectric one. The coupling parameter (or interaction strength) is found as

$$V_{\mathbf{q}} = i \left(\frac{2\sqrt{2}\pi\alpha}{V}\right)^{1/2} \frac{1}{q}.$$
 (1.48)

If we now identify ω with ω_{LO} angular frequency of the longitudinal optical phonon modes (the modes that effectively couple with the electron), we obtain the final form of the Froehlich Hamiltonian:

$$H^{Fr} = \sum_{\mathbf{k}} \frac{k^2}{2m^*} c_{\mathbf{k}}^{\dagger} c_{\mathbf{k}} + \hbar \omega_{LO} \sum_{\mathbf{q}} a_{\mathbf{q}}^{\dagger} a_{\mathbf{q}} + \sum_{\mathbf{k}, \mathbf{q}} (V_q c_{\mathbf{k} + \mathbf{q}}^{\dagger} c_{\mathbf{k}} a_{\mathbf{q}} + V_q^* c_{\mathbf{k} - \mathbf{q}} c_{\mathbf{k}} a_{-\mathbf{q}}^{\dagger})$$
(1.49)

where we have dropped the coupling parameter dependence on ${f q}$ direction since it only depends on its modulus.

The main assumptions of this model are:

- Free electron with quadratic dispersion (up to a scalar effective mass m^*).
- Dispersionless optical mode with frequency ω_{LO} .
- "Large" polaron, with characteristic dimension *d* much greater than lattice parameter *a* (continuum approximation).

In this form the model correctly describes only a handful of real materials and it mainly serves as a toy model (we will breafly mention how it can be solved at weak coupling with perturbation theory and at strong coupling variationally), however we will focus on the **Diagrammatic Monte Carlo Method**, a computational method that is capable of solving the polaron problem using some tricks. We will also see how some of the main limitations of the model (namely the scalar effective mass m^* and the single phonon mode ω_{LO}) can be lifted without losing the main assumption (the large polaron approximation). It will be illustrated in particular the case of an anisotropic band with effective mass $m^*(\hat{\mathbf{k}})$ and multiple dispersionless optical modes ω_{LO_j} , already capable of modelling conduction band minima in a wide range of materials.

1.3 Weak coupling limit: perturbation theory

In the weak coupling regime it is possible to apply perturbation theory to the Froehlich Hamiltonian, for this treatment a slightly modified Hamiltonian with respect to the one seen in 1.49 will be used [20]:

$$H^{Fr} = -\frac{\nabla^2}{2m^*} + \omega_{LO} \sum_{\mathbf{q}} (a_{\mathbf{q}}^{\dagger} a_{\mathbf{q}}) + \sum_{\mathbf{q}} (V_{\mathbf{q}} a_{\mathbf{q}} e^{i\mathbf{q}\cdot\mathbf{r}} + V_{\mathbf{q}}^* a_{\mathbf{q}}^{\dagger} e^{-i\mathbf{q}\cdot\mathbf{r}}). \tag{1.50}$$

We will respectively define the non-interacting Hamiltonian ${\cal H}_0^{Fr}$ and the interaction term ${\cal H}_I^{Fr}$ as

$$H_0^{Fr} = -\frac{\nabla^2}{2m^*} + \omega_{LO} \sum_{\mathbf{q}} (a_{\mathbf{q}}^{\dagger} a_{\mathbf{q}}),$$

$$H_I^{Fr} = \sum_{\mathbf{q}} (V_{\mathbf{q}} a_{\mathbf{q}} e^{i\mathbf{q} \cdot \mathbf{r}} + V_{\mathbf{q}}^* a_{\mathbf{q}}^{\dagger} e^{-i\mathbf{q} \cdot \mathbf{r}}).$$
(1.51)

The quantum state of the non-interacting electron is described by $|\mathbf{k}\rangle = \frac{1}{\sqrt{V}}e^{i\mathbf{k}\cdot\mathbf{r}}$, while for the non interacting phonons it is possible to define the average number of excitations $\langle a_{\mathbf{q}}^{\dagger}a_{\mathbf{q}}\rangle = \langle n_{\mathbf{q}}\rangle$, which is equal to 0 at the ground state.

The total wavefunction of the non-interacting system then becomes:

$$|\mathbf{k},0\rangle = e^{i\mathbf{k}\cdot\mathbf{r}}|0\rangle.$$
 (1.52)

The first excited state to which the ground non-interacting state can jump to is the one with electron wavevector $\mathbf{k} - \mathbf{q}$ and one phonon $n_{\mathbf{q}} = 1$, total energy is:

$$\frac{(\mathbf{k} + \mathbf{q})^2}{2m^*} + \omega_{LO} = \frac{k^2}{2m^*},\tag{1.53}$$

while the corresponding wavefunction is

$$|\mathbf{k} - \mathbf{q}, 1\rangle = e^{i(\mathbf{k} - \mathbf{q}) \cdot \mathbf{r}} |1\rangle.$$
 (1.54)

At first order perturbation theory there is no correction to the energy, we then need to go to second order. We consider the matrix element

$$\langle \mathbf{k} - \mathbf{q}, 1 | H_I^{Fr} | \mathbf{k}, 0 \rangle = V_{\mathbf{q}}^*, \tag{1.55}$$

at second order perturbation theory energy then becomes:

$$E_{\mathbf{k}P} = \frac{k^2}{2m^*} - \sum_{\mathbf{q}} \frac{|V_{\mathbf{q}}|^2}{(\mathbf{k} - \mathbf{q})^2 / 2m^* + \omega_{LO} - k^2 / 2m^*},$$
(1.56)

evaluating the sum over the q wavevectors we arrive at

$$E_{\mathbf{k}P} = \frac{k^2}{2m^*} - \frac{\alpha\omega_{LO}\sqrt{2m^*\omega_{LO}}}{k} \arcsin\frac{k}{\sqrt{2m^*\omega_{LO}}},\tag{1.57}$$

with α adimensional parameter defined as (using atomic units) [21]

$$\alpha = \left(\frac{1}{\epsilon_{\infty}} - \frac{1}{\epsilon_0}\right) \left(\frac{m^*}{2\omega_{LO}}\right)^{1/2} \tag{1.58}$$

where ϵ_{∞} is the optical dielectric constant (purely electronic) and ϵ_0 the static dielectric constant (independent from ω and q).

1.57 for $k \ll \sqrt{2m^*\omega_{LO}}$ yields

$$E_{\mathbf{k}P} = \frac{k^2}{2m^*} - \alpha\omega_{LO}.\tag{1.59}$$

The polaron effective mass m_P^* is instead given by:

$$m_P^* = \frac{m^*}{\left(1 - \frac{\alpha}{6}\right)}. (1.60)$$

From the equation it clearly results that the polaron effective mass diverges for $\alpha \to 6^-$ and is negative for $\alpha > 6$. This signals that perturbation theory does not correctly describe the physical system at strong couplings.

1.4 Strong coupling limit: variational treatment

For the strong coupling case a different approach is taken: the main assumption of this model is a localized polaron wavefunction with a gaussian form [22], the Froehlich Hamiltonian is recast in order to write the phonon operators as displacement and conjugate momentum operators:

$$Q_{\mathbf{q}} = \frac{1}{\sqrt{2}} \left(a_{\mathbf{q}} + a_{-\mathbf{q}}^{\dagger} \right), \qquad P_{\mathbf{q}} = -\frac{i}{\sqrt{2}} \left(a_{\mathbf{q}} - a_{-\mathbf{q}}^{\dagger} \right), \tag{1.61}$$

so that the Hamiltonian in 1.50 can be rewritten as

$$H^{Fr} = \frac{p^2}{2m^*} + \frac{\omega_{LO}}{2} \sum_{\mathbf{q}} \left(P_{\mathbf{q}}^2 + Q_{\mathbf{q}}^2 \right) + \sum_{\mathbf{q}} V_{\mathbf{q}} Q_{\mathbf{q}} e^{i\mathbf{q} \cdot \mathbf{r}}.$$
 (1.62)

A wavefunction with dependence both on the electron position ${\bf r}$ and the lattice displacement $Q_{\bf q}$ is needed, for this reason the following gaussian ansatz is used:

$$\Phi(\mathbf{r}, Q_{\mathbf{q}}) = \phi(\mathbf{r})\Psi_n(Q_{\mathbf{q}} + \delta Q_{\mathbf{q}}),$$

$$\phi(r) = \left(\frac{\beta}{\sqrt{\pi}}\right)^{3/2} e^{-\frac{\beta^2}{2}r^2},$$
(1.63)

with β variational parameter, Ψ_n the harmonic oscillator wavefunction and $\delta Q_{\bf q}$ displacement to be calculated.

We now need to take the expectation value of the Hamiltonian operator:

$$H(Q_{\mathbf{q}}) = \langle \phi(r)|H|\phi^*(r)\rangle = \int \phi(r)H\phi(r)d^3r, \tag{1.64}$$

the terms with r dependence are respectively evaluated as:

$$\int \phi^*(\mathbf{r}) \frac{p^2}{2m^*} \phi(\mathbf{r}) d^3 r = \frac{3\beta^2}{4m^*},$$

$$\int \phi^*(\mathbf{r}) e^{i\mathbf{q} \cdot \mathbf{r}} \phi(\mathbf{r}) d^3 r = e^{-q^2/4\beta^2}.$$
(1.65)

The following result is thus obtained:

$$H(Q_{\mathbf{q}}) = \frac{3\beta^2}{4m^*} + \frac{\omega_{LO}}{2} \sum_{\mathbf{q}} (P_{\mathbf{q}}^2 + Q_{\mathbf{q}}^2) + \sum_{\mathbf{q}} L_{\mathbf{q}} Q_{\mathbf{q}}, \qquad L_{\mathbf{q}} = V_{\mathbf{q}} e^{-q^2/4\beta^2}.$$
(1.66)

To cancel out the linear term in $Q_{\bf q}$ it is important to choose the right equilibrium displacement $\delta Q_{\bf q}$ as

$$\delta Q_{\mathbf{q}} = \frac{L_{\mathbf{q}}}{\omega_{LO}},\tag{1.67}$$

which yields the Hamiltonian

$$H(Q_{\mathbf{q}}) = \frac{\omega_{LO}}{2} \sum_{\mathbf{q}} \left[P_{\mathbf{q}}^2 + (Q_{\mathbf{q}} + \delta Q_{\mathbf{q}})^2 \right] + \frac{3\beta}{4m^*} - \frac{1}{2\omega_{LO}} \sum_{\mathbf{q}} L_{\mathbf{q}}^2$$

$$= \frac{\omega_{LO}}{2} \sum_{\mathbf{q}} \left[P_{\mathbf{q}}^2 + (Q_{\mathbf{q}} + \delta Q_{\mathbf{q}})^2 \right] + E(\beta).$$
(1.68)

The three different terms have precise physical meanings: the first term describes the harmonic oscillation of phonons around their new equilibrium position ($Q_{\bf q} + \delta Q_{\bf q}$), the second

15

term represents the kinetic energy of the electron in the gaussian formalism, the third one the interaction energy between the electron and the phonons. To variationally retrieve the lowest energy the β parameter is minimized, we have:

$$\frac{1}{2\omega_{LO}} \sum_{\mathbf{q}} L_{\mathbf{q}}^2 = \alpha \left(\frac{\beta^2 \omega_{LO}}{m^* \pi}\right)^{1/2},$$

$$E(\beta) = \frac{3\beta^2}{4m^*} - \alpha \left(\frac{\beta^2 \omega_{LO}}{m^* \pi}\right)^{1/2}.$$
(1.69)

If we calculate the derivative with respect to β and we minimize it the following result is obtained:

$$\frac{dE}{d\beta} = \frac{3\beta}{2m^*} - \alpha \left(\frac{\omega_{LO}}{m^*\pi}\right)^{1/2} = 0, \tag{1.70}$$

which yields a value for β_0 :

$$\beta_0 = \frac{\alpha}{3} 2m^* \left(\frac{\omega_{LO}}{m^* \pi}\right)^{1/2}. \tag{1.71}$$

Using this result the minimum energy $E(\beta_0)$ is:

$$E(\beta_0) = -\frac{\alpha^2 \omega_{LO}}{3\pi} = -0.106 \alpha^2 \omega_{LO},$$
 (1.72)

with a quadratic dependence on the coupling strength α different from the one found using perturbation theory (linear).

A more refined treatment of the strong coupling limit [23] yields the following result:

$$\lim_{a \to \infty} E_0(\alpha) = -\omega_{LO} \left[-0.1085\alpha^2 + 2.836 + O(1/\alpha^2) \right], \tag{1.73}$$

not so different from our obtained result.

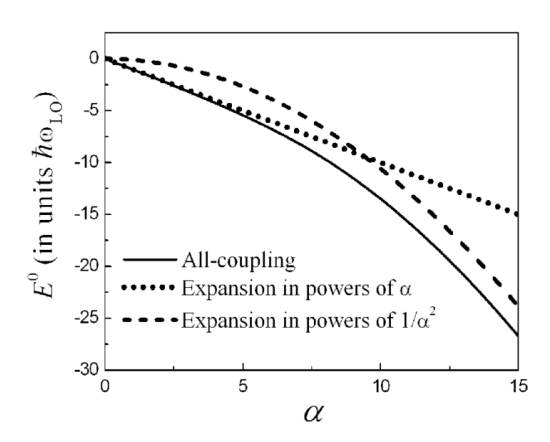


Figure 1.2: Computed polaron energy using perturbation theory, strong coupling theory and all coupling Feynman technique [2].

1.5 Froehlich Hamiltonian: degenerate bands and multiple phonon modes

The Hamiltonian in 1.49 only describes an extremely limited number of real cases, namely a non-degenerate isotropic electron band with effective mass m^* coupled to a single LO phonon mode. Although this relatively simple model is already quite challenging, some of its assumptions can be relaxed to obtain a more general framework.

Here we will be describing the **generalized Froehlich cubic model**: while mantaining some core simplification already seen in the original Froehlich model such as an isotropic dielectric tensor ϵ_0 and ϵ_∞ together with a phonon dispersion ω_{jLO} which does not depend on the wavevector direction (an even more general model not restrained to the cubic case is described in [7]) \hat{k} , it is still a quite relevant and useful model since it can be used to describe multiple materials such as various oxides (BaO, CaO, MgO), II-VI compounds (CdS, CdSe, ZnS, ZnTe) and III-V compounds (AlAs, GaAs, GaN, GaP) [4].

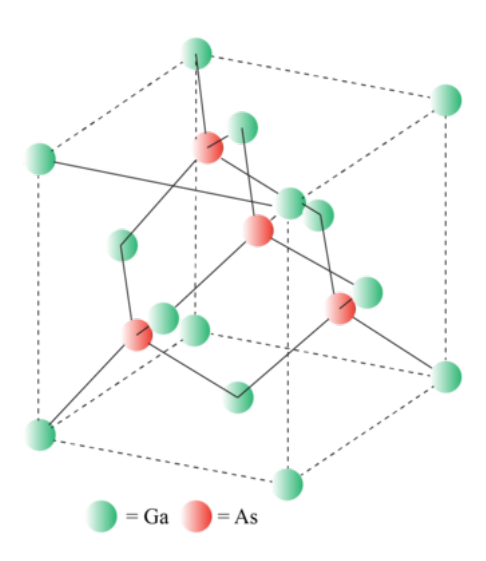


Figure 1.3: GaAs crystal structure, the cubic structure of the zincblende unit cell is here clearly displayed.

We start by defining the new electron term:

$$H_{el}^{cFr} \sum_{\mathbf{k}n} \frac{\sigma k^2}{2m_n^*(\hat{k})} c_{\mathbf{k}n}^{\dagger} c_{\mathbf{k}n}, \tag{1.74}$$

where the sum has been extended to n bands degenerate at the extremum, $\sigma=\pm 1$ depending on the fact that an electron or a hole polaron is taken into consideration. $m_n^*(\hat{k})$ is the new effective mass depending on band index n and wavevector direction \hat{k} (a tensorial quantity in

general).

We also want to extend our Hamiltonian to tackle the case of multiple LO phonon modes present in the material, to this aim we define the following phonon term:

$$H_{ph}^{cFr} = \sum_{\mathbf{q}j} \hbar \omega_{jLO} a_{\mathbf{q}j}^{\dagger} a_{\mathbf{q}j}, \tag{1.75}$$

where the index j represents the different LO modes.

The electron-phonon coupling term gets redefined as:

$$H_{EPC}^{cFr} = \sum_{\mathbf{k}nn',\mathbf{q}j} c_{\mathbf{k}+\mathbf{q}n'}^{\dagger} c_{\mathbf{k}n} \left[V^{cFr}(\mathbf{k}nn',\mathbf{q}j) a_{\mathbf{q}j} + V^{*cFr}(\mathbf{k}nn',\mathbf{q}j) a_{-\mathbf{q}j}^{\dagger} \right].$$
 (1.76)

It should be noted that the new electron-phonon coupling term includes interband transitions (from n to n'). The new coupling strength $V^{cFr}(\mathbf{k}nn',\mathbf{q}j)$ is found to be [4]

$$V^{cFr}(\mathbf{k}nn',\mathbf{q}j) = \frac{i}{q} \frac{4\pi}{\Omega_0} \left(\frac{1}{2\omega_{jLO} V_{BvK}} \right)^{1/2} \frac{p_{jLO}}{\epsilon_{\infty}} \times \sum_{m} s_{n'm}(\hat{k}') s_{nm}^*(\hat{k}), \tag{1.77}$$

with Ω_0 volume of the primitive unit cell, V_{BvK} volume of the Born-von Karman unit cell, p_{jLO} phonon mode polarities, linked to Born effective charges and static dielectric tensor ϵ_0 [24], computed as $p_{jLO}(\hat{q}) = \sum_{\nu} Z_{\nu}^* e_{\nu}(\hat{q})$ isotropic in cubic system, and the s tensors, symmetry dependent unitary matrices which represent specific bands (and have the same symmetry group).

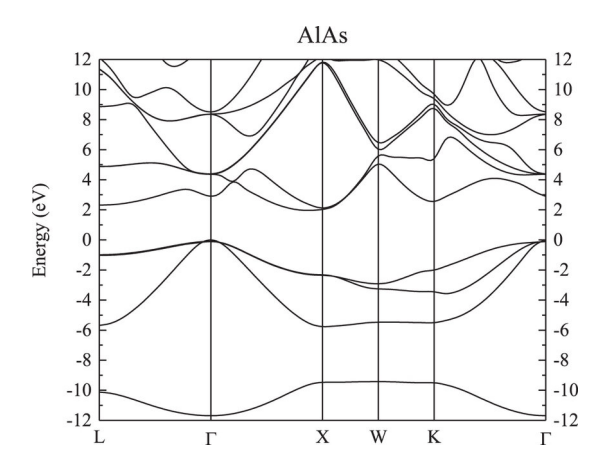


Figure 1.4: DFT calculated AlAs band structure [3], the conduction band minimum is on the high symmetry line Δ between Γ and X.

In our case of interest we restrict to just one anisotropic non-degenerate electron band, which is an accurate model for the conduction band minimum of the materials cited before (usually

located somewhere between Γ and X along the Δ line), in this case the interaction strength simplifies to:

$$V^{cFr}(qj) = \frac{i}{q} \frac{4\pi}{\Omega_0} \left(\frac{1}{2\omega_{jLO} V_{BvK}} \right)^{1/2} \frac{p_{jLO}}{\epsilon_{\infty}}, \tag{1.78}$$

and the full Hamiltonian reads:

$$H^{cFr} = \sum_{\mathbf{k}} \frac{\sigma k^2}{2m^*(\hat{k})} c_{\mathbf{k}}^{\dagger} c_{\mathbf{k}} + \sum_{\mathbf{q}j} \hbar \omega_{jLO} a_{\mathbf{q}j}^{\dagger} a_{\mathbf{q}j} + \sum_{\mathbf{k},\mathbf{q}j} c_{\mathbf{k}+\mathbf{q}}^{\dagger} c_{\mathbf{k}} \left[V^{cFr}(qj) a_{\mathbf{q}} + V^{*cFr}(qj) a_{\mathbf{q}}^{\dagger} \right]. \tag{1.79}$$

The effective mass $m^*(\hat{k})$ dependence on the wavevector \mathbf{q} direction is expressed in the following way:

$$\frac{1}{m^*(\hat{k})} = \frac{\hat{k}_x^2}{m_x^*} + \frac{\hat{k}_y^2}{m_y^*} + \frac{\hat{k}_z^2}{m_z^*},\tag{1.80}$$

with m_x^st , m_y^st and m_z^st effective mass values on the three cartesian axes.

Alternatively, the following formula for the electron energy as a function of k can be employed:

$$\epsilon(\mathbf{k}) = \frac{\sigma}{2} \left(\frac{k_x^2}{m_x^*} + \frac{k_y^2}{m_y^*} + \frac{k_z^2}{m_z^*} \right). \tag{1.81}$$

For the scope of this thesis, we will rearrange the coupling strength term in 1.78 in a way that makes it more similar to the coupling strength of the original Froehlich model.

To this aim we introduce the adimensional coupling term $\alpha(\hat{\mathbf{q}})$ as [21]

$$\alpha(\hat{\mathbf{q}}) = \frac{4\pi}{\sqrt{2}\Omega_0} \left(\frac{m^*(\hat{\mathbf{q}})}{\omega_{jLO}}\right)^{1/2} \left(\frac{p_{jLO}}{\epsilon_\infty \omega_{jLO}}\right)^2, \tag{1.82}$$

which can be rewritten in a similar form to 1.58:

$$\alpha(\hat{\mathbf{q}}) = \frac{1}{\epsilon_j^*} \left(\frac{m^*(\hat{\mathbf{q}})}{2\omega_{jLO}} \right)^{1/2} \tag{1.83}$$

with ϵ_i^* dielectric response of the phonon mode defined as

$$\epsilon_j^* = \frac{4\pi}{\Omega_0} \left(\frac{p_j LO}{\epsilon_\infty \omega_{jLO}} \right)^2. \tag{1.84}$$

The following relation is also true [4]:

$$\frac{1}{\epsilon_{\infty}} = \frac{1}{\epsilon_0} + \sum_{j} \frac{1}{\epsilon_j^*}.$$
 (1.85)

In this way the coupling strength term, similarly to 1.48, can be rewritten as

$$V^{cFr}(qj) = \frac{i}{q} \left(\frac{2\sqrt{2}\pi}{\Omega_0 V_{BvK}} \frac{\omega_{jLO}^{3/2}}{m(\hat{\mathbf{q}})^{1/2}} \alpha(\hat{\mathbf{q}}) \right)^{1/2},$$
(1.86)

which is not dependent on the orientation of ${\bf q}$ since the $\hat{{\bf q}}$ -dependent terms (the effective mass) gets simplified.

It is possible to use perturbation theory to compute the ground state energy of the polaron with an anisotropic electron band and multiple phonon modes. In fact, at the lowest order of perturbation theory we get [21]

$$E_P(0) = -\sum_{j} \frac{\sigma}{\sqrt{2}\Omega_0} \int_{4\pi} d\hat{\mathbf{q}} (m^*(\hat{\mathbf{q}}))^{1/2} (\omega_{jLO}(\hat{\mathbf{q}}))^{-3/2} \left(\frac{p_{jLO}}{\epsilon_{\infty}}\right)^2,$$
 (1.87)

which, using the expression for $\alpha(\hat{\mathbf{q}})$ in 1.82, becomes

$$E_P(0) = -\sigma \sum_{j} \langle \alpha_j(\hat{\mathbf{q}}) \rangle_{\hat{\mathbf{q}}} \, \omega_{jLO}. \tag{1.88}$$

If we rewrite

$$\alpha_j = \langle \alpha_j(\hat{\mathbf{q}}) \rangle_{\hat{\mathbf{q}}} = \langle (m^*(\hat{\mathbf{q}}))^{1/2} \rangle_{\hat{\mathbf{q}}} \frac{1}{\epsilon_j^*} \frac{1}{\sqrt{2\omega_{jLO}}}$$
(1.89)

we obtain the final formula for the polaron ground state energy (for a conduction band):

$$E_P(0) = -\left\langle (m^*(\hat{\mathbf{q}}))^{1/2} \right\rangle_{\hat{\mathbf{q}}} \left(\sum_j \frac{\sqrt{\omega_{jLO}}}{\epsilon_j^* \sqrt{2}} \right). \tag{1.90}$$

The effective mass of the polaron can also be retrieved in perturbation theory, we start by observing that, up to the second order [4]

$$E_P(\mathbf{k}) = E_P(0) + \frac{\sigma}{2} \left(\frac{k_x^2}{m_{Px}^*} + \frac{k_y^2}{m_{Py}^*} + \frac{k_z^2}{m_{Pz}^*} \right),$$
 (1.91)

from which it follows that

$$\frac{1}{m_{Pi}^*} = \frac{1}{m_i^*} + \sigma \left(\frac{d^2 \Sigma(\mathbf{k}, \epsilon(\mathbf{k}))}{dk_i^2} \right)_{k=0}, \tag{1.92}$$

with $\Sigma(\mathbf{k}, \epsilon(\mathbf{k}))$ the energy variation exclusively due to electron-phonon coupling (the component due to the electron band is not included). We now define

$$I_P(\mathbf{k}, \omega_{jLO}, m_i^*) = \int \frac{d^3q}{4\pi q^2} \frac{1}{\sigma\left(\epsilon(\mathbf{k}) - \epsilon(\mathbf{k} - \mathbf{q}) - \omega_{iLO}\right)},\tag{1.93}$$

with $\epsilon(\mathbf{k})$ given as 1.81, we thus get

$$\Sigma(\mathbf{k}, \epsilon(\mathbf{k})) = \frac{\sigma}{\pi} \sum_{i} \frac{\omega_{jLO}}{\epsilon_{j}^{*}} I_{P}(\mathbf{k}, \omega_{jLO}, m_{i}^{*}).$$
 (1.94)

For $\mathbf{k} = 0$ we have [4]

$$I_P(0,\omega_{jLO},m_i^*) = (\omega_{jLO})^{-1/2}I_P(0,1,m_i^*),$$

$$\left(\frac{\partial^2 I_P}{\partial k_i^2}\right)_{k=0} = -2\left(\frac{\partial^2 I_P}{\partial \omega_{jLO}\partial m_i^*}\right)_{k=0,\omega=1} \sum_j \frac{1}{\epsilon_j^*} \frac{1}{\sqrt{2\omega_{jLO}}},$$
(1.95)

which, combined, give the result

$$\left(\frac{d^2\Sigma(\mathbf{k},\epsilon(\mathbf{k}))}{dk_i^2}\right)_{k=0} = \frac{\sigma}{\pi} \left(\frac{\partial I_P}{\partial m_i^*}\right)_{k=0,\omega=1} \sum_j \frac{1}{\epsilon_j^*} \frac{1}{\sqrt{2\omega_{jLO}}}.$$
(1.96)

The obtained expression clearly shows the decomposition between the band dispersion (from the electronic band masses m_i^*) and the phonon modes, in fact, for the electron polaron (conduction band) we have:

$$I_P(0,1,m_i^*) = \int \frac{d^3q}{4\pi q^2} \frac{1}{\frac{1}{2} \left(\frac{q_x^2}{2m_x^*} + \frac{q_y^2}{2m_y^*} + \frac{q_z^2}{2m_z^*}\right) + 1},$$
(1.97)

separating the q_i components in their radial and angular parts following 1.81 we obtain:

$$I_P(0, 1, m_i^*) = \frac{\pi}{\sqrt{2}} \langle m^{*1/2} \rangle.$$
 (1.98)

We thus obtain the expression for the polaron effective mass

$$\frac{1}{m_{Pi}^*} = \frac{1}{m_i^*} - \frac{\partial \left\langle m^{*1/2} \right\rangle}{\partial m_i^*} \sum_j \frac{1}{\epsilon_j^*} \frac{1}{\sqrt{2\omega_{jLO}}},\tag{1.99}$$

which, for an isotropic effective band mass, reduces to the expression in 1.60. In the non-degenerate anisotropic uniaxial case, which describes cubic materials with conduction band gaps in X or L, where we have $m_x^*=m_y^*=m_\perp^*$ and the ratio μ^* defined as

$$\mu^* = \frac{m_{\perp}^*}{m_z^*},\tag{1.100}$$

the square root of the average electronic effective mass becomes

$$\langle m^{*1/2} \rangle = m_{\perp}^* S(\mu^* - 1)$$
 (1.101)

with S(x) defined as

$$S(x) = \begin{cases} \frac{\arcsin(x^{1/2})}{x^{1/2}}, & x > 0, \\ \frac{\arcsin(-x)^{-1/2}}{(-x)^{1/2}}, & x < 0, \end{cases}$$
 (1.102)

we obtain the following expression for the polaron effective mass: for $m_{P\perp}^*$ we have

$$m_{P\perp}^* = m_{\perp}^* \left(1 - \frac{1}{f_{\perp}(\mu^*)} \sum_j \alpha_j \right)^{-1},$$

$$f_{\perp}(\mu^*) = 4(1 - \mu^*) \left[1 - \frac{(\mu^*)^{1/2}}{S(\mu^* - 1)} \right]^{-1},$$
(1.103)

while for m_{Pz}^* we obtain

$$m_{Pz}^* = m_z^* \left(1 - \frac{1}{f_z(\mu^*)} \sum_j \alpha_j \right)^{-1},$$

$$f_z(\mu^*) = 2 \frac{1 - \mu^*}{\mu^*} \left[\frac{(\mu^*)^{-1/2}}{S(\mu^* - 1)} - 1 \right]^{-1}.$$
(1.104)

The limit for which the perturbation approach breaks down is different from the isotropic limit of $\alpha=6$ [4] and depends on the value for which $f_{\perp}(\mu^*)$ and $f_z(\mu^*)$ equal $\sum_j \alpha_j$.

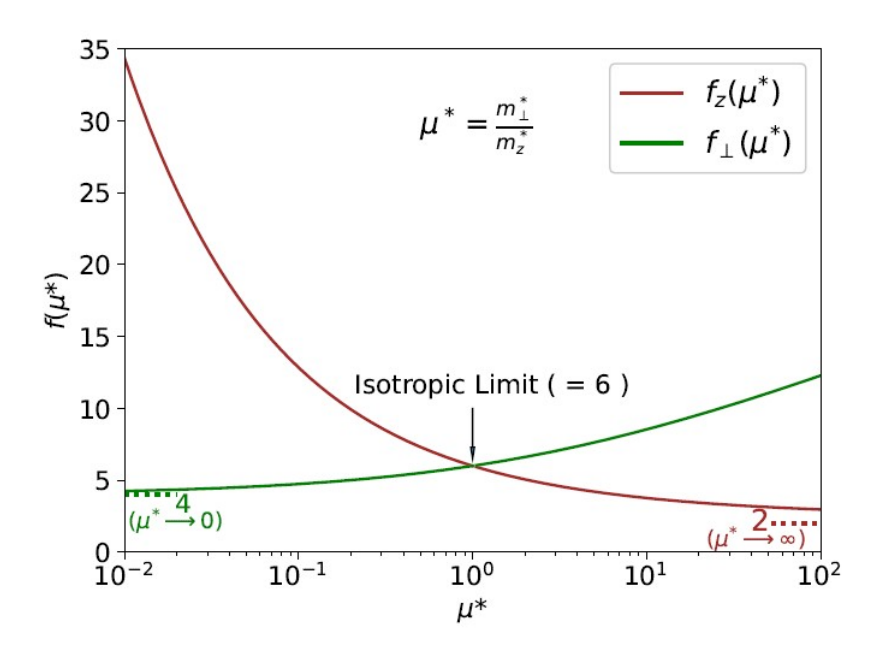


Figure 1.5: Polaron effective mass breakdown limit in the uniaxial case [4].

1.6 Feynman variational method

The Feynman variational approach [25] uses a different method to solve the Froehlich Hamiltonian: it starts by rewriting the Hamiltonian into a Lagrangian by replacing the electron and phonon operators with the corresponding position and conjugate momentum and then using a Legendre tranformation. After having integrated over the momenta, only a path integral over the configuration space remains, which is Gaussian in the phonon coordinates and thus can be evaluated.

We then obtain as a result an effective action of an electron coupled to a fictitious particle with a non-Coulomb potential [4]:

$$Z = Tr[e^{-\beta H^{Fr}}] \approx \int_{\mathbf{r}(0) = \mathbf{r}'(\beta)} D\mathbf{r}(\tau) e^{-S[\mathbf{r}(\tau)]}, \tag{1.105}$$

where τ is the imaginary time (discussed in detail in Chapter 2 and akin to an inverse temperature), $\beta=k_BT$, Z is the partition function for the electron (which starts at $\tau=0$ and finishes in the same position at $\tau=\beta$). S (the model action) is defined as:

$$S[\mathbf{r}(\tau)] = \frac{m^*}{2} \int_0^\beta d\tau \left(\frac{d\mathbf{r}(\tau)}{d\tau}\right)^2 + \frac{\omega_{LO}^{3/2}\alpha}{(8m^*)^{1/2}} \int_0^\beta d\tau \int_0^\beta d\tau' |\mathbf{r}(\tau) - \mathbf{r}(\tau')|^{-1} e^{-\omega_{LO}|\tau - \tau'|},$$
(1.106)

where it is assumed that β is large with respect to ω_{LO} . Since the formula for S is difficult to evaluate, we employ **Jensen's inequality**

$$\langle \exp\left(f\right) \rangle \geq \exp\left\langle f \right\rangle$$
 (1.107)

to approximate the action S into S_0 :

$$S_0[\mathbf{r}(\tau)] = \frac{m^*}{2} \int_0^\beta d\tau \left(\frac{d\mathbf{r}(\tau)}{d\tau}\right)^2 + \frac{C}{2} \int_0^\beta d\tau \int_0^\beta d\tau' \left(\mathbf{r}(\tau) - \mathbf{r}(\tau')\right)^2 e^{-w|\tau - \tau'|}. \tag{1.108}$$

In this way an upper bound for the free energy F can be calculated:

$$F \le F_{S_0} + \frac{1}{\beta} \langle S - S_0 \rangle_{S_0}$$
, (1.109)

with F_{S_0} free energy of the approximate system and $\langle S - S_0 \rangle_{S_0}$ expectation value of the difference between the two actions taken with respect to S_0 .

The ground state energy E_P is found for $T \to 0 \ (\beta \to +\infty)$:

$$Tr\left[e^{-\beta H}\right] \approx e^{-\beta E_P},$$
 (1.110)

and we find

$$E_P \le \frac{3\omega_{LO}}{4v}(v-w)^2 - \frac{\alpha\omega_{LO}}{\sqrt{\pi}} \frac{v}{w} \int_0^{+\infty} d\tau \frac{e^{-\tau}}{\sqrt{\tau D(\tau)}},$$

$$D(\tau) = 1 + \frac{v(1-w^2/v^2)(1-e^{-v\tau})}{\tau w^2}, \qquad v^2 = w^2 + \frac{4C}{w}.$$
(1.111)

This is a variational approach in terms of v (the frequency of the harmonic oscillator made of the electron and the fictitious particle) and w (the exponential decay of the coupling in imaginary time).

If we set $v=(1+\epsilon)w$ with ϵ small (expression valid for the weak-coupling limit) and expand the expression for the energy we find that the energy is minimized for:

$$\frac{E_P}{\omega_{LO}} \le -\alpha - 1.23 \left(\frac{\alpha}{10}\right)^2. \tag{1.112}$$

In the strong-coupling limit we have instead $w/v\ll 1$ and the energy is minimized for

$$\frac{E_P}{\omega_{LO}} \le -\frac{\alpha^2}{2\pi} - \frac{3}{2}(2\log 2 + \gamma) - \frac{3}{4} + O(\frac{1}{\alpha^2}),\tag{1.113}$$

with $\gamma \approx 0.5772$ the Euler-Mascheroni constant.

In this framework, the polaron effective mass m_P^* is retrieved by assuming that the electron has a small velocity ${\bf v}$ and moves from 0 to ${\bf r}={\bf v}\beta$ with β the imaginary time. Assuming that the energy dispersion is quadratic

$$E_P(\mathbf{v}) = E_P(0) + \frac{1}{2}m_P^*v^2,$$
 (1.114)

we retrieve the polaron effective mass as

$$m_P^* = m^* \left[1 + \frac{\alpha}{3\pi} \left(\frac{v}{w} \right)^3 \int_0^{+\infty} d\tau \frac{e^{-\tau} \tau^{1/2}}{[D(\tau)]^{3/2}} \right]. \tag{1.115}$$

In the weak-coupling case we retrieve the expression:

$$m_P^* = m^* (1 + \frac{\alpha}{6} + 0.025\alpha^2 + ...),$$
 (1.116)

while in the strong-coupling we have

$$m_P^* = m^* \frac{160}{81} \left(\frac{\alpha}{\pi}\right)^4.$$
 (1.117)

2 Froehlich polaron: Feynman diagrams

In order to deeply understand a many-body system such as the Froehlich polaron it is necessary to use a more powerful formalism derived from quantum many body theory, we will first briefly introduce Green's functions as an effective mean to describe meaningful quantities of our system and we will then shift to the **Matsubara imaginary time** formalism, much more useful in the context of Diagrammatic Monte Carlo. At the end of this journey the connection between the Froehlich polaron and Feynman diagrams will be explicated.

2.1 Green's function formalism

Green functions are useful objects to perturbatively solve systems that are really hard to correctly treat in any other way [26].

If we take for example a time-dependent Schroedinger equation in the following way:

$$[i\partial_t - H_0(\mathbf{r}) - V(\mathbf{r})] \,\psi(\mathbf{r}, t) = 0, \tag{2.1}$$

with the non-interacting diagonizable term H_0 and the perturbation V. It is possible to define the corresponding Green's functions as:

$$[i\partial_t - H_0(\mathbf{r})] G_0(\mathbf{r}, \mathbf{r}'; t, t') = \delta(\mathbf{r} - \mathbf{r}') \delta(t - t'),$$

$$[i\partial_t - H_0(\mathbf{r}) - V(\mathbf{r})] G(\mathbf{r}, \mathbf{r}'; t, t') = \delta(\mathbf{r} - \mathbf{r}') \delta(t - t').$$
(2.2)

We can define $G_0^{-1}(\mathbf{r};t')$ and $G^{-1}(\mathbf{r};t)$ as:

$$G_0^{-1}(\mathbf{r};t) = i\partial_t - H_0(\mathbf{r}),$$

$$G^{-1}(\mathbf{r};t) = i\partial_t - H_0(\mathbf{r}) - V(\mathbf{r}),$$
(2.3)

The Schroedinger equation can then be recast as

$$\left[G_0^{-1}(\mathbf{r},t) - V(\mathbf{r})\right]\psi(\mathbf{r},t) = 0 \tag{2.4}$$

and it is possible to rewrite the system as an integral equation

$$\psi(\mathbf{r},t) = \psi^{0}(\mathbf{r},t) + \int d^{3}r' \int dt' G_{0}(\mathbf{r},\mathbf{r}';t,t') V(\mathbf{r}')\psi(\mathbf{r}',t')$$
 (2.5)

which can be solved iteratively. In fact:

$$\psi = \psi^{0} + G_{0}V\psi^{0} + G_{0}VG_{0}V\psi^{0} + G_{0}VG_{0}VG_{0}V\psi^{0} + \dots$$

$$= \psi^{0} + (G_{0} + G_{0}VG_{0} + G_{0}VG_{0}VG_{0} + \dots)V\psi_{0}.$$
(2.6)

Noting that 2.5 can be also written as:

$$\psi(\mathbf{r},t) = \psi^{0}(\mathbf{r},t) + \int d^{3}r' \int dt' G(\mathbf{r},\mathbf{r}';t,t') V(\mathbf{r}') \psi^{0}(\mathbf{r}',t'), \tag{2.7}$$

it is possible to identify G with

$$G = G_0 + G_0 V G_0 + G_0 V G_0 V G_0 + \dots$$

= $G_0 + G_0 V (G_0 + G_0 V G_0 + \dots),$ (2.8)

and the well-known **Dyson equation** is retrieved:

$$G = G_0 + G_0 V G. (2.9)$$

The one described above is the **single particle Green's function**, also called propagator since it "propagates" the wavefunction: in fact, if the wavefunction is known at time t' the wavefunction at a later time can be obtained in the following way:

$$\psi(\mathbf{r},t) = \int d^3r' \int dt' G(\mathbf{r}t,\mathbf{r}'t')\psi(\mathbf{r}'t'), \qquad (2.10)$$

which is a solution to 2.3. The Green's function can also be written as

$$G(\mathbf{r}t, \mathbf{r}'t') = -\theta(t - t')\langle \mathbf{r}|e^{-iH(t - t')}|\mathbf{r}'\rangle, \tag{2.11}$$

and is more precisely known as the retarded Green's function.

Focusing now on a many-body system the Green's function is defined as

$$G^{R}(\mathbf{r}\sigma t, \mathbf{r}'\sigma't') = -i\theta(t - t')\langle [\psi_{\sigma}(\mathbf{r}, t), \psi_{\sigma'}^{\dagger}(\mathbf{r}', t')]_{B,F}\rangle, \tag{2.12}$$

where $[,]_{B,F}$ is the commutator [,] for bosons and the anticommutator $\{,\}$ for fermions. In the case of translation-invariant systems (such as lattices) Green's functions can only depend on $\mathbf{r} - \mathbf{r}'$ and it is natural to adopt the usual \mathbf{k} formalism:

$$G^{R}(\mathbf{r} - \mathbf{r}', \sigma t, \sigma' t') = \frac{1}{V} \sum_{\mathbf{k}} e^{i\mathbf{k} \cdot (\mathbf{r} - \mathbf{r}')} G^{R}(\mathbf{k}, \sigma t, \sigma' t'),$$

$$G^{R}(\mathbf{k}, \sigma t, \sigma' t') = -i\theta(t - t') \langle [a_{\mathbf{k}\sigma}, a_{\mathbf{k}'\sigma'}^{\dagger}]_{B,F} \rangle.$$
(2.13)

The goal is now to find explicit expressions for the various Green's function of relevance, in the special case of a free electron the Hamiltonian assumes the simple form

$$H = \sum_{\mathbf{k}\sigma} \epsilon(k) c_{\mathbf{k}\sigma}^{\dagger} c_{\mathbf{k}\sigma}, \tag{2.14}$$

and the time dependence of the creation/annihilation operators is simply defined as

$$c_{\mathbf{k}\sigma}(t) = e^{iHt}c_{\mathbf{k}\sigma}e^{-iHt} = c_{\mathbf{k}\sigma}e^{-i\xi_k t}.$$
(2.15)

The retarded Green's function then becomes:

$$G^{R}(\mathbf{k}\sigma, t - t') = -i\theta(t - t')e^{-i\xi_{k}(t - t')}.$$
(2.16)

2.2 Perturbation theory for Green's functions

Given an Hamiltonian which can be written as a sum of two terms

$$H = H_0 + V,$$
 (2.17)

where H_0 is diagonizable and V is an interaction term which can be treated perturbatively, we want to obtain a perturbative expansion of the Green's function. The issue with this approach is that in the expression for a generic Green's function it is require to take the expectation value over a ground state $(\langle \cdot \rangle)$ which is not known, namely the ground state of the interacting system.

It is thus important to link the ground state of the interacting system to the ground state of the non-interacting one, to this mean we introduce **adiabatic switching on of the interaction** [27].

The core feature of this method is turning a time-independent problem into a time-dependent one by slowly switching on the perturbation, the Hamiltonian is transformed in the following way:

$$H_{\alpha}(t) = H_0 + V e^{-\alpha|t|}, \qquad \alpha > 0,$$
 (2.18)

such that the system is non-interacting for $t \to \pm \infty$ and goes back to 2.17 for $t \to \infty$,

$$\lim_{t\to\pm\infty}H_{\alpha}(t)=H_0, \qquad \lim_{t\to0}H_{\alpha}(t)=H. \tag{2.19}$$

In this setup, it is natural to suppose that the ground state of the interacting system $|\Phi_0\rangle$ evolves continuously starting from the ground state of the non-interacting one $|\Psi_0\rangle$.

We introduce the interaction representation for the operators, for the interaction term of the Hamiltonian we have

$$V_I e^{-\alpha|t|} = e^{iH_0 t} V e^{-iH_0 t} e^{-\alpha|t|}, (2.20)$$

the time-evolution operator in the interaction representation is written as

$$U_{I\alpha}(t,t_0) = \sum_{n=0}^{\infty} \frac{1}{n!} (-i)^n \int_{t_0}^t dt_1 \cdots \int_{t_0}^t dt_n e^{-\alpha(|t_1|+\ldots+|t_n|)} T_t \left[V_I(t_1) \cdots V_I(t_n) \right], \qquad \text{(2.21)}$$

and defines the evolution of the system in the following way:

$$|\psi_{I\alpha}(t)\rangle = U_{I\alpha}(t, t_0)|\psi_{I\alpha}(t_0)\rangle.$$
 (2.22)

The equation of motion is obtained as

$$i\frac{d}{dt}|\psi_{I\alpha}(t)\rangle = e^{-\alpha|t|}V_I(t)|\psi_{I\alpha}(t)\rangle, \qquad (2.23)$$

from this it follows that

$$i\frac{d}{dt}|\psi_{I\alpha}(t\pm\infty)\rangle=0,$$
 (2.24)

which means that the state is time-independent. We can thus take the ground state of the non-interacting system as the ground state for the interacting one when $t \to \pm \infty$, the expression at the two times can differ up to a phase factor:

$$|\psi_{I\alpha}(t\to -\infty)\rangle = |\Psi_0\rangle, \qquad |\psi_{I\alpha}(t\to \infty)\rangle = e^{i\phi}|\Psi_0\rangle.$$
 (2.25)

It is now possible to link the non-interacting ground state at $t \to -\infty$ with the interacting one at t using the time-evolution operator

$$|\psi_{I\alpha}(t)\rangle = U_I(t, -\infty)|\Psi_0\rangle,$$
 (2.26)

at t=0 the interaction is completely switched on. Moreover, if the switching on is performed really slowly (adiabatically) it can be excluded that the wavefunction $|\psi_{I\alpha}(t)\rangle$ depends on the parameter α and the exact ground state should be computed starting from the non-interacting ground state.

However, since it is required that $\alpha > 0$, there is no certainty that the limit

$$|\Phi_0\rangle = \lim_{\alpha \to 0} |\psi_{I\alpha}(0)\rangle$$
 (2.27)

exists, and in fact it does not exist.

For this reason the **Gell-Mann-Low theorem** [28] is used, which is a theorem that fixes the eigenstate which evolves from the non-interacting ground state during the adiabatic switching on of the interaction.

The statement of the theorem is the following: given a state

$$\lim_{\alpha \to 0} \frac{U_{I\alpha}(0, -\infty) |\Psi_0\rangle}{\langle \Psi_0 | U_{I\alpha, -\infty} |\Psi_0\rangle} = \lim_{\alpha \to 0} \frac{|\psi_{I\alpha}(0)\rangle}{\langle \Psi_0 | \psi_{I\alpha}(0)\rangle}$$
(2.28)

which exists for every order of the perturbation theory, then this state is an eigenstate $|\Phi_0\rangle$ of the full Hamiltonian H_0 .

The importance of this theorem consists on the fact that it fixes the eigenstate during its evolution starting from the non-interacting ground state, a further important assumption is thus the requirement that no crossings of the states occur during their evolution from the free states. This is not a problem in our case since in the Froehlich Hamiltonian no transitions of this type occur, differently from what happens, for example, in superconductivity.

Since Green's functions are defined as expectation values of Heisenberg operators, these expectation values should be evaluated over the ground state (at T=0). Using Gell-Mann-Low theorem it was demonstrated that the ground state of the interacting system $|\Phi_0\rangle$ can be retrieved from the non interacting one $|\Psi_0\rangle$, the normalized ground state is then

$$|\Phi_0\rangle_{norm} = \frac{|\Phi_0\rangle}{\left(\langle\Phi_0|\Phi_0\rangle\right)^{1/2}}.$$
 (2.29)

Given a generic Green's function (in terms of the parameter α)

$$G_{\alpha}(\mathbf{k}t, \mathbf{k}'t') = -i\langle T_t c_{\mathbf{k}}(t) c_{\mathbf{k}'}^{\dagger}(t') \rangle, \tag{2.30}$$

the creation and annihilation operators in the Heisenberg representation can be cast in the interaction one:

$$c_{\alpha \mathbf{k}}(t) = U_{I\alpha}(0, t)c_{I\alpha \mathbf{k}}(t)U_{I\alpha}(t, 0).$$
 (2.31)

The expectation value of the Heisenberg operator can now be computed:

$$norm \langle \Psi_{0} | c_{\mathbf{k}}(t) c_{\mathbf{k}'}^{\dagger}(t') | \Psi_{0} \rangle_{norm} = \frac{\langle \Psi_{0} | c_{\alpha \to 0\mathbf{k}} c_{\alpha \to 0\mathbf{k}'}^{\dagger} | \Psi_{0} \rangle}{\langle \Psi_{0} | \Psi_{0} \rangle}$$

$$= \lim_{\alpha \to 0} \frac{\langle \Psi_{0} | U_{I\alpha}(+\infty, t) c_{I\mathbf{k}}(t) U_{I\alpha}(t, t') c_{I\mathbf{k}'}^{\dagger}(t') U_{I\alpha}(t', -\infty) | \Psi_{0} \rangle}{\langle \Psi_{0} | U_{I\alpha}(+\infty, -\infty) | \Psi_{0} \rangle}.$$
(2.32)

Using this formula it is possible to perturbatively treat any Green's function by expanding it in a power series.

Given a generic Heisenberg operator A(t) and the power expansion for the time-evolution operator in 2.21 we may write:

$$norm \langle \Psi_0 | A(t) | \Psi_0 \rangle_{norm} = \lim_{\alpha \to 0} \frac{1}{\langle \Psi_0 | U_{I\alpha}(+\infty, -\infty) | \Psi_0 \rangle} \sum_{n=0}^{+\infty} \frac{1}{n!} (-i)^n \cdot \int_{-\infty}^{+\infty} dt_1 \cdots \int_{-\infty}^{+\infty} dt_n e^{-\alpha(|t_1| + \dots + |t_n|)} \langle \Psi_0 | T(V_I(t_1) \cdots V_I(t_n)) | \Psi_0 \rangle.$$

$$(2.33)$$

It is then possible to compare 2.33 with 2.21 to obtain the following identity:

$$\sum_{n=0}^{+\infty} \frac{1}{n!} (-i)^n \int_{-\infty}^{+\infty} dt_1 \cdots \int_{-\infty}^{+\infty} dt_n e^{-\alpha(|t_1|+...+|t_n|)} T_t \left(V_I(t_1) \cdots V_I(t_n) A(t) \right) = U_{I\alpha}(+\infty, t) A(t) U_{I\alpha}(t, -\infty).$$
(2.34)

The same argument can be made for a single particle Green's function, obtaining a similar expansion:

$$iG(\mathbf{k},t,t') = \sum_{n=0}^{+\infty} \frac{1}{n!} (-i)^n \int_{-\infty}^{+\infty} dt_1 \cdots \int_{-\infty}^{+\infty} dt_n \cdot e^{-\alpha(|t_1|+\dots+|t_n|)} \langle \Psi_0 | T_t \left(V_I(t_1) \cdots V_I(t_n) c_{\mathbf{k}}(t) c_{\mathbf{k}}^{\dagger}(t') \right) | \Psi_0 \rangle.$$

$$(2.35)$$

2.3 Matsubara formalism for imaginary time Green's functions

The usual Green's functions are complex-valued objects that are not fit to be used in the Diagrammatic Monte Carlo method since they provide negative values that cannot be easily

sampled from a distribution without losing precision.

For this reason we now describe the imaginary time formalism for Green's functions, which is also useful to evaluate systems that are at non-zero temperature. The relevant substitution is the following:

$$it \to \tau$$
, (2.36)

the retarded Green's function previously defined in 2.13 thus becomes the following Matsubara Green's function:

$$G(\mathbf{k}, \sigma \tau, \sigma' \tau') = -\theta(\tau - \tau') \langle [a_{\mathbf{k}\sigma}, a_{\mathbf{k}'\sigma'}^{\dagger}]_{B,F} \rangle, \tag{2.37}$$

where the thermal average $\langle A(\tau)B(\tau')\rangle$ is defined as:

$$\langle \Psi_0 | A(\tau) B(\tau') | \Psi_0 \rangle \qquad T = 0,$$

$$\frac{1}{Z} Tr \left[e^{-\beta H} A(\tau) B(\tau') \right] \qquad T > 0.$$
(2.38)

where Ψ_0 is the ground state and Z the partition function.

Given a system with a Hamiltonian characterized by a diagonizable term H_0 and a perturbation $V(\tau)$, we can define the imaginary time Heisenberg picture for an operator A as

$$A(\tau) = e^{-\tau H} A e^{\tau H},\tag{2.39}$$

and similarly the imaginary time interaction picture as

$$A_I(\tau) = e^{\tau H_0} A e^{-\tau H_0}. (2.40)$$

We can define the imaginary time-evolution operator in the interaction picture as

$$U_I(\tau, \tau') = e^{\tau H_0} e^{-(\tau - \tau')H} e^{-\tau' H_0}, \tag{2.41}$$

an explicit expression for the interaction picture time-evolution operator in the imaginary time formalism is found in analogy with the real time counterpart

$$\frac{\partial}{\partial \tau} U_I(\tau, \tau') = e^{\tau H_0} (H_0 - H) e^{-(\tau - \tau')H} e^{-\tau' H_0} = -V_I(\tau) U_I(\tau, \tau'), \tag{2.42}$$

which can be solved iteratively:

$$U_{I}(\tau, \tau') = \sum_{n=0}^{\infty} \frac{1}{n!} (-1)^{n} \int_{\tau'}^{\tau} d\tau_{1} ... \int {\tau'}^{\tau} d\tau_{n} T_{\tau} \left[V_{I}(\tau_{1}) ... V_{I}(\tau_{n}) \right]$$

$$= T_{\tau} \exp\left(-\int_{\tau'}^{\tau} d\tau_{1} V_{I}(\tau_{1})\right),$$
(2.43)

where T_{τ} is the τ ordering operator.

It is also important to stress that the partition function Z is naturally treated in the imaginary time formalism, in fact:

$$e^{-\beta H} = e^{-\beta H_0} U_I(\beta, 0) = e^{-\beta H_0} T_{\tau} exp \left(-\int_0^{\beta} d\tau_1 V_I(\tau_1) \right),$$
 (2.44)

and we have

$$\langle T_{\tau}A(\tau)B(\tau')\rangle = \frac{1}{Z}Tr\left[e^{-\beta H}T_{\tau}(A(\tau)B(\tau'))\right]$$

$$= \frac{1}{Z}Tr\left[e^{-\beta H_{0}}U_{I}(\beta,0)T_{\tau}(U_{I}(0,\tau)A_{I}(\tau)U_{I}(\tau,\tau')B_{I}(\tau')U_{I}(\tau',0))\right]$$

$$= \frac{1}{Z}Tr\left[e^{-\beta H_{0}}T_{\tau}(U_{I}(\beta,0)A_{I}(\tau)B_{I}(\tau'))\right]$$

$$= \frac{\langle T_{\tau}U_{I}(\beta,0)A_{I}(\tau)B_{I}(\tau')\rangle_{0}}{\langle U_{I}(\beta,0)\rangle_{0}},$$
(2.45)

where the expectation value is taken on the non-interacting system, in agreement with the previously found result for T=0.

We now go back to the definition of single particle Green's functions in imaginary time formalism, we can define them both in real space and in k space:

$$G(\mathbf{r}t, \mathbf{r}'t') = -\langle T_{\tau} \left(\psi(\mathbf{r}, \tau), \psi^{\dagger}(\mathbf{r}', \tau') \right) \rangle,$$

$$G(\mathbf{k}\tau, \mathbf{k}'\tau') = -\langle T_{\tau} \left(c_{\mathbf{k}}(\tau) c_{\mathbf{k}'}^{\dagger}(\tau') \right) \rangle,$$
(2.46)

neglecting the spin σ degree of freedom (not relevant for our treatment).

In the non-interacting case the Matsubara single particle Green's functions can be evaluated in the same way as the retarded Green's functions, in fact:

$$H_0 = \sum_{\mathbf{k}} \xi_{\mathbf{k}} c_{\mathbf{k}}^{\dagger} c_{\mathbf{k}}, \tag{2.47}$$

and the creation/annihilation operators in the Heisenberg picture read

$$c_{\mathbf{k}}(\tau) = e^{\tau H_0} c_{\mathbf{k}} e^{-\tau H_0} = c_{\mathbf{k}} e^{-\xi_{\mathbf{k}} \tau}, \qquad c_{\mathbf{k}}^{\dagger}(\tau) = e^{\tau H_0} c_{\mathbf{k}}^{\dagger} e^{-\tau H_0} = c_{\mathbf{k}}^{\dagger} e^{\xi_{\mathbf{k}} \tau}.$$
 (2.48)

The non-interacting Matsubara Green's function is then defined as

$$G_{0}(\mathbf{k}, \tau, \tau') = -\langle T_{\tau} \left(c_{\mathbf{k}}(\tau) c_{\mathbf{k}}^{\dagger}(\tau') \right) \rangle$$

$$= -\theta(\tau - \tau') \langle c_{\mathbf{k}}(\tau) c_{\mathbf{k}}^{\dagger}(\tau') \rangle - (\pm)_{B,F} \theta(\tau' - \tau) \langle c_{\mathbf{k}}^{\dagger}(\tau') c_{\mathbf{k}}(\tau) \rangle$$

$$= -\left[\theta(\tau - \tau') \langle c_{\mathbf{k}} c_{\mathbf{k}}^{\dagger} \rangle - (\pm)_{B,F} \theta(\tau' - \tau) \langle c_{\mathbf{k}}^{\dagger} c_{\mathbf{k}} \rangle \right] e^{-\xi_{\mathbf{k}}(\tau - \tau')}.$$
(2.49)

31

2.4 Equation of motion and Wick's theorem

For a general Green's function the process to find its expression goes through the equation of motion technique, for an operator in the imaginary time formalism the time derivative is

$$\partial_{\tau} A(\tau) = \partial(\tau) \left(e^{\tau H} A e^{-\tau H} \right) = e^{\tau H} [H, A] e^{-\tau H} = [H, A](\tau), \tag{2.50}$$

if we derive with respect to imaginary time a Matsubara Green's function, the following result is obtained:

$$-\frac{\partial}{\partial \tau} \left(T_{\tau} \langle A(\tau)B(\tau') \rangle \right) = \delta(\tau - \tau') \langle (AB - (\pm)_{B,F}BA \rangle) + \langle T_{\tau} \left([H, A](\tau)B(\tau') \right) \rangle, \quad (2.51)$$

which for the single particle Green's function in momentum space becomes

$$-\frac{\partial}{\partial \tau}G(\mathbf{k}\tau,\mathbf{k}'\tau') = \delta(\tau - \tau')\delta_{\mathbf{k}\mathbf{k}'} + \langle T_{\tau}\left([H,c_{\mathbf{k}}](\tau)c_{\mathbf{k}'}^{\dagger}(\tau')\right)\rangle. \tag{2.52}$$

In the case of a Green's function for a non-interacting system G_0 with an Hamiltonian $H_0 = \sum_{\mathbf{k}\mathbf{k}'} t_{\mathbf{k}\mathbf{k}'} c_{\mathbf{k}'}^{\dagger} c_{\mathbf{k}'}$ this equation simplifies to

$$-\frac{\partial}{\partial \tau}G_0(\mathbf{k}\tau, \mathbf{k}'\tau') = \delta(\tau - \tau')\delta_{\mathbf{k}\mathbf{k}'} + \sum_{\mathbf{k}''} t_{\mathbf{k}\mathbf{k}''}G_0(\mathbf{k}''\tau, \mathbf{k}'\tau'), \tag{2.53}$$

and the solution is found as previously defined.

We now introduce **Wick's theorem**, an important result which states that higher order (greater than 1) Green's functions for non-interacting systems $G_0^{(n)}$ can be factorized into products of single particle Green's functions G_0 .

The n-particle Green's function is defined as:

$$G_0^{(n)}(\nu_1 \tau_1, \cdots, \nu_n \tau_n; \nu_1' \tau_1', \cdots \nu_n' \tau_n') =$$

$$= (-1)^n \langle T_\tau \left[c_{I\nu_1}(\tau_1) \cdots c_{I\nu_n}(\tau_n) c_{I\nu_n'}^{\dagger}(\tau_n') \cdots c_{I\nu_1'}^{\dagger}(\tau_1') \right] \rangle.$$
(2.54)

This expression is quite complicated and difficult to handle, we first define an easier notation to handle all the operators:

$$l_{j}(\gamma_{j}) = \begin{cases} c_{I\nu_{j}}(\tau_{j}) & \in [0, n], \\ c^{\dagger}_{I\nu'_{2n+1-j}}(\tau'_{2n+1-j}) & \in [n+1, 2n], \end{cases}$$
 (2.55)

and we define the permutation of the 2n operators as:

$$P(l_1(\gamma_1)\cdots l_{2n}(\gamma_{2n})) = l_{P1}(\gamma_{P1})\cdots l_{P_{2n}}(\gamma_{P_{2n}}), \tag{2.56}$$

with P_i j-th variable in the permutation P.

The correct order of permutation depends on the the time arguments ordering, for this reason it is possible to rewrite 2.54 taking into account these considerations:

$$G_0^{(n)}(j_1 \cdots j_{2n}) = (-1)^n \sum_{P \in S_{2n}} (\pm)_{B,F}^P \theta(\gamma_{P_1} - \gamma_{P_2}) \cdots \theta(\gamma_{P_{n-1}} - \gamma_{P_n}) \times \langle l_{P_1}(\gamma_{P_1}) \cdots l_{P_{2n}}(\gamma_{P_{2n}}) \rangle.$$
(2.57)

We can now take the derivative with respect to one of the time variables of $G_0^{(n)}$ and use the equation of motion:

$$\left[-\frac{\partial}{\partial \tau_1} G^{(n)_0} \right]_{2nd-term} =$$

$$= -(-1)^n \left\langle T_\tau \left[H_0, c_{I\nu_1}(\tau_1) \cdots c_{I\nu_n}(\tau_n) c_{I\nu_n}^{\dagger}(\tau_n') \cdots c_{I\nu_1}^{\dagger}(\tau_1') \right] \right\rangle$$
(2.58)

We now focus on the case where τ_i is next to τ_j' , two terms like this are present in 2.57, one where $\tau_i < \tau_j'$ and one where $\tau_i > \tau_j'$ (the permutation order is obviously different). The Green's function is written as

$$G_0^{(n)} = \left[\cdots \theta(\tau_i - \tau_j') \cdots \right] \left\langle \cdots c_{I\nu_i}(\tau_i) c_{I\nu_j'}^{\dagger}(\tau_j') \cdots \right\rangle$$

$$(\pm)_{B,F} \left[\cdots \theta(\tau_j' - \tau_i) \cdots \right] \left\langle \cdots c_{I\nu_j'}^{\dagger}(\tau_j') c_{I\nu_i}(\tau_i) \right\rangle.$$
(2.59)

Differentiating these two terms with respect to τ_i gives two contributions from the heavyside function $\theta(\cdot)$:

$$-\left[\frac{\partial}{\partial \tau_{i} G_{0}^{(n)}}\right]_{1st-term} = \left([\cdots]\langle \cdots c_{I\nu_{i}}(\tau_{I})c_{I\nu'_{j}}^{\dagger}(\tau'_{j})\cdots\rangle\right)$$

$$(\mp)_{B,F}[\cdots]\langle \cdots c_{\nu'_{j}}^{\dagger}(\tau'_{j})c_{\nu_{i}}(\tau_{i})\cdots\rangle\right)\delta(\tau_{i}-\tau'_{j}).$$
(2.60)

We now observe that

$$\left[c_{\nu_i}(\tau_i), c_{\nu'_j}^{\dagger}(\tau_i)\right]_{B.F} = \delta_{\nu_i, \nu'_j},$$
 (2.61)

in the same way, for a couple of terms $c_{\nu_i}(\tau_i)$ and $c_{\nu_i}(\tau_i)$ we have:

$$\left[c_{\nu_i}(\tau_i), c_{\nu_j}(\tau_i)\right]_{BF} = 0,$$
 (2.62)

and the same is true for two creation operators.

In this way the number of creation and annihilation operators has been reduced by one each and we have demonstrated that a n order Green's function can written in terms of a n-1

order Green's functions (which is a sum of different terms). For fermionic Green's functions, the sign of G_0^{n-1} depends on the specific τ'_i . Apart from that, the equation of motion is now:

$$G_{0i}^{-1}G_{0}^{(n)} = \sum_{j=1}^{n} \delta_{\nu_{i},\nu'_{j}} \delta(\tau_{i} - \tau'_{j})(\pm 1)_{B,F}^{x} G_{0}^{(n-1)}(\underbrace{\nu_{1}\tau_{1}, \cdots, \nu_{n}\tau_{n}}_{\text{without } i}; \underbrace{\nu'_{1}\tau'_{1}, \cdots, \nu'_{n}\tau'_{n}}_{\text{without } j}). \tag{2.63}$$

The sign $(-1)^x$ for fermions is determined as $(-1)^{n-i+n-j}=(-1)^{-(i+j)}=(-1)^{i+j}$ due to the fact that it is required that the annihilation operator $c_{I\nu_i}(\tau_i)$ is moved i positions to the right while the creation operator $c_{\nu'_i}^{\dagger}(\tau'_i)$ is moved j positions to the left.

It is now possible to write the explicit decomposition of the n-order Green's function into a sum of $n\ (n-1)$ -order ones:

$$G_0^{(n)} = \sum_{i=0}^n (\pm)_{B,F}^{i+j} G_0(\nu_1 \tau_1, \nu_j' \tau_j') G_0^{(n-1)}(\underbrace{\nu_1 \tau_1, \cdots, \nu_n \tau_n}_{\text{without } i}; \underbrace{\nu_1' \tau_1', \cdots, \nu_n' \tau_n'}_{\text{without } j}). \tag{2.64}$$

It is clear from the obtained result that this method can be naturally generalized to iteratively obtain any non-interacting n-order Green's function as sum of terms only containing products of single particle non-interacting Green's functions. The final result of Wick's theorem is thus obtained:

$$G_0^{(n)}(1,\cdots,n;n',\cdots,1') = \begin{vmatrix} G_0(1,1') & \cdots & G_0(1,n') \\ \vdots & \ddots & \vdots \\ G_0(n,1') & \cdots & G_0(n,n') \end{vmatrix}_{B,F}, \qquad i \equiv (\nu_i,\tau_i) \quad (2.65)$$

where the result is given as a determinant for fermions and as a permanent for bosons.

2.5 Green's functions for the Froehlich Hamiltonian

We may now consider the Froehlich Hamiltonian previously defined in 1.79 using the new imaginary time formalism, defining the non-interacting Hamiltonian H_0^{cFr} as

$$H_0^{cFr} = \sum_{\mathbf{k}} \frac{\sigma k^2}{2m(\hat{k})} c_{\mathbf{k}}^{\dagger} c_{\mathbf{k}} + \sum_{\mathbf{q}j} \omega_{LO} a_{\mathbf{q}j}^{\dagger} a_{\mathbf{q}j}. \tag{2.66}$$

Since our model consists of a single electron (hole) in the minimum (maximum) of the conduction (valence) band interacting with a cloud of phonon, we may consider our system to be at zero temperature and the ground state wavefunction $|\Psi_0\rangle$ to be the vacuum:

$$|\Psi_0\rangle = |0\rangle, \qquad \langle \cdot \rangle = \langle 0| \cdot |0\rangle.$$
 (2.67)

It is then possible to explicitely compute the electron free propagator using 2.49:

$$G_{0}(\mathbf{k}, \tau, \tau') = -\left[\theta(\tau - \tau')\langle 0|c_{\mathbf{k}}c_{\mathbf{k}}^{\dagger}|0\rangle + \theta(\tau' - \tau)\langle 0|c_{\mathbf{k}}^{\dagger}c_{\mathbf{k}}|0\rangle\right]e^{k^{2}/2m(\hat{k})(\tau - \tau')}$$

$$= -\theta(\tau - \tau')e^{(k^{2}/2m(\hat{k}))(\tau - \tau')},$$
(2.68)

which for $\tau' = 0$ becomes

$$G_0(\mathbf{k}, \tau) = -\langle 0|c_{\mathbf{k}}(\tau)c_{\mathbf{k}}^{\dagger}|0\rangle = -e^{-(k^2/2m(\hat{k}))\tau}, \qquad \tau \ge 0.$$
 (2.69)

The Matsubara Green's function for a free electron propagator assumes the simple form of an exponential function, which can be easily sampled.

$$\begin{matrix} \bullet & & \bullet & \bullet \\ 0 & (\epsilon(\mathbf{k}), \mathbf{k}) & \tau \\ \\ -G_0(\mathbf{k}, \tau) = e^{-(k^2/2m(\hat{k}))\tau} \end{matrix}$$

Figure 2.1: Feynman diagram of the free electron propagator together with its Green's function.

$$0 \qquad (\omega_{jLO}, \mathbf{q}) \qquad \tau$$
$$-D_0(\mathbf{q}, \tau) = e^{-\omega_{jLO}\tau}$$

Figure 2.2: Feynman diagram of the free phonon propagator together with its Green's function.

In the same way, it is possible to find an explicit form for the phonon free propagator:

$$D_0(\mathbf{q}j,\tau) = -\langle 0|a_{\mathbf{q}}(\tau)a_{\mathbf{q}}^{\dagger}|0\rangle = -e^{-\omega_{jLO}\tau}, \qquad \tau \ge 0,$$
 (2.70)

which is again a simple exponential function.

We now take into consideration the interaction part of the Froehlich Hamiltonian:

$$V = \sum_{\mathbf{k}, \mathbf{q}j} c_{\mathbf{k}+\mathbf{q}}^{\dagger} c_{\mathbf{k}} \left[V^{cFr}(qj) a_{\mathbf{q}} + V^{*cFr}(qj) a_{-\mathbf{q}}^{\dagger} \right], \tag{2.71}$$

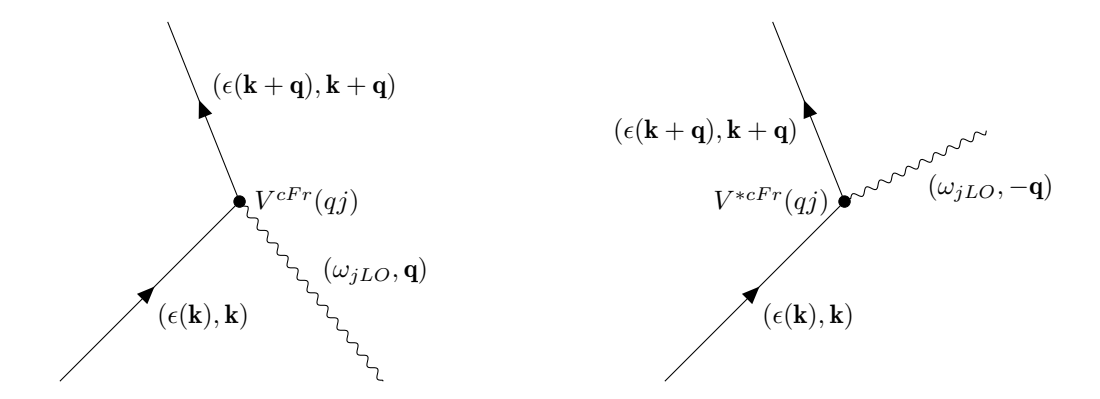


Figure 2.3: Feynman diagrams of the electron-phonon interaction.

the basic Feynman diagram that describes this interaction is an interaction between two free electron propagators (one with momentum \mathbf{k} gets annihilated and one with momentum $\mathbf{k}+\mathbf{q}$ gets created) and a free phonon propagator which can be either annihilated (momentum \mathbf{q}) or created (momentum $-\mathbf{q}$), the strength of the interaction at the vertex is given by $V^{cFr}(qj)$ (2.3).

We have now obtained the fundamental building blocks which can be used to obtain the total Green's function for the Froehlich polaron $G(\mathbf{k}, \tau)$, a generic one-electron Matsubara Green's function for the polaron is written as [29]

$$G(\mathbf{k}, \tau - \tau') = -\langle c_{\mathbf{k}}(\tau) c_{\mathbf{k}}^{\dagger}(\tau') \rangle = -\langle 0 | c_{\mathbf{k}}(\tau) c_{\mathbf{k}}^{\dagger}(\tau') | 0 \rangle. \tag{2.72}$$

The creation and annihilation operators here defined do not have the simple form described above for the free propagators, it is thus necessary to use the interaction picture and transform the operators:

$$c_{I\mathbf{k}}(au) = e^{\tau H_0^{cFr}} c_{\mathbf{k}} e^{-\tau H_0^{cFr}}, \qquad c_{I\mathbf{k}}^{\dagger}(au) = e^{\tau H_0^{cFr}} c_{\mathbf{k}}^{\dagger} e^{-\tau H_0^{cFr}}.$$
 (2.73)

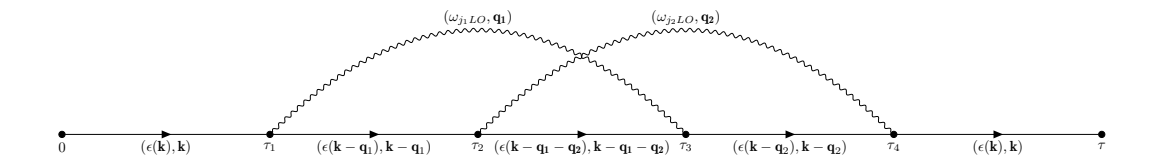


Figure 2.4: Order 4 diagram.

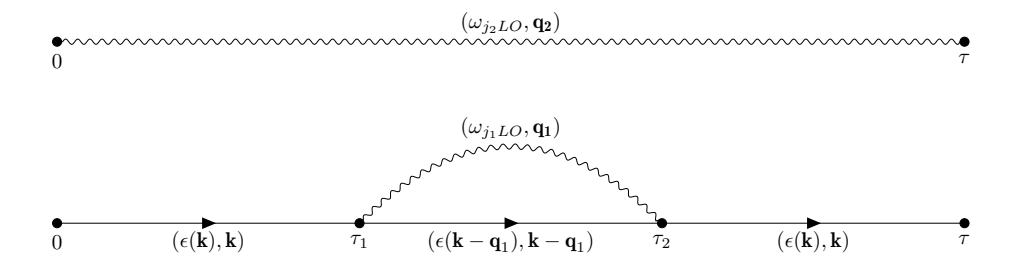


Figure 2.5: Disconnected order 4 diagram.

In the interaction picture the Green's function for the Froehlich polaron assumes the form [30]:

$$G(\mathbf{k}, \tau) = -\left\langle 0 \left| T_{\tau} \left[c_{I\mathbf{k}}(\tau) c_{\mathbf{k}}^{\dagger} \exp\left(-\int_{0}^{+\infty} V_{I}(\tau') d\tau' \right) \right] \right| 0 \right\rangle_{\text{conn}},$$
 (2.74)

where the expectation value is restricted to connected diagrams, which means that no integral over the internal variables $d\tau_i'$ can be represented by an external factor (the difference between a connected and disconnected diagram is easily recognizable in 2.4 and 2.5).

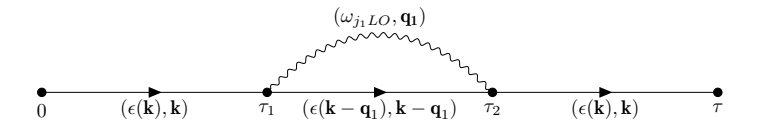


Figure 2.6: Order 2 diagram.



Figure 2.7: Order 4 diagram.

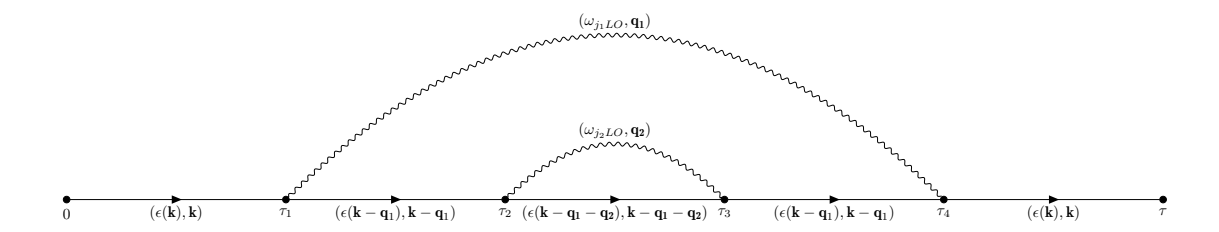


Figure 2.8: Order 4 diagram.

Using Wick's theorem, the product of n chronologically ordered operators $\{\tau_1, \tau_2, ..., \tau_n\}$ can be evaluated as the sum of products of pairs of operators, such that it is possible to expand the Green's function as an infinite series of terms of the following form:

$$G(\mathbf{k},\tau) = -\sum_{n=0,2,4...}^{+\infty} \sum_{\xi_n} \int d\tau_1 \cdots \int d\tau_n D_n^{\xi_n}(\mathbf{k},\tau;x_1,...,x_n),$$
 (2.75)

where n indexes the rank of the term (only terms with an even number of internal variables are allowed), ξ_n indexes the topology of the term (which depends on how the phonon lines are arranged, see the difference between 2.4, 2.7 and 2.8), x_i are the internal variables which index the imaginary times at which a vertex $V^{cFr}(qj)$ is present (and a phonon is created or annihilated), the index j of the phonon mode which interacts with the electron propagators and the momentum q of the created/annihilated phonon line.

As an example, the 0-order term is just the free electron propagator $G_0(\mathbf{k},\tau)=-e^{-\epsilon(\mathbf{k})\tau}$, the 2-order term (with internal variables (τ_1,j_1) and (τ_2,j_2)) represents a diagram with 3 free electron propagators, 1 free phonon propagator and 2 vertices.

 $D_2(\mathbf{k},\tau;x_1,x_2,)$ can thus be represented using Green's function as

$$D_{2}(\mathbf{k}, \tau; x_{1}, x_{2},) = |V^{cFr}(qj)|^{2} D_{0}(\mathbf{q}j, \tau_{2} - \tau_{1}) G_{0}(\mathbf{k}, \tau - \tau_{2}) \times G_{0}(\mathbf{k} - \mathbf{q}, \tau_{2} - \tau_{1}) G_{0}(\mathbf{k}, \tau_{1}),$$
(2.76)

which translates to

$$D_2(\mathbf{k}, \tau; x_1, x_2,) = |V^{cFr}(qj)|^2 e^{-\omega_{jLO}(\tau_2 - \tau_1)} e^{-\epsilon(\mathbf{k})(\tau - \tau_2)} e^{-\epsilon(\mathbf{k} - \mathbf{q})(\tau_2 - \tau_1)} e^{-\epsilon(\mathbf{k})\tau_1}.$$
 (2.77)

It should be noted that in our computation instead of 2.75 the result without the minus sign will be taken: this is just a convention used in order to obtain a definite positive distribution for the Monte Carlo sampling and it does not affect the physical significance of the calculated Green's functions.

Having seen the one-electron Green's function we now introduce another related Green's function: the one-electron N-phonons Green's function $G^N(\mathbf{k}, \sum_{j=1}^N \tilde{\mathbf{q}}_j, \tau)$. Differently from

the one-electron Green's function, the one-electron N-phonons Green's function is a more complex object consisting of N phonons and one electron, and better describes the polaron physics, especially if the strength of the interaction is intense. Its expression, using Wick's theorem, can be written as [31]:

$$G^{N}(\mathbf{k}, \sum_{j=1}^{N} \tilde{\mathbf{q}}_{j}, \tau) = \left\langle 0 | a_{\tilde{\mathbf{q}}_{1}}(\tau) ... a_{\tilde{\mathbf{q}}_{N}}(\tau) c_{\mathbf{p}}(\tau) c_{\mathbf{p}}^{\dagger} a_{\tilde{\mathbf{q}}_{N}} ... a_{\tilde{\mathbf{q}}_{1}} | 0 \right\rangle, \tag{2.78}$$

where $\mathbf{p} = \mathbf{k} - \sum_{j=1}^N \tilde{\mathbf{q}}_j$.

It is worth noting that $G^N(\mathbf{k}, \sum_{j=1}^N \tilde{\mathbf{q}}, \tau)$ will only take into account connected one-electron N-phonons Green's functions since in the other cases the external phonons can just be neglected. The related expansion can be given as:

$$G^{N}(\mathbf{k}, \sum_{j=1}^{N} \tilde{\mathbf{q}}_{j}, \tau) = \sum_{n=0,2,4...}^{+\infty} \sum_{\xi_{n}} \int d\tilde{\mathbf{q}}_{1} \cdots \int d\tilde{\mathbf{q}}_{N} \cdot \int d\tau_{1} \cdots \int d\tau_{n} D_{n}^{\xi_{n}}(\mathbf{k}, \sum_{j} \tilde{\mathbf{q}}_{j}, \tau; x_{1}, ..., x_{n}),$$

$$(2.79)$$

where the minus sign has been dropped.

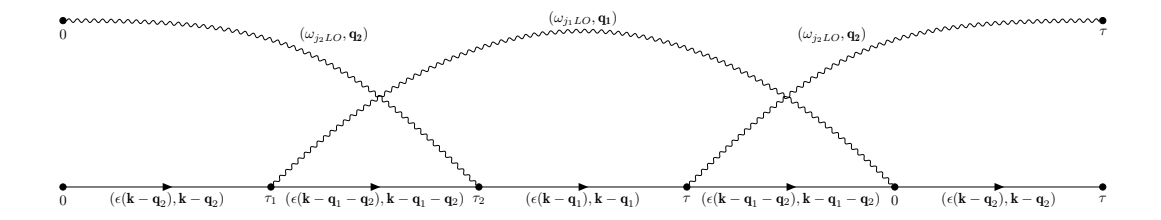


Figure 2.9: Order 2 diagram with one external phonon.

It is thus useful to consider the full function $P(\mathbf{k}, \tau)$ defined as follows:

$$P(\mathbf{k},\tau) = G(\mathbf{k},\tau) + \sum_{N=1}^{+\infty} G^N(\mathbf{k}, \sum_{j=1}^N \tilde{\mathbf{q}}_j, \tau),$$
 (2.80)

which more accurately describes our polaron model, including both the "free" polaron and its interaction with the phonon cloud.

39

2.6 Green's function: retrieving physical quantities

From the treatment of the Green's function performed up to now it is not immediately clear which physical information is stored inside the polaron's Green's function. We begin by reminding what the 1-electron Green's function is defined as

$$G(\mathbf{k}) = \langle 0|c_{\mathbf{k}}(\tau)c_{\mathbf{k}}^{\dagger}|0\rangle,$$
 (2.81)

with $c_{\bf k}(\tau)=e^{H\tau}c_{\bf k}e^{-H\tau}$, we can expand the Green's function as [29]

$$G(\mathbf{k},\tau) = \sum_{\nu} |\langle \nu | c_{\mathbf{k}}^{\dagger} | 0 \rangle|^2 e^{-(E_{\nu}(\mathbf{k}) - E_0)\tau}, \tag{2.82}$$

with $|\nu\rangle$ a complete set of eigenstates of the Froehlich Hamiltonian for a given momentum ${\bf k}$ such that

$$H|\nu(\mathbf{k})\rangle = E_{\nu}(\mathbf{k})|\nu(\mathbf{k})\rangle.$$
 (2.83)

Given that the ground state energy in our case E_0 is exactly 0 (electron at the ground state energy and no phonon excitations for T=0), we can neglect this term.

We can then rewrite the Green's function in terms of the spectral function $g_{\mathbf{k}}(\omega)$:

$$G(\mathbf{k}, \tau) = \int_{0}^{+\infty} d\omega g_{\mathbf{k}}(\omega) e^{-\omega \tau},$$

$$g_{\mathbf{k}}(\omega) = \sum_{\nu} \delta[\omega - E_{\nu}(\mathbf{k})] |\langle \nu | c_{\mathbf{k}}^{\dagger} | 0 \rangle|^{2}.$$
(2.84)

The spectral function $g_{\mathbf{k}}(\omega)$ is defined to have poles at frequencies for which a stable quasiparticle state exists. For this reason if a stable polaron exists for a given \mathbf{k} we will have

$$g_{\mathbf{k}}(\omega) = Z_0^{\mathbf{k}} \delta[\omega - E(\mathbf{k})] + \dots$$
 (2.85)

where $Z_0^{\mathbf{k}}$ is the overlap between the polaronic state and the free electron one:

$$Z_0^{\mathbf{k}} = |\langle \text{polaron } (\mathbf{k})| \text{ free electron } (\mathbf{k}) \rangle|^2.$$
 (2.86)

It can also be demonstrated that, if the polaron is at the ground state, for large τ values the Z factor and its energy can be retrieved:

$$G(\mathbf{k}, \tau \gg \omega^{-1}) \to Z_0^{\mathbf{k}} e^{-E_P(\mathbf{k})\tau}$$
. (2.87)

The same thing can be done with $P(\mathbf{k},\tau)$ sum of all the possible 1-electron N-phonons Green's functions, we have $Z_N^{\mathbf{k}}$ defined as:

$$Z_N^{\mathbf{k}}(\tilde{\mathbf{q}}_1,...,\tilde{\mathbf{q}}_N) = |\langle \mathsf{polaron} \ (\mathbf{k})| \ \mathsf{free} \ \mathsf{electron} \ (\mathbf{p}) + \ \mathsf{free} \ \mathsf{phonons} \ (\tilde{\mathbf{q}}_1,...,\tilde{\mathbf{q}_N}) \rangle|^2, \quad \text{(2.88)}$$

40

from which it follows that

$$G^{N}(\mathbf{k}, \tau \gg \omega^{-1}, \tilde{\mathbf{q}}_{1}, ..., \tilde{\mathbf{q}}_{N}) = Z_{N}^{\mathbf{k}} e^{-E_{P}(\mathbf{k})\tau}.$$
 (2.89)

and the formula for $P(\mathbf{k},\tau)$ is retrieved:

$$P(\mathbf{k},\tau) = \sum_{N} Z_{N}^{\mathbf{k}} e^{-E_{P}(\mathbf{k})\tau}.$$
 (2.90)

3 The Diagrammatic Monte Carlo method

3.1 The Monte Carlo sampling method

The Monte Carlo method is not a specific technique, but rather a wide set of similar methods which employ probability to solve problems that are otherwise too complex for an analytic solution and too resource demanding to solve with a numerical method.

The basic idea behind Monte Carlo is to use a statistical approach in the resolution of difficult integral and differential equations [32] by the means of a precisely defined set of rules and a random number generator.

This method is an *iterative stochastic procedure*, or in layman terms, a technique that is iterative: it needs to be applied many times in order to produce an extremely large number of measurements from which it is possible to build an estimate for a determined quantity, using the **central limit theorem** and the law of large numbers, and stochastic: it uses random numbers to obtain all sorts of distributions, usually through a precisely defined set of rules with a **Markov chain**.

It is in fact possible, using a Monte Carlo method, to estimate the ground state of the time-independent Schroedinger equation [5]

$$-\nabla^2 \psi(x, y, z) = [E - U(x, y, z)] \, \psi(x, y, z) \tag{3.1}$$

using the following ansatz for the wavefunction:

$$u(x, y, z, \tau) = \psi(x, y, z)e^{-E\tau}, \tag{3.2}$$

thus introducing a fictitious imaginary time-dependence. In this way u(x,y,z,t) follows the diffusion equation

$$\frac{\partial u}{\partial \tau} = \nabla^2 u - Uu,\tag{3.3}$$

which can be framed in a Monte Carlo representation as a set of weighted particles which independently perform a random walk with an exponential decay in imaginary time and a rate governed by the energy eigenvalue E, together with a particle distribution which can be used to determine an estimate for the wavefunction $\psi(x,y,z)$.

Note that the transformation performed on the wavefunction (first done by Fermi) is exactly the already seen transformation used for the Matsubara Green's functions 2.36, which turns the standard time-dependent Schroedinger equation

$$i\frac{\partial \psi}{\partial t} = -\nabla^2 \psi + U\psi \tag{3.4}$$

into

$$\frac{\partial \psi}{\partial \tau} = \nabla^2 \psi - U \psi. \tag{3.5}$$

3.2 Direct Monte Carlo 42

This observation already stresses the importance of imaginary time in our computation. We list three main types of Monte Carlo simulations [14]:

- **Direct Monte Carlo**, where the generation of random numbers directly models a physical system (usually with a random walk) without directly defining the complexities which characterizes it. An example is the aforementioned model to solve the ground state of the Schroedinger equation.
- Monte Carlo integration, a method that is specifically used to compute hard integrals with random numbers.
- Markov chain Monte Carlo, which generates the distribution of a system using a Markov chain. This method is used to study the properties of classical and quantum systems.

3.2 Direct Monte Carlo

In direct Monte Carlo the expectation value $\langle I \rangle$ of a variable is estimated, which means that we compute its mean. In order to do so the deterministic problem must be recast in a probabilistic form. Since $\langle I \rangle$ is a number, it can be seen as the result of an integration.

Given X a random variable defined on a set Ω , we can define $\langle I \rangle$ as the expectation value E(X) of the random variable. In statistics, the expectation value E(X) and the variance $\sigma^2(X)$ have the following definitions:

$$\langle I \rangle = E(X) = \int_{\Omega} dp X, \qquad \sigma_I^2 = \sigma^2(X) = \int_{\Omega} dp (X - E(X))^2,$$
 (3.6)

where p is the probability measure [33].

An approximate estimate for the value I is obtained by producing an independent sequence of random event ω_i according to the probability law p with value

$$\bar{I}_N = E(X_N) = \frac{1}{N} \sum_{i=1}^N X(\omega_i),$$
 (3.7)

with \bar{I}_N the arithmetic mean of N random events.

Given the fact that I_N is just an estimate of the expectation value $\langle I \rangle$, it is important to also provide an estimation of its deviation from the exact value, to this reason we introduce the **Chebyshev's inequality** [34], which states that no more than $1/k^2$ of the distribution values can be more than k standard deviations from the mean value:

$$P(|x - \langle x \rangle| > k\sigma) \le \frac{1}{k^2}.$$
 (3.8)

Chebyshev's inequality makes no assumptions on the distribution and is thus very general, yet it provides an upper bound for the probability to find random values far from the mean.

3.2 Direct Monte Carlo 43

In the case of N independent random variable for which

$$P(x_1, x_2, ..., x_N) = P(x_1)P(x_2)...P(x_N)$$
(3.9)

holds true, it is possible to consider a new random variable z which is the sum of the N original random variables. If the random variables X_i have generic distribution functions, then the distribution function of the sum has a complicated form, the important consideration is that, under very broad assumptions, it is possible to obtain an asymptotically exact form for the distribution function of z when the number N of independent variables becomes very large. Given

$$\bar{x}_N = \frac{1}{N} \sum_{i=0}^{N} x_i,$$
 (3.10)

both the expectation value and the variance of \bar{x}_N can be easily computed, since all the N terms of the sum give an identical contribution equal to $\langle x \rangle$, resulting in

$$\langle \bar{x}_N \rangle = \langle x \rangle. \tag{3.11}$$

This results holds also in the case where the N random variables x_i are not independent. The variance of \bar{x}_N is easily obtained in the following way:

$$\sigma_{\bar{x}_N}^2 = \langle \bar{x}_N^2 \rangle - \langle \bar{x}_N \rangle^2 = \frac{\sigma^2}{N}.$$
 (3.12)

We thus have for $N\to\infty$ the random variable $\bar x_N$ which has a very narrow distribution centered about the true expectation value of the random variable X (noting that $\sigma^2_{\bar x_N}\to 0$). This result is called the **weak law of large numbers**.

With the **central limit theorem** instead we obtain the asymptotic probability distribution of the sum z of a large number of random variables which are independent and equally distributed.

Let us define the random variable Y as

$$Y = \frac{1}{\sqrt{N}} \sum_{i=1}^{N} y_i = \sqrt{N}(\bar{x}_N - \langle x \rangle), \tag{3.13}$$

which has the expectation value

$$\langle Y \rangle = 0. {(3.14)}$$

The characteristic function of Y is given by

$$\phi_Y(t) = \left[\phi_y\left(\frac{t}{\sqrt{N}}\right)\right]^N,\tag{3.15}$$

assuming that all the y_i are independent and identically distributed.

Expanding the characteristic function up to second order and taking the limit for $N \to \infty$ we get:

$$\lim_{N \to \infty} \phi_Y(t) = \exp\left(-\frac{\sigma^2 t}{2}\right),\tag{3.16}$$

which is the characteristic function of a gaussian random variable:

$$P(Y) = \frac{1}{\sqrt{2\pi\sigma^2}} \exp\left(-\frac{Y^2}{2\sigma^2}\right),\tag{3.17}$$

and we obtain for $\bar{x}_N = \langle x \rangle + Y/\sqrt{N}$ the same gaussian distribution with mean $\langle x \rangle$ and variance σ^2/N .

Having now stated these necessary elements from probability and statistics it is easy to see how a direct Monte Carlo method works: we directly employ random numbers to compute quantities, exploiting the fact that given N iterations and $N \to \infty$, we will obtain a convergent solution for the modelled problem. The big issue is, of course, representing the investigated phenomenon in a way that makes it possible to use random numbers.

3.3 Monte Carlo integration

The Monte Carlo integration method is a technique specifically developed to compute integrals. Consider a generic integral of a smooth generic function $f(\mathbf{x})$ of vector \mathbf{x} and d components:

$$I = \int f(\mathbf{x})d\mathbf{x},\tag{3.18}$$

in Monte Carlo integration we recast this integral in the following way using a probability distribution p(x), ($\int p(x) = 1$):

$$\left\langle \frac{f(\mathbf{x})}{p(\mathbf{x})} \right\rangle = \int \frac{f(\mathbf{x})}{p(\mathbf{x})} p(\mathbf{x}) d\mathbf{x} = \int f(\mathbf{x}) d\mathbf{x}.$$
 (3.19)

The integral recast in this form is the expectation value of the function $f(\mathbf{x})$ divided by the probability distribution $p(\mathbf{x})$. The central limit theorem then implies that it is possible to estimate the integral I (deterministic) as the average value of f(x) over a large number of sampling of the random variable \mathbf{x}_i with distribution $p(\mathbf{x})$:

$$I \approx I_N = \frac{1}{N} \sum_{i=1}^{N} \frac{f(\mathbf{x}_i)}{p(\mathbf{x}_i)},$$
 (3.20)

where the random variables \mathbf{x}_i are sampled according to $p(\mathbf{x}_i)$.

For large N I_N is normally distributed with mean equal to I and variance σ^2/N computed as

$$\sigma^2 = \left\langle \left(\frac{f(\mathbf{x})}{p(\mathbf{x})} \right)^2 \right\rangle - \left\langle \frac{f(\mathbf{x})}{p(\mathbf{x})} \right\rangle^2, \tag{3.21}$$

thus for $N \to +\infty$ I_N tends to the deterministic value I.

It is now relevant to address the main issue with this method: generating configurations \mathbf{x}_i that are distributed according to $p(\mathbf{x})$ and then computing $f(\mathbf{x}_i/p(\mathbf{x}_i))$. When it is possible to directly generate samples from $p(\mathbf{x})$ we are employing **direct MC sampling**, this is possible if we are using a uniform or exponential distribution (or other similar simple distributions). The samples generated with this method are independent, but we are limited in the type of distribution that can be used, which could make the convergence to the exact value extremely slow.

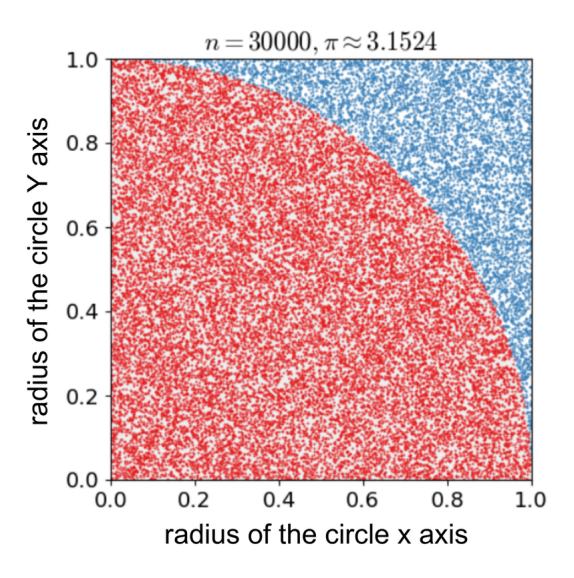


Figure 3.1: Graphical representation of π estimation using the simple direct Monte Carlo integration method.

The simplest way to show the direct sampling method for integrals is through the computation of π : suppose that we have a square of side 1 and, inside it, the quadrant of a circle (of radius 1). It is known from high school geometry that:

$$\frac{\pi}{4} = \frac{1}{4} \frac{\pi(1)^2}{(1)^2} = \frac{1}{4} \frac{A_{\text{quadrant}}}{A_{\text{square}}},\tag{3.22}$$

from which it follows that we can compute the value of π from the ratio between the two areas. We now express the areas in terms of integrals

$$\frac{\pi}{4} = \frac{\int_{\text{circle}} dx dy}{\int_{\text{square}} dx dy} = \int_{\text{square}} f(x, y) p(x, y) dx dy, \tag{3.23}$$

with

$$p(x,y) = \frac{1}{\int_{\text{square}} dx dy} \tag{3.24}$$

and f(x, y) defined in the following way:

$$f(x,y) = \begin{cases} 1, & \text{if } \sqrt{x^2 + y^2} < 1\\ 0, & \text{otherwise.} \end{cases} \tag{3.25}$$

Since p(x,y) is non-negative and normalized, it can be treated as a probability distribution. We can thus say that

$$\frac{\pi}{4} \approx \frac{1}{N} \sum_{i=1}^{N} f(x_i, y_i),$$
 (3.26)

the obtained result can be interpreted visually considering that we are filling the total area of the square with randomly distributed dots and counting how many of them end inside the circle compared to the total.

This simple method can be used (at least in theory) to compute every possible integral, nevertheless using a uniform distribution may result impractical when estimating functions that have sharp peaks: in this case most of the guesses made end up "outside" the region of interest and do not contribute to the estimation of the integral. Of course, this problem becomes more and more relevant the more dimensions we have.

In these cases, it is appropriate to use as a probability function that has a similar shape with respect to the target function we want to integrate, consider the following one-dimensional case:

$$I = \int_{a}^{b} f(x)dx,\tag{3.27}$$

where f(x) has a sharp peak in a limited interval between a and b and is close to 0 everywhere else. Operating in the same way as before we obtain the following expression:

$$I = \int_a^b \frac{f(x)}{p(x)} p(x) dx,$$
(3.28)

and we can approximate the integral as

$$I \approx I_N = \frac{1}{N} \sum_{i=1}^{N} \frac{f(x_i)}{p(x_i)},$$
 (3.29)

while the variance of our estimation is found as

$$s^{2} = \frac{1}{N} \sum_{i=1}^{N} \left[\frac{f(x_{i})}{p(x_{i})} \right]^{2} - \left[\frac{1}{N} \sum_{i=1}^{N} \frac{f(x_{i})}{p(x_{i})} \right]^{2},$$
 (3.30)

analyzing the expression for the variance estimator it becomes clear that it is minimized if p(x) is chosen to be as close as possible to the target function f(x), with the best result $s^2 = 0$ obtained for p(x) = cf(x) (which would mean that it is possible to analytically integrate f(x)).

This means that with a careful choice of the probability distribution it is possible to minimize the statistical fluctuations of our estimate and thus obtain the same accuracy with a smaller number of samples N.

Since multiple algorithms have been studied in order to build pseudonumber generators in the interval (0,1) that are efficient, provide long periods for sequences of values and have uniform distribution in n-dimensional spaces (for example the Mersenne-Twister algorithm, used in this thesis [35]), it is important to find ways to sample from other more complex (continuous) distributions p(x), the easiest way to do so is through **CDF inversion** (cumulative density function inversion), which, as the name suggests, can be used when the analytical form of the cumulative distribution P(x) is known.

Choosing for example the exponential distribution

$$\exp(x;\lambda) = \lambda e^{-\lambda x} \qquad \text{for } x > 0, \tag{3.31}$$

for which we can obtain the expression for the cumulative density function easily:

$$P(x) = \int_0^x \lambda e^{-\lambda x} dx = 1 - e^{-\lambda x}.$$
 (3.32)

We now solve for x to obtain

$$x = -\frac{1}{\lambda} \log (1 - P(x)). \tag{3.33}$$

Since by definition the image of P(x) is [0,1], we can substitute it in the equation with the standard uniform random variable defined in [0,1] r:

$$x = -\frac{1}{\lambda} \log (1 - r),$$
 (3.34)

and we obtain a random variable x that follows the exponential distribution $p(x; \lambda)$.

3.4 Markov Chain Monte Carlo

The procedure illustrated in the previous section only works when an analytical expression for the cumulative distribution exists, this is not true in general and a different method is thus needed for a general distribution p(x). To this scope **Markov chains** are used.

Let us define the random vector X as a sequence of n random samples that are drawn one after the other:

$$\mathbf{X} = (X_1, X_2, ..., X_n), \tag{3.35}$$

we call this vector an uncorrelated chains if each one of the variables x_i are independent and thus uncorrelated, the probability of obtaining the chain \mathbf{X} is then given by the product of the individual elements of the chain:

$$P_n(\mathbf{X}) = P_1(X_1)P_2(X_2)\cdots P_n(X_n).$$
 (3.36)

In a Markov chain this is not true and the random samples are correlated: a sequence of samples is said to be Markovian if the conditional probability of each sample of the sequence satisfies

$$P(X_i|X_{i-1}...X_1) = P(X_i|X_{i-1}). (3.37)$$

This means that the probability of X_i only depends on the previous element X_{i-1} (and nothing else), with the exception of the first element of the chain. From this it follows that the order of the variables is important in the determination of the probability of the full random vector:

$$P_n(X_1, X_2, ..., X_n) = P_1(X_1)P(X_2|X_1) \cdots P(X_n|X_{n-1})$$
(3.38)

where $P(X_i|X_{i-1})$ is the transition probability from X_{i-1} to X_i . We define $p_i^{(1)}$ ($\sum_i p_i^{(1)} = 1$) the initial probability and $P(X_i|X_j) = P_{ij}$ the transition probability from j to i. The transition probabilities are normalized for each j such that $\sum_i P_{ij} = 1$, in this way for every k step $\sum_k p_i^{(k)} = 1$ is obtained (note that, in continuous distribution, the sum is replaced by an integral).

Apart from the (obvious) normalization constraint, the single probabilities $p_i^{(k)}$ at the step k (which are steps in time) are in general different from the probabilities $p_i^{(k-1)}$, the important mathematical result that is obtained under very general assumptions is that, after a necessary relaxation time that is different from system to system, the distribution relaxes to a stationary state p_i which satisfies the relation

$$p_i = \sum_j P_{ij} p_j \tag{3.39}$$

for every k step in the simulation.

The conditions required for this to happen are:

- **connectedness**: every configuration of the distribution that we want to obtain must be accessible from any other configuration of the system in a finite number of steps.
- **no periodicity**: which means that, after having visited a specific configuration, it must be false that the same configuration will be accessible again only after nk steps with n positive integer and k fixed.

A Markov chain that satisfies these two conditions is called **ergodic** [5].

Since the objective is to obtain a target stationary distribution p_i , we need a mean to do so starting from a more generic distribution (such as the uniform distribution in [0,1]), which means that a specific expression for the transition probabilities P_{ij} is needed. The solution proposed by Metropolis [36] is to require the following relation for the transition probability P_{ij} to be true:

$$P_{ij}p_j = P_{ii}p_i, (3.40)$$

which is the **detailed balance condition**. This means that the probability of transitioning from j to i is the same as the probability of transitioning from i to j. This relation can be demonstrated using the **Master equation**:

$$p_i^{(k)} - p_i^{(k-1)} = -\sum_j P_{ji} p_i^{(k-1)} + \sum_j P_{ij} p_j^{(k-1)}, \tag{3.41}$$

the stationary condition is obtained for

$$p_i^{(k)} = p_i^{(k-1)} = p_i, (3.42)$$

From this it follows that

$$\sum_{j} P_{ji} p_i = \sum_{j} P_{ij} p_j, \tag{3.43}$$

for every i, j pair.

An obvious solution to this equation is found if 3.40 holds.

We now recast the transition probability matrix P_{ij} in the form

$$P_{ij} = T_{ij}A_{ij}, (3.44)$$

where T_{ij} is the symmetric matrix $(T_{ij} = T_{ji})$ of the trial transition proposal probabilities with the additional properties $0 \le T_{ij} \le 1$ and $\Sigma_i T_{ij} = 1$, while A_{ij} are the elements of the acceptance matrix, whose form is

$$A_{ij} = \min\left\{1, \frac{p_i}{p_j}\right\} \qquad i \neq j. \tag{3.45}$$

Using this configuration we can show that the condition of detailed balance is obeyed by assuming $p_i < p_j$ (we are not posing any constraint on the system by doing this since the choice of the indices is arbitrary) and observing that

$$P_{ij} = T_{ij} \frac{p_i}{p_j} = T_{ji} \frac{p_i}{p_j} = T_{ji} \cdot 1 \cdot \frac{p_i}{p_j} = P_{ji} \frac{p_i}{p_j},$$
(3.46)

from which 3.40 follows.

The complete algorithm, known as the **Metropolis algorithm**, proposes a new i state given the present j with trial transition probability T_{ij} , then uses the A_{ij} elements of the acceptance matrix to accept i or reject it (and thus keep j). Whether the new i state is accepted or rejected depends on the uniform random variable defined in [0,1] r: if $r < A_{ij}$ i is accepted, otherwise it is rejected.

Algorithm 3 Metropolis algorithm.

```
Input: Proposal probability T, limiting distribution p, configuration j.

Sample an i from T_{ij};

Generate a uniform random number \zeta \in [0, 1];

if \zeta \leq p_i/p_j then

j \leftarrow i;

end if

return j.
```

Figure 3.2: Schematic representation of the Metropolis algorithm procedure [5].

It is possible to generalize the algorithm to one that does not have a symmetric trial transition probability matrix T_{ij} : given a generic acceptance ratio R_{ij} such that $A_{ij} = \min\{1, R_{ij}\}$ defined as

$$R_{ij} = \frac{S_{ij}}{1 + \frac{T_{ij}p_j}{T_{ji}p_i}},\tag{3.47}$$

with S_{ij} non-negative symmetric matrix, if S_{ij} is chosen to be:

$$S_{ij} = \begin{cases} 1 + \frac{T_{ji}p_i}{T_{ij}p_j}, & T_{ij}p_j \ge T_{ji}p_i, \\ 1 + \frac{T_{ij}p_j}{T_{ji}p_i}, & T_{ji}p_1 \ge T_{ij}p_j, \end{cases}$$
(3.48)

the **Metropolis-Hasting algorithm** is obtained with acceptance ratio R_{ij} :

$$R_{ij} = \frac{T_{ji}p_i}{T_{ij}p_i}. (3.49)$$

In the special case where we want to obtain a random variable X distributed as a generic continuous function f(x) (not necessarily normalized) using as a prior distribution a known distribution h(x), we may identify the trial transition probability from a state x to a state x' with

$$T_{x'x} = \pi(x')dx \tag{3.50}$$

independent on the current state x, the acceptance ratio $R_{x'x}$ then becomes

$$R_{x'x} = \frac{T_{xx'}p_{x'}}{T_{x'x}p_x} = \frac{\pi(x)dxf(x')dx}{\pi(x')dxf(x)dx} = \frac{\pi(x)f(x')}{\pi(x')f(x)},$$
(3.51)

with acceptance probability $A_{x'x}$:

$$A_{x'x} = \min\left\{1, \frac{\pi(x)f(x')}{\pi(x')f(x)}\right\}. \tag{3.52}$$

Using the above formulation (easily generalizable at least in theory to N dimensions) it is possible to sample random variables from any generic continuous unnormalized function. The main drawbacks of this method are the fact that a relaxation to the stationary distribution is necessary (and the number of steps required is not known a priori) and that the obtained samples are correlated.

3.5 Diagrammatic Quantum Monte Carlo

In Chapter 2 we have seen that the polaron model can be solved by perturbatively expanding the related Green's function (which is a solution to the equation of motion of the system) in the imaginary time formalism. Since the Green's function in this formalism can be cast in a form that makes it real and non-negative, it can be sampled as if it were a distribution using the methods provided by Markov Chain Monte Carlo.

To this objective, we need a method to ergodically represent all the possible configurations of the polaron system. This approach can be used in many different condensed matter physics systems where a similar expansion is possible, provided that the weight of negative diagrams (which in our specific case do not appear, but are generally present in fermionic systems) does not hinder the accuracy of the estimated quantity [37].

Given a function represented as 2.75 (without the minus sign) it is possible to sample it as a distribution $Q(\{y\})$ which depends on a set of variable y:

$$Q(\{y\}) = \sum_{n=0}^{+\infty} \sum_{\xi_n} \int dx_1 \cdots \int dx_n D_n(\xi_n, y, x_1, ..., x_n),$$
 (3.53)

with $\{y\}$ external variables and $\{x_i\}$ internal variables (to be integrated out).

Using the Metropolis-Hastings algorithm it is possible to sample variables from this distribution and in the limit of a large number of samples retrieve the full function up to a normalization constant \mathcal{C} with no approximations:

$$Q_i(\{y\}) = C \ G(\mathbf{k}, \tau). \tag{3.54}$$

The fundamental difference with respect to an usual Monte Carlo integration is the fact that the parameter space of internal variables varies between different iterations of the simulation: ways to model transitions between these different states together with the correct trial transition probability are required.

In order to do so, a number of elementary updates are defined such that there are at least enough to satisfy the ergodicity requirement [5] for the Markov chain which relaxes to the target distribution (the system under study). The Metropolis-Hastings algorithm in DMC uses as acceptance probabilities for transitions between two different states characterized by the variables $i=\{y_i,\xi_i,\mathbf{x}_i\}$ and $i=\{y_j,\xi_j,\mathbf{x}_j\}$ respectively the relative weight of the two diagrams.

In fact, given the two diagrams $D_{n_i}(i)$ and $D_{n_j}(j)$ (which may be different in the value of one or more variables, whether internal or external, and more importantly in the *number* of internal variables if the rank of the two diagrams is different), the acceptance ratio R_{ij} is proportional to:

$$R_{ij} \propto \frac{D_{n_i}(i)}{D_{n_i}(j)} = \frac{C \ D_{n_i}^*(i)}{C \ D_{n_i}^*(j)} = \frac{D_{n_i}^*(i)}{D_{n_i}^*(j)},$$
 (3.55)

where the $D_{n_k}^*(k)$ are the properly normalized weights, different from the weights of the generated distribution up to a normalization constant [6].

When negative-valued diagrams are present, the acceptance ratio is performed on the absolute values of the weights. Operating in this way, however, we expose ourselves to the **negative sign problem**: when we want to compute an observable O from the Monte Carlo simulation, whether it be the (normalized) distribution or any other quantity of interest, we must take into account the negative weights:

$$O = O_N = \left(\frac{1}{N} \sum_{i=1}^{N} |O_i(D(i))|\right) \left(\frac{N^+ - N^-}{N}\right)^{-1} = \frac{1}{N^+ - N^-} \sum_{i=1}^{N} |O_i(D(i))|, \quad (3.56)$$

and the variance of the Monte Carlo estimate diverges for $N^+ - N^- \approx 0$. Two basic classes of elementary updates can be recognized [38][29]:

- class I updates: they change one or more variables (internal or external), the new variables \mathbf{x} are proposed using a suitable distribution $\pi(\mathbf{x})$ (some distribution might be more suited than others depending on the specific system), and the acceptance ratio is computed using the standard Metropolis-Hastings algorithm (3.49 and 3.51 depending on the type of variable and prior distribution)
- class II updates: in this class of updates the order of the diagram is changed, and thus the number of internal variables is increased or reduced. Considering an update where the order of the diagram is increased, the new m internal variables are sampled from a distribution $\rho(\mathbf{x})$ and the acceptance ratio R_{ij} is computed as follows:

$$R_{ij} = \frac{p_A}{p_B} \frac{D_{n_i = n_j + m}(i)}{\rho(x_1, ..., x_n) D_{n_j}(j)},$$
(3.57)

where p_A and p_B are the so-called **context factors** that take into account the ways it is possible to transition from state A to state B and thus depend on how the processes are organized (it does not usually reduce to the simple relation $p_A/p_B=1$) [33]. The opposite process which reduces the order of the diagram from n to n-m is found to be

$$R_{ji} = \frac{1}{R_{ij}},\tag{3.58}$$

in agreement with the detailed balance requirement.

Employing these rules and carefully crafting prior distributions and acceptance ratios, it is possible to sample a distribution that is equal up to a normalization constant a Green's function in imaginary time formalism, provided that it can be expanded in a similar way to 2.74.

```
Input: initial configuration X^{(0)} = (\{y\}; \xi_n, x_1, \dots, x_n)
          update procedures \{U_1, \ldots, U_k\}
Output: histogram of Q(\{y\})
histogram[];
start from initial diagram \mathcal{D} \leftarrow X^{(0)};
while not enough samples do
    choose an update U_i from \{U_1, \ldots, U_k\};
    propose a new configuration X' = (\{y'\}; \xi_{n'}, x_{1'}, \dots, x_{n'}) according to U_i;
    calculate acceptance ratio R;
   if R \geq 1 then
     \mathcal{D} \leftarrow X';
   else
        draw random uniform number r;
        if r \leq R then
         \mathcal{D} \leftarrow X';
    end
   histogram[{y}].add(1);
end
return histogram;
```

Figure 3.3: Diagrammatic Monte Carlo algorithm procedure [6].

The specific updates, however, greatly vary between different systems considering issues such as ergodicity requirements, context factors and the sign problem.

4 Diag MC for the Froehlich Polaron

In Chapter 2 we have seen that it is possible to perturbatively expand the Matsubara Green's function for the Froehlich polaron in a series of integrals 2.5, while in chapter 3 we have shown that series of this type can be computed using a special type of Markov chain Monte Carlo called Diagrammatic Monte Carlo which is able to take into account all the possible perturbative expansions of the full function and sample from it.

We now focus on the specific Diagrammatic Monte Carlo technique employed for the Froehlich Polaron case. Let us consider the Froehlich Hamiltonian H^{cFr} in the specific case of a single anisotropic electron band and multiple phonon modes. We take into account the non-interacting term

$$H_0^{cFr} = \sum_{\mathbf{k}} \left(\frac{k^2}{2m(\hat{k})} - \mu \right) c_{\mathbf{k}}^{\dagger} c_{\mathbf{k}} + \sum_{\mathbf{q}j} \omega_{jLO} a_{\mathbf{q}j}^{\dagger} a_{\mathbf{q}j}, \tag{4.1}$$

where we consider only the electron polaron (the only difference in the hole polaron case would be negative electron energy dispersion). The chemical potential μ is put inside the electron term as a renormalization constant (**fictitious potential renormalization** [29][33]) which can be tuned in order to obtain a non-divergent distribution that decays as an exponential for long τ in the stationary limit.

The interaction term reads:

$$V^{cFR} = \sum_{\mathbf{k},\mathbf{q}j} c_{\mathbf{k}+\mathbf{q}}^{\dagger} c_{\mathbf{k}} \left(V_{\mathbf{q}j}^{cFr} a_q + V_{\mathbf{q}j}^{*cFr} a_{-\mathbf{q}}^{\dagger} \right), \tag{4.2}$$

where the interaction vertex V^{cFr} has formula

$$V^{cFr}(qj) = \frac{i}{q} \left(\frac{2\sqrt{2}\pi}{\Omega_0 V_{BvK}} \frac{\omega_{jLO}^{3/2}}{m(\hat{\mathbf{q}})^{1/2}} \alpha(\hat{\mathbf{q}}) \right)^{1/2}.$$
 (4.3)

We need a technique to translate the Green's functions defined in chapter 2 to the formalism of Diagrammatic Monte Carlo. To this aim we identify the stationary distribution $Q(\{y\})$ with the two Green's functions of interest: the one-electron Green's function $G(\mathbf{k},\tau)$, where no external phonon lines are present:

$$G(\mathbf{k},\tau) = \sum_{n=0,2,4,\dots}^{+\infty} \sum_{\xi_n} \int d\tau_1 \cdots \int d\tau_n \int d\mathbf{q}_1 \frac{V_{q_1 j_1}}{(2\pi)^3} \cdots \int d\mathbf{q}_{n/2} \frac{V_{q_{n/2} j_{n/2}}}{(2\pi)^3} \times D_n^{\xi_n}(\mathbf{k},\tau;\tau_1,\dots,\tau_n,\mathbf{q}_1,\dots,\mathbf{q}_{n/2},j_1,\dots,j_{n/2}),$$
(4.4)

and $P(\mathbf{k}, \tau)$, a function that is the sum of the single electron Green's function and all the possible one-electron N-phonons Green's function configurations (weighted accordingly):

$$P(\mathbf{k},\tau) = G(\mathbf{k},\tau) + \sum_{N=1}^{+\infty} G^{(N)}(\mathbf{k}\tilde{\mathbf{q}}_1,...,\tilde{\mathbf{q}}_N, j_1,...,j_N,\tau),$$
(4.5)

where $G^{(N)}(\mathbf{k}, \tau)$ is diagrammatically expanded in

$$G^{(N)}(\cdots) = \sum_{\xi_n} \int d\tau_1 \cdots \int d\tau_n \int d\mathbf{q}_1 \frac{V_{q_1 j_1}}{(2\pi)^3} \cdots \int d\mathbf{q}_{n/2} \frac{V_{q_{n/2} j_{n/2}}}{(2\pi)^3} \times D_n^{\xi_n}(\mathbf{k}, \tilde{\mathbf{q}}_1, ..., \tilde{\mathbf{q}}_N, \tilde{j}_1, ..., \tilde{j}_N, \tau; \tau_1, ..., \tau_n, \mathbf{q}_1, ..., \mathbf{q}_{n/2}, j_1, ..., j_{n/2}).$$
(4.6)

It is now important to distinguish between external variables y and the internal ones $\{x_1, ..., x_n\}$. We identify them as

$$\{y\} \to \{\mathbf{k}, \tilde{\mathbf{q}}_{1}, \tilde{j}_{1}, ..., \tilde{\mathbf{q}}_{N}, \tilde{j}_{N}, \tau\},
n \to \{0, 2, 4, ...\},
\{x_{1}, ..., x_{n}\} \to \{\tau_{1}, ..., \tau_{n}, \mathbf{q}_{1}, j_{1}, ..., \mathbf{q}_{n/2}, j_{n/2}\}.$$
(4.7)

The algorithm that computes our simulation must satisfy the ergodicity requirement of Markov chain Monte Carlo: for this reason it is necessary to implement updates that change the external variables $\{y\}$, the internal ones $\{x_i\}$, and the order of the diagram n.

We start by saying that no updates have been implemented in order to sample from the free electron momentum \mathbf{k} , which will be fixed for each individual simulation: this was made in order to have a more precise control about the region of k-space that we want to simulate, in particular the $\mathbf{k}=0$ point where the electron is at the bottom (top) of the conduction (valence) band.

The chemical potential μ is also implemented in the simulations as a normalizing factor, in this way a free electron propagator becomes:

$$G_0(\mathbf{k}, \tau) \to G_0(\mathbf{k}, \mu, \tau) = e^{-(\epsilon(\mathbf{k}) - \mu)\tau},$$
 (4.8)

the effect of which can be easily reversed by rescaling the result.

Due to the finite memory of computers, it is then necessary to fix for each simulation a maximum imaginary time value τ_{max} , a maximum internal order n_{max} (the number of internal phonon propagators would be $n_{max}/2$) and a maximum number of external phonon propagators N_{max} .

Having decided this, it is then necessary to state the electron effective mass on the three main axes m_x^* , m_y^* and m_z^* together with the number of phonon modes that couple to the electron band n_{ph} together with their energy ω_{jLO} and their phonon mode polarities p_j or another equivalent quantity from which their value can be recovered [21].

Other quantities that needs to be specified are the size of the unit cell Ω_0 , the size of the Bornvon Karman cell V_{BvK} , the optical dielectric tensor (a scalar in the case of cubic materials) ϵ_{∞} , the number of thermalization steps N_{relax} set to achieve the stationary distribution condition and the number of simulation steps N_{steps} .

It is now important to define how the diagram was effectively modelled in the computer: to this aim three data structures were defined. The **Vertex**: this data structure encapsulates all

the data which describes the vertices of the electron-phonon interaction (also the diagram beginning and end) together with all the relevant information about the associated phonon propagator, its components are:

- τ_i , the imaginary time value of the vertex, 0 and τ for the extrema
- type, integer parameter which differentiates between extrema (0), internal phonon vertices (+1 for outgoing phonon propagators and -1 for incoming ones), external phonon vertices (+2 for outgoing phonon propagators and -2 for incoming ones).
- **linked**, integer value which shows to which other vertex the current vertex is linked to, and thus the length of the phonon propagator (whether we have an internal or external one).
- \mathbf{q}_i , the three momentum components of the free phonon propagator which is created or annihilated at the vertex.
- **index**, the phonon mode which is involved in the electron-phonon interaction at the vertex.

The **Propagator**: this data structure represents the free electron propagators, it is defined by the three electron momentum components \mathbf{k}_i .

The **Effective_Mass**: this data structure represents the effective mass $m_i^*(\hat{k})$ of the electron for each electron propagator \mathbf{k}_i , it is computed using the formula in 1.80.

At the start of each simulation, an array of dimension $n_{max}+2N_{max}+2$ of Vertex data type is created, while an array of dimension $n_{max}+2N_{max}+1$ is created for the Propagator and Effective_Mass data type. At the beginning of the simulation all the single elements of the three data types are initialized to default values with the exception of the first 2 Vertex elements and the first Propagator and Effective_Mass element: the latter two are initialized using the ${\bf k}$ value given as input and by computing the related effective mass (default to 1 in the case that ${\bf k}=0$), while the τ values of the first two Vertex elements are initialized to 0 and τ respectively, where τ is retrieved using the **Diagram Length** update, which will be explained in detail in the following section.

4.1 Updates

Updates are necessary to obtain a Markov chain for the system which is ergodic, there is no single way to implement them in order to achieve this aim and different choices have been proposed about the way new parameters are proposed and how updates are implemented [29][31], here it is thus shown just a proposal that is sufficient but is nevertheless not necessarily the best or fastest choice.

The first update that is described is the **Diagram Length** update (class I), which updates the length of the last electron propagator: it thus changes the value of the external variable τ .

Since the last electron propagator is a free electron propagator, which decays exponentially with τ as

$$G_0(\mathbf{k}, \tilde{\mathbf{q}}_1, ..., \tilde{\mathbf{q}}_N, \tau) = \exp\left\{-\left(\frac{p^2}{2m^*(\hat{p})} - \sum_j \omega_{jLO} n_{jph} - \mu\right) (\tau - \tau_{last})\right\}, \tag{4.9}$$

with τ_{last} time of last vertex before the diagram end, we have:

$$\mathbf{p} = \mathbf{k} - \sum_{i=0}^{N} \tilde{\mathbf{q}}_{i},$$

$$\sum_{j} n_{jph} = N,$$
(4.10)

with N total number of external phonons in the current diagram and j phonon mode index. The weight ratio between two diagrams with length τ and τ' thus becomes:

$$\frac{D_n(\cdots,\tau')}{D_n(\cdots,\tau)} = \frac{e^{-\Delta E(\tau'-\tau_{last})}}{e^{-\Delta E(\tau-\tau last)}},\tag{4.11}$$

where ΔE is the computed energy in 4.9.

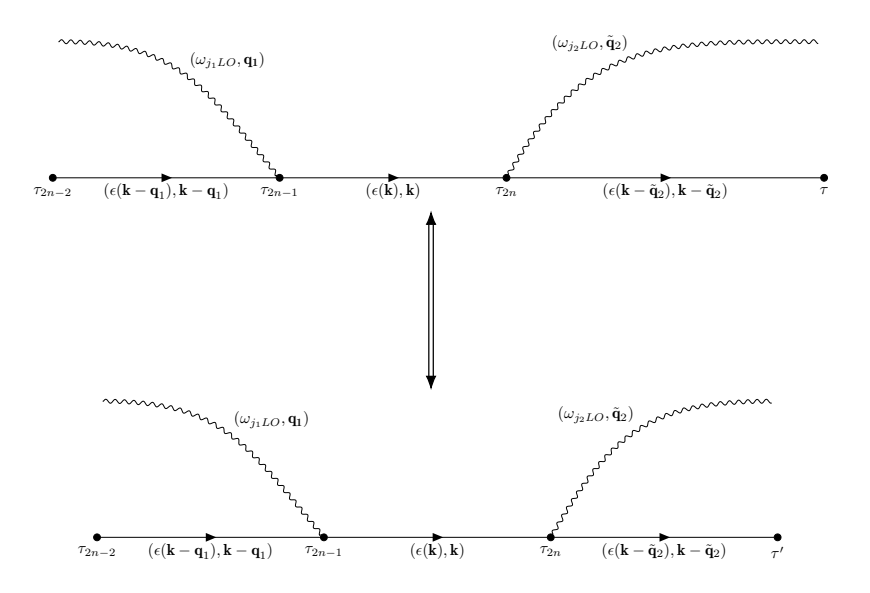


Figure 4.1: Diagram length update.

If we thus take an exponential distribution as the proposal distribution for new values of the imaginary time value τ' built as follows

$$\tau' = \tau_{last} - \frac{\log(1-r)}{\Delta E},\tag{4.12}$$

with r uniform random variable in [0,1] we obtain a new value that is always accepted apart from the case where $\tau' > \tau_{max}$. In fact the acceptance ratio is

$$R_{\tau'\tau} = \frac{\exp\left(\tau; \tau_{last}, \Delta E\right) e^{-\Delta E(\tau' - \tau_{last})}}{\exp\left(\tau'; \tau_{last}, \Delta E\right) e^{-\Delta E(\tau - \tau_{last})}} = \frac{\Delta E e^{-\Delta E(\tau - \tau_{last})} e^{-\Delta E(\tau' - \tau_{last})}}{\Delta E e^{-\Delta E(\tau' - \tau_{last})} e^{-\Delta E(\tau - \tau_{last})}} = 1, \tag{4.13}$$

which is always accepted.

The next update to be described is the **add internal phonon**, a class II update. The new (internal) variables that have to be proposed are the time value of the outgoing vertex τ' , the time value of the incoming vertex τ'' , the phonon mode index j and the phonon propagator momentum ${\bf q}$. If proposing the diagram means that $n+2>n_{max}$ maximum allowed internal order is true, then the update is rejected.

An electron propagator (from the first one to the last for a total of n+1 possible choices) is chosen at random, then the value of τ' is generated using a uniform distribution between τ_{left} and τ_{right} vertices of the chosen free electron propagator.

The phonon mode j is then chosen at random between the ones given in input, and the value of the second vertex of the phonon propagator τ'' is generated using the following exponential distribution

$$P(\tau''|\tau',j) = \tau' - \frac{\log(1-r)}{\omega_{jLO}},$$
 (4.14)

where τ'' is not restrained to any particular free electron propagator. The update is straight-up rejected if $\tau'' > \tau$ length of the full diagram or if it is too close to another vertex ($|\tau'' - \tau_i| < 10^{-9}$).

The phonon momentum values \mathbf{q} are then proposed using a probability $P(\mathbf{q}|\tau',\tau'',j)$ dependent on a gaussian distribution with mean 0 and variance $(\tau''-\tau')^{-1}$.

The ratio of the two diagrams is

$$\frac{D_{(n+2)}(\mathbf{k}, \tau, \dots, \tau', \tau'', \mathbf{q}, \dots)}{D_n(\mathbf{k}, \tau, \dots)} =$$

$$= \exp \left\{ -\left(\sum_i \epsilon(\mathbf{k}_i - \mathbf{q}) - \epsilon(\mathbf{k}_i) \Delta \tau_i - \omega_{LO}(\tau'' - \tau') \right) \right\} |V_{\mathbf{q}j}|^2 d\tau' d\tau'' \frac{\Omega_0}{(2\pi)^3} d\mathbf{q}, \tag{4.15}$$

where the sum over i is extended over all the phonon propagators between the two phonon vertices τ' and τ'' , while $\Delta \tau_i$ is computed as $\tau_i - \tau_{i-1}$ where the two extrema are τ' and τ'' . The infinitesimals are required because they are not cancelled in the ratio since they are new proposed variables.

The full distribution from which the new values are sampled is written as

$$P(\tau', \tau'', \mathbf{q}, j) = P(\tau')P(\tau''|\tau', j)P(\mathbf{q}|\tau', \tau'', j) = \frac{1}{\tau_{right} - \tau_{left}} \underbrace{\omega_{jLO}e^{-\omega_{jLO}(\tau''-\tau')}}_{P(\tau''|\tau', j)} \underbrace{\left(\frac{\tau'' - \tau'}{2\pi}\right)^{3/2} e^{-\frac{q^2}{2}(\tau''-\tau')}}_{P(\mathbf{q}|\tau', \tau'', j)}.$$
(4.16)

The acceptance ratio thus becomes:

$$R_{add} = \frac{p_A}{p_B} \frac{D_{n+2}(\mathbf{k}, \tau, ..., \tau', \tau'', \mathbf{q}, ...)}{D_n(\mathbf{k}, \tau, ...) P(\tau', \tau'', \mathbf{q}, j)},$$
(4.17)

the context factors p_A and p_B take into account the number of free electron propagators from which a vertex can be generated and the total number of internal phonon propagators which can be removed, their ratio is

$$\frac{p_A}{p_B} = \frac{p_{(rem \, int)}}{p_{(add \, int)}} \frac{n + 2N + 1}{n/2 + 1},\tag{4.18}$$

for example at order n=2 and 1 external phonon we can choose from $2+2\cdot 1+1=5$ electron propagators, while to go back to order 2 from order n+2=4 we can choose between 2/2+1=2 phonon propagators. The two variables $p_{(rem\ int)}$ and $p_{(add\ int)}$ measure the probability of choosing the add internal and remove internal updates in the main Monte Carlo simulation.

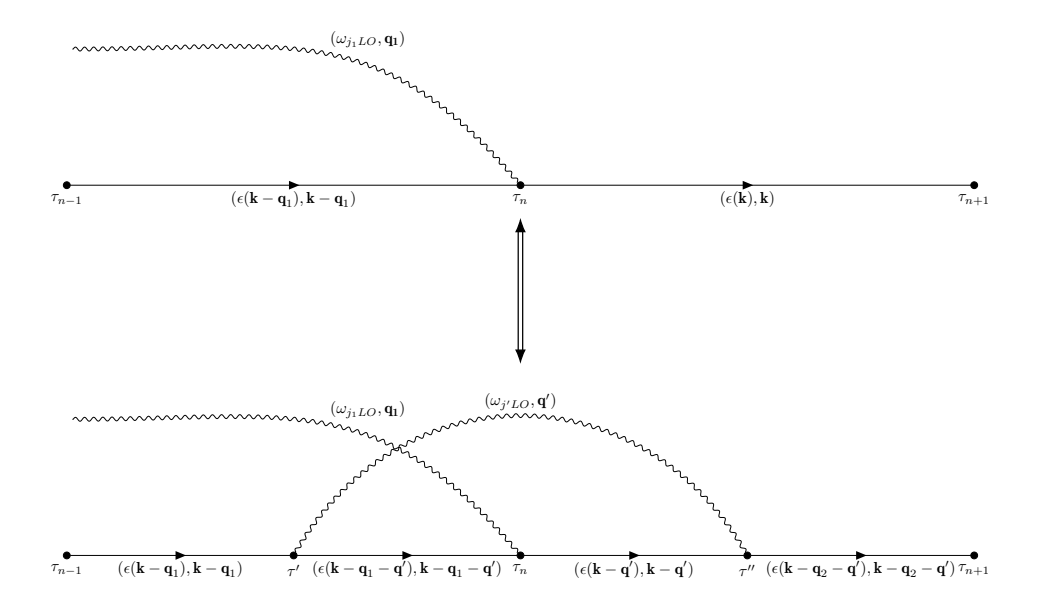


Figure 4.2: Diagram add/remove internal phonon update.

The **remove internal phonon** is also a class II update, no new parameters are proposed but instead a random internal phonon propagator with vertices at τ' and τ'' and momentum ${\bf q}$ is chosen to be removed. The update is automatically rejected if it is true that the internal order n=0 and is accepted with acceptance ratio $R_{rem}=1/R_{add}$ calculated for the add internal phonon update.

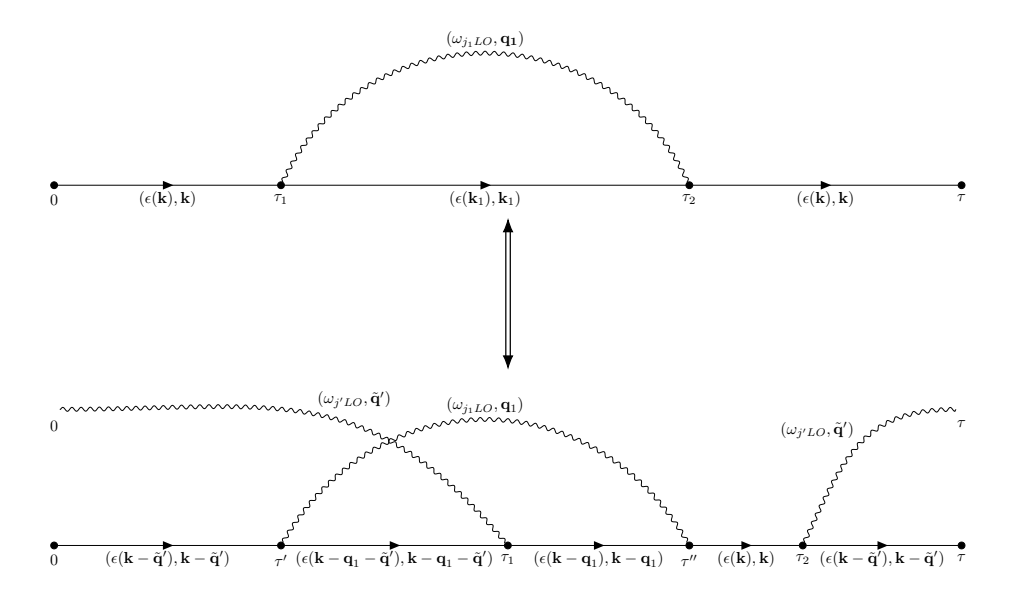


Figure 4.3: Diagram add/remove external phonon update.

Another necessary update to implement is the **add external phonon** update, a class II update which adds an external phonon to the current diagram, if the number of external phonon propagators is already N_{max} the update is automatically rejected.

The new variables that need to be proposed are the time values of the vertices τ' and τ'' , the phonon mode index j and the phonon momentum $\tilde{\mathbf{q}}$. After having chosen the proposed phonon mode index j we want to write the full probability as:

$$P(\tau', \tau'', \tilde{\mathbf{q}}, j) = P(\tau'|j)P(\tau''|j)P(\tilde{\mathbf{q}}|\tau', \tau'', j),$$
 (4.19)

in order to do so we choose the following proposal distribution for τ' :

$$\tau' = 0 - \frac{\log(1-r)}{\omega_{iLO}},$$
 (4.20)

where r is a uniform random variable in [0,1], if a value of $\tau'>\tau$ length of the current diagram is chosen the update is rejected. For τ'' the following similar exponential distribution is used

$$\tau'' = \tau + \frac{\log\left(1 - r\right)}{\omega_{jLO}},\tag{4.21}$$

if $\tau''<0$ the update is directly rejected. The update is also rejected if any of the two values τ' and τ'' lie too close to any other vertex $|\tau',\tau''-\tau_i|<10^{-9}$. New values for the momentum $\tilde{\mathbf{q}}$ are then proposed using the normal distribution with mean 0 and variance $1/(\tau-\tau''+\tau')$,

which takes into account the imaginary time length of the external phonon propagator. The full probability thus becomes:

$$P(\tau', \tau'', \tilde{\mathbf{q}}, j) = P(\tau'|j)P(\tau''|j)P(\tilde{\mathbf{q}}|\tau', \tau'', j) =$$

$$= \underbrace{\omega_{jLO}e^{-\omega_{jLO}\tau'}}_{P(\tau'|j)}\underbrace{\omega_{jLO}e^{-\omega_{jLO}\tau''}}_{P(\tau''|j)}\underbrace{\left(\frac{\tau - \tau'' + \tau'}{2\pi}\right)^{D/2}}_{P(\mathbf{q}|\tau', \tau'', j)} e^{-\frac{\tilde{\mathbf{q}}}{2}(\tau - \tau'' - \tau')}. \tag{4.22}$$

It is now important to evaluate the ratio of the two diagrams, two different cases are possible:

- $\tau' < \tau''$, in this case the internal part of the two diagrams is the same
- $\tau' > \tau''$, here the two diagrams are completely different, in particular the free electron propagators all have different momenta.

Let us start with the first case, we have

$$\frac{D_{n+2}(\mathbf{k}, \tau, ..., \tau', \tau'', \tilde{\mathbf{q}}, ...)}{D_{n}(\mathbf{k}, \tau, ...)} =$$

$$= \exp \left\{ -\left(\sum_{i_{1}} \left[\epsilon(\mathbf{k}_{i_{1}} - \tilde{\mathbf{q}}) - \epsilon(\mathbf{k}_{i_{1}}) \right] \Delta \tau_{i_{1}} + \sum_{i_{2}} \left[\epsilon(\mathbf{k}_{i_{2}} - \tilde{\mathbf{q}}) - \epsilon(\mathbf{k}_{i_{2}}) \right] \Delta \tau_{i_{2}} \right) \right\}$$

$$\cdot \exp \left\{ \left(-\omega_{jLO}(\tau - \tau'' + \tau') \right) \right\} |V_{\tilde{q}j}|^{2} d\tau' d\tau'' \frac{\Omega_{0}}{(2\pi)^{3}} d\tilde{\mathbf{q}},$$
(4.23)

where i_1 indexes a sum over the propagators below τ' , i_2 one over the propagators above τ'' , and $\Delta \tau_{i_1}$, $\Delta \tau_{i_2}$ are computed in the same way as performed for the add internal phonon update (considering the boundaries for the two sums as τ' and τ'' respectively). In the second case, we instead have the expression

$$\frac{D_{n+2}(\mathbf{k}, \tau, ..., \tau', \tau'', \tilde{\mathbf{q}}, ...)}{D_{n}(\mathbf{k}, \tau, ...)} =$$

$$= \exp \left\{ -\left(\sum_{i_{1}} \left[\epsilon(\mathbf{k}_{i_{1}} - \tilde{\mathbf{q}}) - \epsilon(\mathbf{k}_{i_{1}}) \right] \Delta \tau_{i_{1}} + \sum_{i_{2}} \left[\epsilon(\mathbf{k}_{i_{2}} - \mathbf{q}) - \epsilon(\mathbf{k}_{i_{2}}) \right] \Delta \tau_{i_{2}} \right) \right\}$$

$$\cdot \exp \left\{ -\left(\sum_{i_{3}} \left[\epsilon(\mathbf{k}_{i_{3}} - 2\tilde{\mathbf{q}}) - \epsilon(\mathbf{k}_{i_{3}}) \right] - \omega_{jLO}(\tau - \tau'' + \tau') \right) \right\} |V_{\tilde{q}j}|^{2} d\tau' d\tau'' \frac{d\tilde{\mathbf{q}}}{(2\pi)^{3}},$$
(4.24)

where i_1 and i_2 run over the electron propagators below τ'' and over τ' respectively, with $\Delta \tau_{i_k}$ computed as before, while the sum over i_3 runs over the propagators between τ'' and τ' with

 $\Delta \tau_{i_3}$ defined in the same way as in the add internal phonon update. In both cases, the full expression for the acceptance ratio thus becomes:

$$R_{add} = \frac{p_A}{p_B} \frac{D_{(n+2)}(\mathbf{k}, \tau, \dots, \tau', \tau'', \tilde{\mathbf{q}})}{D_n(\mathbf{k}, \tau, \dots) P(\tau', \tau'', \tilde{\mathbf{q}}, j)}.$$
(4.25)

In this case the context factors are defined as such: when adding a phonon propagator no restriction on the position is made, and thus $p_B = p_{(add\; ext)} \cdot 1$, when removing it is possible to choose between N external phonons (or better N+1 considering that at the moment of the update the new one has not been accepted yet), and we have $p_A = p_{(rem\; ext)}(N+1)$. The acceptance ratio is then fully defined.

The **remove external phonon** update (class II) chooses an external phonon propagator at random (if they are not already 0, then it is automatically rejected) and removes it from the total diagram with acceptance ratio $R_{rem} = 1/R_{add}$ inverse of that of the add external phonon update. Besides that, no new variables are proposed.

The updates illustrated up to now are sufficient to obtain an ergodic simulation, nevertheless other 3 updates were implemented. The first one of these is the **swap phonon** update (class I): this update takes two adjacent internal phonon vertices and proposes to swap their phonon propagators, the update is automatically rejected if the two adjacent vertices belong to the same internal phonon propagator or they do not belong to two internal phonon propagators (for example an external one).

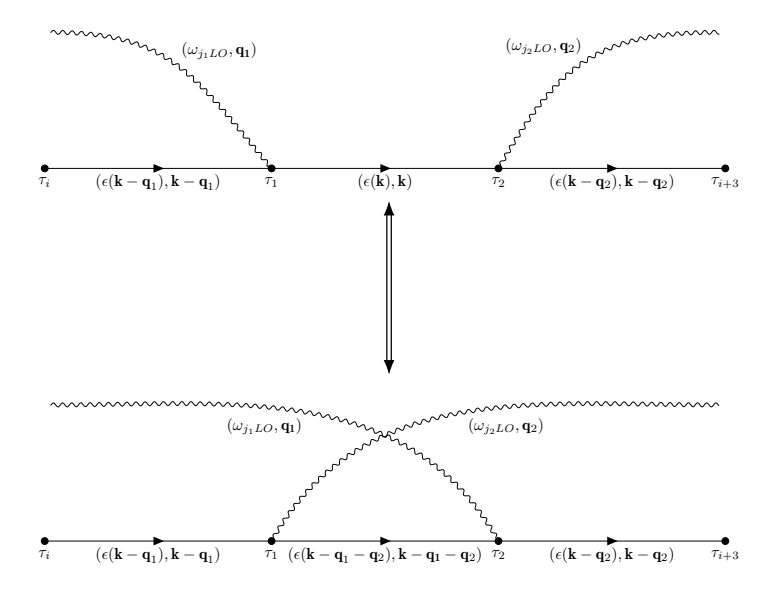


Figure 4.4: Diagram swap update.

Let us call the two phonon propagator that we want to swap 1 and 2. We have that the two phonon propagators have momentum \mathbf{q}_1 and \mathbf{q}_2 with energy ω_{j_1LO} and ω_{j_2LO} and imaginary

time τ_1 and τ_2 , given that the electron propagator between the two vertices has momentum \mathbf{k}_{el} we have that the acceptance ratio of the update is simply given by the ratio between the 2 diagrams:

$$R_{swap} = \frac{D_n^{\xi_n'}(\mathbf{k}, \tau, \dots)}{D_n^{\xi_n}(\mathbf{k}, \tau, \dots)} =$$

$$= \exp\left\{-\left(\epsilon(\mathbf{k}_{el} + c_1\mathbf{q}_1 - c_2\mathbf{q}_2) - \epsilon(\mathbf{k}_{el}) - \left(c_1\omega_{j_1LO} - c_2\omega_{j_2LO}\right)\right)(\tau_2 - \tau_1)\right\},$$
(4.26)

where c_1 and c_2 are integer variables that store the type of the vertex ($c_i = +1$ for an outgoing vertex, linked to a vertex with time $\tau' > \tau_i$, -1 for an incoming one with $\tau' < \tau_i$).

The next class I update is the **shift phonon** update: in this update a single phonon interaction vertex τ_i is shifted between the two adjacent phonon vertices τ_{left} and τ_{right} . Given \mathbf{k}_{i-1} and \mathbf{k}_i the momenta of the two free electron propagators that are linked to the phonon vertex we have that the new imaginary time value τ_i' is found as

$$\tau_i' = \tau_{left} - \frac{\log\left(1 - r(1 - e^{-\Delta E(\tau_{right} - \tau_{left})})\right)}{\Delta E},\tag{4.27}$$

where the value of ΔE is retrieved with the following relation

$$\Delta E = \epsilon(\mathbf{k}_i) + \epsilon(\mathbf{k}_{i-1}) - c_i \omega_{i,i,LO}, \tag{4.28}$$

where c_i is the phonon vertex type (+1 for outgoing vertices, -1 for incoming ones). The update is always accepted as long that the new proposed value is not too close to the two extrema (< 10^{-9}).

The last update that was implemented is the **stretch diagram** update (class I). In this update the whole diagram is stretched or compressed like a spring: each electron propagator, together with the phonon propagators that are active at the two selected times τ_i and τ_{i+1} . The imaginary time value of each vertex is shifted (from the first vertex with time value τ_1 to

The imaginary time value of each vertex is shifted (from the first vertex with time value τ_1 to the last $\tau_{2n+1} = \tau$ length of the diagram, while the first vertex at 0 is of course fixed) using the following formula:

$$\tau_i' = \tau_{i-1}' - \frac{\log(1-r)}{\epsilon(\mathbf{k}_{i-1}) - \mu + \sum_j \omega_{jLO} n_j},$$
 (4.29)

where n_j is the number of phonon propagator with mode j that are active at the index j (they were created to the left of the i vertex and and annihilated to the right of it). The update is rejected only if each new proposed value τ_i' is too close to the previously proposed vertex τ_{i-1}' or if $\tau_i' \geq \tau_{i+1}$ next vertex in the diagram.

The full simulation decides which of the 8 updates to choose based on a uniform random variable r in [0,1].

4.2 Collected quantities and MC estimators

After having implemented the features of the Diagrammatic Monte Carlo simulation, methods to collect results and analyze them are necessary. The simplest estimator that can be built is an **histogram method** to reconstruct the shape of the Green's function that we are simulating: a fixed number of bins N_{bins} from 0 to τ_{max} is set at the beginning of the simulation such as every bin has width $\Delta \tau = \tau_{max}/N_{bins}$ and is centered at the value $\tau_j = j\tau_{max}/N_{bins} + \Delta \tau/2$ with j integer between 0 and $N_{bins} - 1$.

After every iteration of the simulation, the diagram length τ_k is given as input to the histogram: if the value τ_k falls in the range $(\tau_j - \Delta \tau/2, \tau_j + \Delta \tau/2)$ the number of counts n_j is updated by 1.

At the end of the simulations we will have N_{bins} each with a different number of counts n_j . The shape of the Green's function can already be assessed in this form, but to obtain the right value at each bin a normalization factor is needed: the obvious normalization factor that is needed is the bin width $\Delta \tau$, but is not enough to get the actual Green's function. In fact, given that we have fixed a maximum imaginary time value τ_{max} , the obtained Green's function is actually normalized over the $(0,\tau_{max})$ range: this is not how the Green's function is defined, since its domain is $(0,+\infty)$. For this reason we exploit the properties of the 0-order diagrams $D_0(\mathbf{k},\tau)$, which we know to have the simple exponential form

$$D_0(\mathbf{k}, \tau) = e^{-(\epsilon(\mathbf{k}) - \mu)\tau},\tag{4.30}$$

since we know how to integrate this function we can use the integral value I_0 of the zero order diagrams to reconstruct the correct normalization factor. The following integral value I_0 is then computed:

$$I_0 = \int_0^{\tau_{max}} e^{-(\epsilon(\mathbf{k}) - \mu)\tau} d\tau = \frac{1 - e^{-(\epsilon(\mathbf{k}) - \mu)\tau_{max}}}{\epsilon(\mathbf{k}) - \mu},$$
(4.31)

and the Green's function has the value

$$P(\mathbf{k}, \tau_j) = \frac{n_j I_0}{N_0 \Delta \tau},\tag{4.32}$$

with N_0 number of 0-order diagrams in the simulation.

Although it is possible to estimate the **ground state energy** $E_P(0)$ of the polaron (also known as the **zero-point renormalization** or **ZPR**), by fitting an exponential function to the Green's function estimated as previously mentioned for large τ values [33], we can build an exact estimator that is able to compute a value for the ground state energy that has no discretization errors (due to the finite width of the bins in the histogram).

The estimator follows from these considerations [29]: given a quantity A specified by the diagrammatic expansion

$$A = \sum_{\nu} D_A(\nu),\tag{4.33}$$

with $D_A(\nu)$ diagrams for which the quantity A is computed, ν internal variables of the diagram with summation over discrete variables and integration over continuous ones, and a quantity $B = \sum_{\nu} D_B(\nu)$ defined similarly, it is possible to estimate the ratio of the two quantities as

$$\frac{B}{A} = \frac{\left(\sum_{MC_A\{\nu\}} Q_{\nu}\right)}{\sum_{MCA\{\nu\}} 1} = \langle Q_{\nu} \rangle_{MC},$$

$$Q_{\nu} = \frac{D_B(\nu)}{D_A(\nu)},$$
(4.34)

with $MC_A\{\nu\}$ set of internal parameters generated during the Monte Carlo simulation. Given the definition, it might not be clear how this expression is useful in order to build an exact energy estimator. To start let us consider the fact that the two quantities A and B are usually the same Green's function (same expansion of the internal variables) taken with some variations in the external parameters. For the ground state energy this reduces to

$$Q_{\nu} = \frac{P(\mathbf{k}, (1+\lambda)\tau)}{P(\mathbf{k}, \tau)} \to \exp\left(-\lambda E_{P}(\mathbf{k})\tau\right)$$
(4.35)

for large au values and λ small parameter. If we approximate the exponential with a Taylor expansion in λ we get

$$\exp(-\lambda E_P(\mathbf{k})\tau) = 1 - \lambda E_P(\mathbf{k})\tau + O(\lambda^2). \tag{4.36}$$

The quantity Q_{ν} can be diagrammatically expanded as

$$Q_{\nu} = \frac{D_{A}(\nu)}{D_{B}(\nu)} = \frac{D_{n_{\nu}}^{\xi_{n_{\nu}}}(\mathbf{k}, (1+\lambda)\tau, \nu)}{D_{n_{\nu}}^{\xi_{n_{\nu}}}(\mathbf{k}, \tau, \nu)},$$
(4.37)

where the ν are the (same) internal variables up to a λ scaling factor. Explicitly, we get the following ratio:

$$Q_{\nu} = (1 + \lambda)^n \left\{ \prod_{l} \exp\left(-\epsilon(\mathbf{k}_l) \Delta \tau_l\right) \prod_{m} \exp\left(-\omega_{jLO} \Delta \tau_m\right) \right\}, \tag{4.38}$$

where the index l lists the free electron propagators while m the free phonon ones. If we now impose $\lambda \to 0$ we get

$$Q_{\nu} \xrightarrow[\lambda \to 0]{} 1 + \lambda \left(n - \sum_{l} \epsilon(\mathbf{k}_{l}) \Delta \tau_{l} - \sum_{m} \omega_{jLO} \Delta \tau_{m} \right) + O(\lambda^{2}), \tag{4.39}$$

which, when compared with 4.36, gives the explicit expression for the energy estimator

$$E_P(\mathbf{k}) = \left\langle \frac{1}{\tau_k} \left(\sum_{l} \epsilon(\mathbf{k}_l) \Delta \tau_l - \sum_{m} \omega_{jLO} \Delta \tau_m - n_k \right) \right\rangle_{MC}. \qquad \tau_k \to +\infty$$
 (4.40)

The ground state energy $E_P(0)$ is found for $\mathbf{k} = 0$.

The next estimator that is defined is for the **effective mass** $m_p^*(\mathbf{k})$ of the polaron, which is in general anisotropic with respect to momentum (it has the same symmetry properties of the electron effective mass from which it is derived), its theoretical definition is

$$\frac{1}{m_P^*(\hat{\mathbf{k}})} = \left(\frac{d^2 E_P(\mathbf{k})}{d\mathbf{k}^2}\right)_{\mathbf{k}=0}.$$
 (4.41)

While an effective mass exact estimator for the isotropic case has been derived [29], no attempts at defining it for the anisotropic case have been tried (at least to the current knowledge). For this reason the following estimator has been developed: it should not be interpreted as a definitive result and a more accurate expression is for sure obtainable. We begin by noting that

$$Q_{\nu} = \frac{P(\lambda \hat{\mathbf{e}}, \tau)}{P(0, \tau)} \xrightarrow{\tau \to \infty} \exp\left\{-\left(E_{P}(\lambda \hat{\mathbf{e}})\tau - E_{P}(0)\right)\tau\right\} =$$

$$= \exp\left(-\frac{\lambda^{2}\tau}{2m_{P}^{*}(\hat{\mathbf{e}})} - E_{P}(0)\tau + E_{P}(0)\tau\right) = \exp\left(-\frac{\lambda^{2}\tau}{2m_{P}^{*}(\hat{\mathbf{e}})}\right),$$
(4.42)

which, for $\lambda \to 0$ becomes:

$$\exp\left(\frac{\lambda^2 \tau}{2m_P^*(\hat{\mathbf{e}})}\right) \xrightarrow[\lambda \to 0]{} 1 - \frac{\lambda^2 \tau}{2m_P^*(\hat{\mathbf{e}})} + O(\lambda^4). \tag{4.43}$$

The ratio can be explicited in a similar way as it was done in 4.38:

$$Q_{\nu} = \prod_{l} \exp \left\{ -\frac{1}{2} \left[\frac{(\mathbf{k}_{l} + \lambda \hat{\mathbf{e}})^{2}}{m^{*} \left(\frac{\mathbf{k}_{l} + \lambda \mathbf{e}}{\sqrt{k_{l}^{2} + \lambda^{2}}} \right)} - \frac{k_{l}^{2}}{m^{*} (\hat{k}_{l})} \right] \Delta \tau_{l} \right\}. \tag{4.44}$$

The first electronic effective mass in this expression is problematic: the fact that $\lambda \to 0$ in the limit does not help with the evaluation since the mass only depends on the orientation of the momentum, for $\mathbf{k} \to 0$ (which is quite common) the expression is not defined without determining a clear λ value. For this reason we employ the approximation

$$m^* \left(\frac{\mathbf{k}_l + \lambda \mathbf{e}}{\sqrt{k_l^2 + \lambda^2}} \right) \approx m(\hat{\mathbf{e}}).$$
 (4.45)

Using this expression 4.44 becomes solvable at the price of losing accuracy. Given that conduction band minima usually have a prolate effective mass ($m_x^* = m_y^* = m_\perp^* < m_z^*$) this means that our estimation sets a lower bound for the computed m_z^* and an upper bound for

 m_{\perp}^* . In the case $m_x < m_y < m_z$ the behaviour of m_y is not defined a priori. Given 4.45, 4.44 becomes:

$$Q_{\nu} = \prod_{l} \exp \left\{ -\frac{1}{2m^{*}(\hat{\mathbf{e}})} \left[\mathbf{k}_{l}^{2} + \lambda (\mathbf{k}_{l} \cdot \hat{\mathbf{e}}) + \lambda^{2} - k_{l}^{2} \right] \Delta \tau_{l} \right\} =$$

$$= \prod_{l} \exp \left\{ -\frac{1}{2m^{*}(\hat{\mathbf{e}})} \left[\lambda (\mathbf{k}_{l} \cdot \hat{\mathbf{e}}) + \lambda^{2} \right] \Delta \tau_{l} \right\},$$
(4.46)

which for $\lambda \to 0$ becomes

$$Q_{\nu} \xrightarrow[\lambda \to 0]{} 1 - \lambda \sum_{l} \frac{(\mathbf{k}_{l} \cdot \hat{\mathbf{e}})}{m^{*}(\hat{\mathbf{e}})} \Delta \tau_{l} - \lambda^{2} \sum_{l} \frac{\Delta \tau_{l}}{m^{*}(\hat{\mathbf{e}})} + \frac{\lambda^{2}}{2} \left(\sum_{l} \frac{(\mathbf{k}_{l} \cdot \hat{\mathbf{e}})}{m^{*}(\hat{\mathbf{e}})} \Delta \tau_{l} \right)^{2} + O(\lambda^{3}). \tag{4.47}$$

Combining this equation with 4.43 and identifying the corresponding λ terms, we see that

$$\frac{1}{m_P^*(\hat{\mathbf{e}})} = \frac{1}{m^*(\hat{\mathbf{e}})} - \frac{1}{m^*(\hat{\mathbf{e}})^2} \left\langle \frac{1}{\tau_k} \left(\sum_l (\mathbf{k}_l \cdot \hat{\mathbf{e}}) \Delta \tau_l \right)^2 \right\rangle_{MC}. \tag{4.48}$$

The formula for m_{Px}^* , m_{Py}^* and m_{Pz}^* are retrieved for $\hat{\bf e}=\hat{x}$, $\hat{\bf e}=\hat{y}$ and $\hat{\bf e}=\hat{z}$ respectively. The last exact estimator which is shown is the Green's function exact estimator, which removes the discretization error in the Green's function estimation that is present in the histogram method, which inevitably introduces systematic errors.

We begin by observing that [29]

$$P(\mathbf{k}, \tau_j) = \sum_{\nu} D(\mathbf{k}, \tau_j, \nu) = \int d\tau \sum_{\nu} D(\mathbf{k}, \tau, \nu) \delta(\tau - \tau_0),$$
 (4.49)

with $P(\tau_j)$ value of the Green's function at τ_j .

Given a width $\Delta \tau$ fixed around the τ_i value (the procedure to define the τ_i values and the width $\Delta \tau$ is the same as previously done for the histogram method), we can define a Monte Carlo estimator for $P(\tau_i)$ as:

$$P(\mathbf{k}, \tau_j) = \left\langle \frac{1}{\Delta \tau} \frac{D_{n_k}(\mathbf{k}, \tau_k, \dots)}{D_{n_k}(\mathbf{k}, \tau_j, \dots)} \theta \left(|\tau_k - \tau_j| - \frac{\Delta \tau}{2} \right) \right\rangle_{MC}, \tag{4.50}$$

where $\theta(\cdots)$ is the Heaviside step function, which takes into account only τ_k values that are inside the interval $(\tau_j - \frac{\Delta \tau}{2}, \tau_j + \frac{\Delta \tau}{2})$. In alternative, an estimator for $G^{(N)}(\mathbf{k}, \tau_j)$ which only takes into account diagrams with N

external phonons can be defined:

$$G^{(N)}(\mathbf{k}, \tau_j) = \left\langle \frac{1}{\Delta \tau} \frac{D_{n_k}(\mathbf{k}, \tau_k, \dots)}{D_{n_k}(\mathbf{k}, \tau_j, \dots)} \theta \left(|\tau_k - \tau_j| - \frac{\Delta \tau}{2} \right) \delta_{N_k, N} \right\rangle_{MC}, \tag{4.51}$$

where the Kronecker delta $\delta_{N_k,N}$ only takes into account diagrams with $N_k=N$ number of external phonon propagators.

5 Methods and results

The program developed was used to simulate the electron polaron of a range of cubic materials (zincblende structrure) both with isotropic (CBM at Γ) and anisotropic (CBM at X point or along the $X-\Gamma$ high symmetry line) electronic band structure. For each one of them one single phonon mode was considered since from the phonon band structure only one longitudinal optical mode is retrieved [4] (which means that the add internal/external update cannot choose between different phonon energies and is restricted to one ω_{LO} and j=1).

5.1 Input data

Material	a (bohr)	edge	m_{\perp}^{*}	m_z^*	ω_{LO} (meV)	ϵ_{∞}	ϵ_0	$\langle \alpha \rangle$
AlAs-zb	10.825	X	0.243	0.897	47.3	9.49	11.51	0.184
AlP-zb	10.406	X	0.252	0.809	59.9	8.12	10.32	0.184
GaN-zb	8.598	Γ	0.144	0.144	86.0	6.13	11.00	0.345
GaP-zb	10.294	X^*	0.230	1.062	48.6	10.50	12.53	0.152
SiC-zb	8.227	X	0.228	0.677	117.0	6.97	10.30	0.280
ZnSe-zb	10.833	Γ	0.089	0.089	29.3	7.35	10.73	0.276

Table 1: Input values used for the simulations from [7] and [4], the coupling strengths are given as averages over the solid angle 4π .

The 6 simulated materials were AlAs, AlP, GaN, GaP, SiC and ZnSe: the values of their effective masses, phonon energy, cell size, static dielectric tensor and optical dielectric tensor were computed with first-principle methods using GGA-PBE retrieved from [7] and [4] (Supplementary data). Their values are visible in 1 together with the computed average coupling strength as reference, which was found as

$$\langle \alpha \rangle = \left(\frac{1}{\epsilon_{\infty}} - \frac{1}{\epsilon_{0}}\right) \sqrt{\frac{\langle m^{*}(\hat{\mathbf{q}}) \rangle}{2\omega_{LO}}}.$$
 (5.1)

All the simulated electron polarons originated from an electron band which was isotropic (in Γ) or anisotropic uniaxial (in X or in X^* , which is a short-hand notation for the high symmetry line $X-\Gamma$) and the longitudinal optical phonon energies were between $30 \mathrm{meV}$ and $117 \mathrm{meV}$ covering an order of magnitude.

The lattice parameter (and thus the volume, computed as $a^3/4$) is reported for completeness even if it is by no means necessary in the simulation, in agreement with the large polaron approximation proper of the used Froehlich model.

5.2 Methods 69

The dielectric response ϵ^* , which in the case of a single optical phonon mode simply reduces to

$$\frac{1}{\epsilon^*} = \left(\frac{1}{\epsilon_\infty} - \frac{1}{\epsilon_0}\right),\tag{5.2}$$

is independent of the nuclear masses since both ϵ_{∞} (purely electronic) and ϵ_0 (static) are. It measures the ionicity of the material and thus the strength of the electron-phonon coupling: for $\epsilon^* \to +\infty$ there is no coupling: this is the case for covalent materials such as diamond-C and diamond-Si where no polarization is possible between the atoms in the basis and $\epsilon_{\infty} = \epsilon_0$.

5.2 Methods

For each one of the studied materials 20 independent simulations were performed in order to get an estimation together with an error, the estimate was computed with a simple mean while the error with the formula for the sample variance:

$$\bar{x} = \frac{1}{20} \sum_{i} x_{i}, \qquad \Delta x = \sqrt{\frac{\sum_{i} (x_{i} - \bar{x})^{2}}{19}}.$$
 (5.3)

The simulations were performed using a fixed τ value in order to have better-converged results for the ground state energy and the polaron effective masses. The τ value was set to 2000 for AlAS, AlP, SiC and ZnSe, 3000 for GaP, 10000 for GaN (to see if a bigger value for τ could improve the obtained result). As a rule of thumb, it is always better to have a greater fixed τ value for energy and effective mass computation, especially if the energy of the optical phonon is small or the coupling strength is high. This of course means that the computation times are inevitably longer. For effective masses, in the isotropic case only the computed value for m_{Px}^* were used for the result, in the anisotropic case only m_{Px}^* (m_1^*) and m_{Pz}^* .

5.3 Results

material	DMC (meV)	Perturbative (meV)	Feynman avg (meV)		
AlAs-zb	-10.52 ± 0.11	-8.8	-9.6		
AIP-zb	-15.83 ± 0.19	-14.0	-15.1		
GaN-zb	-30.11 ± 0.42	-29.6	-29.7		
GaP-zb	-8.59 ± 0.24	-7.4	-8.3		
SiC-zb	-34.72 ± 0.42	-32.7	34.8		
ZnSe-zb	-8.66 ± 0.09	-8.1	-8.1		

Table 2: Obtained polaron ground state energy with DMC (0 is the reference for the conduction band minimum), the values for Froehlich and Feynman were retrieved from [4].

5.3 Results 70

The results obtained for the ground state energy of the polaron (or Zero-Point Renormalization ZPR) are shown in 2 together with the values computed with a generalized Froehlich formalism and the average (in the anisotropic case) values obtained with the Feynman variational approach, the values are to be interpreted as a renormalization of the conduction band minimum (and thus are all negative). The data obtained shows that all the computed parameters are estimated to be lower than what is found with the Feynman technique, as it should be since this is a variational technique which provides an upper bound to the renormalization energy. In the case of an anisotropic electronic band, the Feynman result was found as

$$E_{Pavg}^{F} = \frac{2E_{P\perp}^{F} + E_{Pz}^{F}}{3}.$$
 (5.4)

	DMC		Pertur	bative	Feynman	
material	$m_{P\perp}^*$ (a.u.)	m_{Pz}^st (a.u.)	$m_{P\perp}^*$ (a.u.)	m_{Pz}^st (a.u.)	$m_{P\perp}^*$ (a.u.)	m_{Pz}^st (a.u.)
AlAs-zb	0.2564	0.9256	0.2518	0.9155	0.2490	0.9409
AlP-zb	0.2689	0.8423	0.2637	0.8322	0.2602	0.8574
GaN-zb	0.1541	0.1541	0.1523	0.1523	0.1518	0.1518
GaP-zb	0.2413	1.0894	0.2367	1.0786	0.2343	1.1086
SiC-zb	0.2450	0.7089	0.2409	0.7007	0.2372	0.7235
ZnSe-zb	0.0977	0.0977	0.0936	0.0936	0.09344	0.0934

Table 3: Obtained polaron effective masses using DMC, the values for Froehlich and Feynman were retrieved from [4].

In 3 instead the polaron effective masses are shown (error estimations are not given since they are so small they can be neglected). As it can be seen in this case the values obtained have a less clear relationship with the perturbative and variational approaches (differently from what is seen with the ground state energy, which is consistently inferior to the variational value) and it is not clear which one of the computed values better estimates the actual polaron effective mass, also considering that for DMC we have employed the approximation 4.45 to obtain 4.48. Nevertheless the results obtained are still consistent with the symmetry of the model and with the values provided by the other approaches.

Conclusions

In this thesis we have seen how the Diagrammatic Monte Carlo approach can be used to simulate polaronic states inside real cubic materials and obtain estimates about the renormalization of the ground state energy of conduction band minima and about the polaron effective masses in a range of isotropic and anisotropic materials.

In Chapter 1 the failures of the Born-Oppenheimer approximation in modelling polaronic states were first presented, then the basic Froehlich model was derived and illustrated, together with the main approaches that are used to solve it. Then the generalized Froehlich model was illustrated, with a focus in particular on the non-degenerate anisotropic electron band case. Some analytical solution techniques were provided for this model.

In Chapter 2 the formalism provided by Quantum Many Body theory was used to obtain a Green's function (which is the solution to the Hamiltonian) which could be treated with Diagrammatic Monte Carlo, in particular by employing the Matsubara imaginary time formalism, which gets rid of the complex nature of the original Green's function and obtains a real nonnegative representation, and using Wick's theorem, which allows us to treat the original interacting Green's function as a perturbative infinite series of non-interacting Green's functions and interaction vertices (both easy to evaluate).

In Chapter 3 the Monte Carlo method was explained illustrating the basic features of this numerical method, which depends on estimating expectation values of given quantities. Then the direct Monte Carlo method was briefly described, which directly models the investigated system, then the integration method, used to compute hard integrals, and the Markov chain Monte Carlo, a tool capable of generating random samples distributed as a target distribution after a given relaxation time using the Metropolis-Hastings algorithm. The Markov chain Monte Carlo method is at the basis of the Diagrammatic Monte Carlo approach, which extensively uses it to compute transitions from different diagrams using suitable updates.

In Chapter 4 the algorithm used for the Froehlich polaron simulation was discussed, from the way the free propagators and vertices were stored in the computer to the procedure used for each one of the implemented updates. The main estimators which can be used to retrieve information about the Green's function were also described.

In Chapter 5 the obtained results for a range of real materials were shown, together with the input data and basic information about the procedure which was undertaken.

The work done in this thesis can be used as a starting point for a more complete and complex simulation that takes into account degenerate electronic bands, electronic band anharmonicity and phonon mode anisotropy in order to simulate the electron and hole polarons in a wider range of materials.

Acknowledgement

5.4 Acknowledgment

I would like to personally thank Dr. Thomas Hahn for all the support and all the suggestions he has provided during the realization of this thesis, which could not have been possible without his help, and Prof. Franchini, for having believed in my abilities and for having introduced me to the specific topic of Diagrammatic Monte Carlo, of which I did not know anything.

Appendix

All the simulations have been performed using the code in [39], in order to use it you have to include in the compiler list the files main.cpp, Diagram.cpp, GreenFuncNph.cpp, GreenFuncNphBands.cpp, MC_Benchmarking.cpp and progressbar.cpp, the Eigen library is also required and its main directory must be present in the DQMC directory (otherwise specify the path in the include files).

The program was compiled in a Windows machine using the mingw64 g++ compiler and in a Linux machine using the native GNU/GCC compiler.

Three text files must be included in order to start the simulation, **simulation_parameters.txt**, **simulation_settings.txt** and **simulations_probabilities_MC.txt**.

The main options of **simulation_parameters.txt** are:

- type: set "bands" for anisotropic multi-phonon mode calculations.
- thermalization_steps: number of relaxation steps performed.
- **simulation_steps**: number of MC steps performed.
- max_tau_value: maximum allowed tau value in the simulation.
- **dimensions**: number of dimensions of the system to simulate (3).
- **kx**: k_x momentum.
- **ky**: k_y momentum.
- **kz**: k_z momentum.
- chemical_potential: fictitious renormalization potential (provide negative values).
- max_internal_order: maximum number of allowed internal phonon propagator is half this quantity (provide even values).
- max_num_ext_phonon: maximum number of allowed external phonon propagators.
- **num_bands**: number of degenerate electronic bands (1).
- num_phonon_modes: number of phonon modes (1 or more).
- **phonon_mode(i)**: energy of the *i*th phonon mode (starting from 0 to n-1), values must be provided in Hartree (atomic units).
- **dielectric_response(i)**: dielectric response of *i*th phonon mode using atomic units.

- **mx**: effective band mass along k_x .
- my: effective band mass along k_y .
- mz: effective band mass along k_z .
- **V_1BZ**: unit cell volume (not necessary, can be set to 1 since the Froehlich model assumes the continuum hypothesis).
- **V_BvK**: Born-von Karman cell volume (set to 1).
- **diel_const**: ϵ_{∞} in atomic units.

The main options of **simulation_settings.txt** are:

- exact_GF: boolean, computes the Green's function with the exact estimator
- **num_points**: number of points for which the exact GF is evaluated, spacing depends on max_tau_value.
- **selected_order**: number N of external phonons for which the exact GF is computed, if the value is negative the GF is computed for all N.
- histo: boolean, computes the Green's function using the histogram method.
- bins_(histogram): number of bins of the histogram, width depends on max_tau_value.
- **gs_energy**: boolean, computes the ground state energy with the exact estimator.
- **cutoff_tau_(gs_energy)**: tau value cutoff for which the ground state energy is computed (lower bound).
- **effective_mass**: boolean, computes the polaron effective masses with the exact estimator.
- cutoff_tau_(mass): same as for the energy cutoff.
- write_diagram: boolean, method to print and visualize computed diagram, automatically disabled if simulation_steps;25000.
- **time_benchmark**: boolean, computes the average time each update takes and the average time per iteration.
- **stats**: boolean, collects statistics about MC simulation (average order, number of external phonons, number of internal phonons, order 0 diagrams).
- **cutoff_tau_stats**: tau value cutoff for which statistics is computed (lower bound).

• fix_tau_value: boolean, fixes length of diagrams to max_tau_value (and changes update probabilities accordingly), useful to compute ground state energy and effective masses.

The options of **simulation_probabilities_MC.txt** are:

- prob_length: diagram length update probability.
- prob_add_internal: add internal phonon update probability.
- prob_remove_internal: remove internal phonon update probability.
- prob_add_external: add external phonon update probability.
- prob_remove_internal: remove external phonon update probability.
- prob_swap: swap update probability.
- **prob_shift**: shift update probability (currently not working properly).
- prob_stretch: stretch update probability.

If the probabilities given in input do not add to 1, they are properly normalized.

REFERENCES 76

References

[1] Craig Pryor. Predicted band structures of iii-v semiconductors in the wurtzite phase. *Phys. Rev. B*, 81, 08 2009.

- [2] Jozef Devreese and Alexandre Alexandrov. Froehlich polaron and bipolaron: Recent developments. *Reports on Progress in Physics*, 72:066501, 05 2009.
- [3] Jun Da Ng and Aaron Danner. Pseudopotential form factors and electronic band structures for alas, alp, bas, bp, 3c-sic, and cubic-gan. *Physica Scripta*, 96(5):055801, 2021.
- [4] Bogdan Guster, Pedro Melo, Bradley AA Martin, Véronique Brousseau-Couture, Joao C de Abreu, Anna Miglio, Matteo Giantomassi, Michel Côté, Jarvist M Frost, Matthieu J Verstraete, et al. Fröhlich polaron effective mass and localization length in cubic materials: Degenerate and anisotropic electronic bands. *Physical Review B*, 104(23):235123, 2021.
- [5] James Gubernatis, Naoki Kawashima, and Philipp Werner. *Quantum Monte Carlo Methods*. Cambridge University Press, 2016.
- [6] Thomas Hahn. Diagrammatic quantum monte carlo for the fröhlich polaron, 2017.
- [7] Anna Miglio, Véronique Brousseau-Couture, Emile Godbout, Gabriel Antonius, Yang-Hao Chan, Steven G Louie, Michel Côté, Matteo Giantomassi, and Xavier Gonze. Predominance of non-adiabatic effects in zero-point renormalization of the electronic band gap. *npj Computational Materials*, 6(1):167, 2020.
- [8] Herbert Fröhlich. Electrons in lattice fields. Advances in Physics, 3(11):325-361, 1954.
- [9] Th Holstein. Studies of polaron motion: Part i. the molecular-crystal model. *Annals of physics*, 8(3):325–342, 1959.
- [10] Th Holstein. Studies of polaron motion: Part ii. the "small" polaron. *Annals of physics*, 8(3):343–389, 1959.
- [11] Cesare Franchini, Michele Reticcioli, Martin Setvin, and Ulrike Diebold. Polarons in materials. *Nature Reviews Materials*, 6(7):560–586, 2021.
- [12] Felix Bloch. Quantum mechanics of electrons in crystal lattices. *Z. Phys*, 52:555–600, 1928.
- [13] N. W. Ashcroft and N. D. Mermin. Solid State Physics. Holt-Saunders, 1976.
- [14] Jos Thijssen. Computational physics. Cambridge university press, 2007.

REFERENCES 77

[15] Pierre Hohenberg and Walter Kohn. Inhomogeneous electron gas. *Physical review*, 136(3B):B864, 1964.

- [16] W. Kohn and L. J. Sham. Self-consistent equations including exchange and correlation effects. *Phys. Rev.*, 140:A1133–A1138, 11 1965.
- [17] GP Kerker. Non-singular atomic pseudopotentials for solid state applications. *Journal of Physics C: Solid State Physics*, 13(9):L189, 1980.
- [18] Paul Ziesche, Stefan Kurth, and John P Perdew. Density functionals from Ida to gga. *Computational materials science*, 11(2):122–127, 1998.
- [19] Hermann Haken. Quantum Field Theory of Solids. An Introduction. 1976.
- [20] Alexandre S Alexandrov and Jozef T Devreese. *Advances in polaron physics*, volume 159. Springer, 2010.
- [21] Pedro Miguel MC de Melo, Joao C de Abreu, Bogdan Guster, Matteo Giantomassi, Zeila Zanolli, Xavier Gonze, and Matthieu J Verstraete. High-throughput analysis of fröhlichtype polaron models. *npj Computational Materials*, 9(1):147, 2023.
- [22] Gerald D Mahan. Many-particle physics. Springer Science & Business Media, 2013.
- [23] Satoru J Miyake. The ground state of the optical polaron in the strong-coupling case. *Journal of the Physical Society of Japan*, 41(3):747–752, 1976.
- [24] Xavier Gonze and Changyol Lee. Dynamical matrices, born effective charges, dielectric permittivity tensors, and interatomic force constants from density-functional perturbation theory. *Physical Review B*, 55(16):10355, 1997.
- [25] Richard Phillips Feynman. Slow electrons in a polar crystal. *Physical Review*, 97(3):660, 1955.
- [26] Henrik Bruus and Karsten Flensberg. Many-body quantum theory in condensed matter physics: an introduction. Oxford university press, 2004.
- [27] Wolfgang Nolting and William D Brewer. *Fundamentals of many-body physics*, volume 3. Springer, 2009.
- [28] Murray Gell-Mann and Francis Low. Bound states in quantum field theory. *Phys. Rev.*, 84:350–354, 10 1951.
- [29] AS Mishchenko, NV Prokof'Ev, A Sakamoto, and BV Svistunov. Diagrammatic quantum monte carlo study of the fröhlich polaron. *Physical Review B*, 62(10):6317, 2000.

REFERENCES 78

[30] Andrei S Mishchenko. Diagrammatic monte carlo method as applied to the polaron problems. *Physics-Uspekhi*, 48(9):887, 2005.

- [31] Thomas Hahn, Sergei Klimin, Jacques Tempere, Jozef T Devreese, and Cesare Franchini. Diagrammatic monte carlo study of fröhlich polaron dispersion in two and three dimensions. *Physical Review B*, 97(13):134305, 2018.
- [32] Nicholas Metropolis and Stanislaw Ulam. The monte carlo method. *Journal of the American statistical association*, 44(247):335–341, 1949.
- [33] Holger Fehske, Ralf Schneider, and Alexander Weisse. *Computational many-particle physics*, volume 739. Springer, 2007.
- [34] Federico Becca and Sandro Sorella. *Quantum Monte Carlo approaches for correlated systems*. Cambridge University Press, 2017.
- [35] Makoto Matsumoto and Takuji Nishimura. Mersenne twister: a 623-dimensionally equidistributed uniform pseudo-random number generator. ACM Transactions on Modeling and Computer Simulation (TOMACS), 8(1):3–30, 1998.
- [36] Nicholas Metropolis, Arianna W Rosenbluth, Marshall N Rosenbluth, Augusta H Teller, and Edward Teller. Equation of state calculations by fast computing machines. *The journal of chemical physics*, 21(6):1087–1092, 1953.
- [37] Emanuel Gull, Andrew J Millis, Alexander I Lichtenstein, Alexey N Rubtsov, Matthias Troyer, and Philipp Werner. Continuous-time monte carlo methods for quantum impurity models. *Reviews of Modern Physics*, 83(2):349–404, 2011.
- [38] Kris Van Houcke, Evgeny Kozik, Nikolay Prokof'ev, and Boris Svistunov. Diagrammatic monte carlo. *Physics Procedia*, 6:95–105, 2010.
- [39] Dqmc. https://github.com/sda-express-one/DQMC, 2025. [Online; accessed 2025-10-08].